

Spacecraft Thermal Control Coatings References

Lonny Kauder

The NASA STI Program Office ... in Profile

Since its founding, NASA has been dedicated to the advancement of aeronautics and space science. The NASA Scientific and Technical Information (STI) Program Office plays a key part in helping NASA maintain this important role.

The NASA STI Program Office is operated by Langley Research Center, the lead center for NASA's scientific and technical information. The NASA STI Program Office provides access to the NASA STI Database, the largest collection of aeronautical and space science STI in the world. The Program Office is also NASA's institutional mechanism for disseminating the results of its research and development activities. These results are published by NASA in the NASA STI Report Series, which includes the following report types:

- **TECHNICAL PUBLICATION.** Reports of completed research or a major significant phase of research that present the results of NASA programs and include extensive data or theoretical analysis. Includes compilations of significant scientific and technical data and information deemed to be of continuing reference value. NASA's counterpart of peer-reviewed formal professional papers but has less stringent limitations on manuscript length and extent of graphic presentations.
- **TECHNICAL MEMORANDUM.** Scientific and technical findings that are preliminary or of specialized interest, e.g., quick release reports, working papers, and bibliographies that contain minimal annotation. Does not contain extensive analysis.
- **CONTRACTOR REPORT.** Scientific and technical findings by NASA-sponsored contractors and grantees.
- **CONFERENCE PUBLICATION.** Collected papers from scientific and technical conferences, symposia, seminars, or other meetings sponsored or cosponsored by NASA.
- **SPECIAL PUBLICATION.** Scientific, technical, or historical information from NASA programs, projects, and mission, often concerned with subjects having substantial public interest.
- **TECHNICAL TRANSLATION.** English-language translations of foreign scientific and technical material pertinent to NASA's mission.

Specialized services that complement the STI Program Office's diverse offerings include creating custom thesauri, building customized databases, organizing and publishing research results . . . even providing videos.

For more information about the NASA STI Program Office, see the following:

- Access the NASA STI Program Home Page at <http://www.sti.nasa.gov/STI-homepage.html>
- E-mail your question via the Internet to help@sti.nasa.gov
- Fax your question to the NASA Access Help Desk at (301) 621-0134
- Telephone the NASA Access Help Desk at (301) 621-0390
- Write to:
NASA Access Help Desk
NASA Center for AeroSpace Information
7121 Standard Drive
Hanover, MD 21076-1320



Spacecraft Thermal Control Coatings References

Lonny Kauder

NASA/Goddard Space Flight Center, Greenbelt, Maryland

National Aeronautics and
Space Administration

Goddard Space Flight Center
Greenbelt, Maryland 20771

Available from:

NASA Center for AeroSpace Information
7121 Standard Drive
Hanover, MD 21076-1320
Price Code: A17

National Technical Information Service
5285 Port Royal Road
Springfield, VA 22161
Price Code: A10

Table of Contents

	pg
<i>Introduction</i>	ii
I. Electromagnetic Origins of Thermal Properties	1
II. Factors that Affect Emittance	10
2.1 Change in emittance with Temperature	10
2.2 Role of thickness in Effective Emittance	11
2.3 Non-Grey Effects	12
III. Measurement of Thermal Properties	18
3.1 Solar absorptance	18
3.2 Measurement of Emittance	23
3.2.1 Infrared Reflectometry	23
3.2.2 Emittance Calculated from Infrared Reflectance Measurements	25
3.2.3 Calorimetric Technique for Determining Hemispherical Emittance	26
3.2.4 Thermal Balance Method for Determining Hemispherical Emittance	27
3.2.5 Methods of Increasing Emittance	29
3.2.6 Considerations and Lessons Learned	29
3.3 Electrical properties of Thermal Control Coatings.....	30
References	39
IV. Thermal Control Coatings Data	40
4.1 Black Coatings	40
4.2 White and Color Coatings	41
4.3 Conductive Paints	42
4.4 Anodize Aluminum Coatings	43
4.5 Metals and Conversion Coatings	44
4.6 Vapor Deposited Coatings	45
4.7 Solar Cells	46
4.8 Composite Coatings	47
4.9 Films and Tapes	48
V. Total Hemispherical Reflectance Curves for Selected Thermal Control Coatings	50
VI. Total Hemispherical Emittance as a Function of Temperature For Selected Thermal Control Coatings	90

Introduction

The successful thermal design of spacecraft depends in part on a knowledge of the solar absorptance and hemispherical emittance of the thermal control coatings used in & on the spacecraft. The Goddard Space Flight Center has had since its beginning, a group whose mission has been to provide thermal/optical properties data of thermal control coatings to Thermal Engineers. This handbook represents a summary of the data and knowledge accumulated over many years at the GSFC. I would like to thank the many people who have contributed to this data and assisted in the creation of this handbook: Jack Triolo, Wanda Peters, John Henninger, Amani Ginyard, Monali Joshi, & Blake Miller.

I. Electromagnetic Origins of Emittance and Reflectance

The following is a derivation of the parallel and perpendicular components of reflectivity starting from Maxwell's laws. Looking forward to the end result (equation 23 & 24 pg 8 & 9) will not affect the understanding of the topic.

When electromagnetic energy is incident on an opaque surface such as a typical thermal control coating, part of the energy is reflected back into space and part of the energy is absorbed in the material. Maxwell's equations can, at least in theory, be used to describe the interaction of electromagnetic radiation with spacecraft coatings if one happens to know the bulk properties of conductivity, permittivity and permeability of the coating.

The following set of well known Maxwell equations (reference 1) are necessary to describe the interaction of electromagnetic energy absorbed or reflected by metals and dielectrics used in thermal control coatings:

$$\nabla \times \vec{H} = \xi \frac{\partial \vec{E}}{\partial t} + \sigma \vec{E} \quad (1)$$

$$\nabla \times \vec{E} = -\mu \frac{\partial \vec{H}}{\partial t} \quad (2)$$

$$\nabla \cdot \vec{E} = 0 \quad (3)$$

$$\nabla \cdot \vec{H} = 0 \quad (4)$$

Where ξ , μ , σ , are the permittivity, permeability and conductivity of the medium respectively. The electric field vector is represented here by \vec{E} and the magnetic field vector by \vec{H} . Applying an appropriate vector identity (reference 3) and taking the curl of the first two equations and using equations (3 and (4 from above, it's clear that the Electric and Magnetic fields must satisfy the following set of vector wave equations:

$$\nabla^2 \vec{H} = \xi \mu \frac{\partial^2 \vec{H}}{\partial t^2} + \sigma \mu \frac{\partial \vec{H}}{\partial t} \quad (5)$$

$$\nabla^2 \vec{E} = \xi \mu \frac{\partial^2 \vec{E}}{\partial t^2} + \sigma \mu \frac{\partial \vec{E}}{\partial t} \quad (6)$$

Let's assume the general form of an electromagnetic plane wave incident on a surface with a time dependency t and frequency ω :

$$\vec{E}(\vec{r}, t) = \vec{E}_o e^{j(\vec{k} \cdot \vec{r} - \omega t)} \quad (7)$$

$$\vec{H}(\vec{r}, t) = \vec{H}_o e^{j(\vec{k} \cdot \vec{r} - \omega t)} \quad (8)$$

where the direction of propagation is given by the unit vector \mathbf{k} :

$$\vec{k} = k\vec{x} + k\vec{y} + k\vec{z}$$

and any given vector is given by r :

$$\vec{r} = r\vec{x} + r\vec{y} + r\vec{z}$$

where \vec{x} , \vec{y} , \vec{z} are unit vectors in the x,y, and z direction.

Now consider the case of an electromagnetic plane wave in space incident on a thermal control surface with conductivity, permeability and permittivity of σ , μ , and ξ respectively. The following diagrams represents two cases, one in which the electric vector is perpendicular to the normal and the other in which the magnetic vector is perpendicular to the normal.

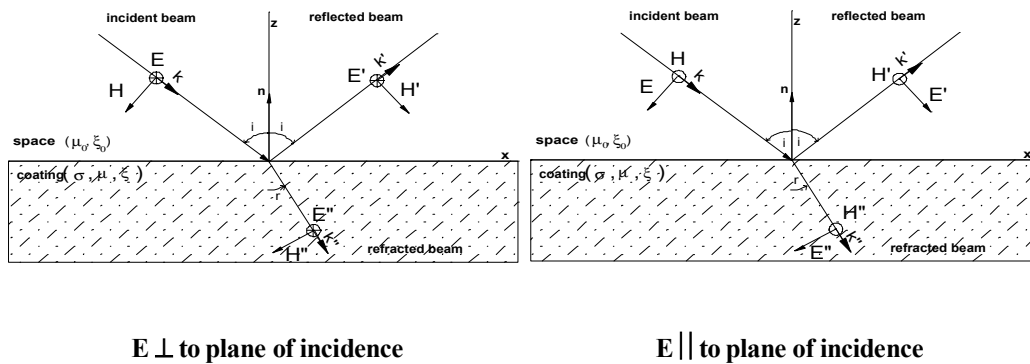


Figure 1.1-1. Electromagnetic waves incident on a thermal control coating

Where n is a unit normal vector, μ_0 and ξ_0 are the permeability and permittivity respectively of space and σ , μ and ξ are the conductivity, permeability and permittivity respectively of the coating. For each case the three waves (incident, reflected and refracted) are represented by:

$\vec{E}(\vec{r}, t) = \vec{E}_o e^{j(\vec{k} \cdot \vec{r} - \omega t)}$	$\vec{H}(\vec{r}, t) = \vec{H}_o e^{j(\vec{k} \cdot \vec{r} - \omega t)}$	Incident wave
$\vec{E}'(\vec{r}, t) = \vec{E}'_o e^{j(\vec{k}' \cdot \vec{r} - \omega t)}$	$\vec{H}'(\vec{r}, t) = \vec{H}'_o e^{j(\vec{k}' \cdot \vec{r} - \omega t)}$	Reflected wave
$\vec{E}''(\vec{r}, t) = \vec{E}''_o e^{j(\vec{k}'' \cdot \vec{r} - \omega t)}$	$\vec{H}''(\vec{r}, t) = \vec{H}''_o e^{j(\vec{k}'' \cdot \vec{r} - \omega t)}$	Refracted wave

The \mathbf{E} field and \mathbf{H} field for an electromagnetic wave are perpendicular and therefore the \mathbf{E} and \mathbf{H} components can only satisfy the wave equation provided that:

$$\vec{E}(\vec{r}, t) = \vec{E}_o e^{j(\vec{k} \cdot \vec{r} - \omega t)} \quad \vec{H}(\vec{r}, t) = \sqrt{\frac{\xi_0}{\mu_0}} \frac{\vec{k} \times \vec{E}_o e^{j(\vec{k} \cdot \vec{r} - \omega t)}}{k} \quad \text{Incident wave}$$

$$\begin{aligned}
\vec{E}'(\vec{r}, t) &= \vec{E}'_o e^{j(\vec{k}' \cdot \vec{r} - \omega t)} & \vec{H}'(\vec{r}, t) &= \sqrt{\frac{\xi_o}{\mu_o}} \frac{\vec{k}' \times \vec{E}'_o e^{j(\vec{k}' \cdot \vec{r} - \omega t)}}{k'} & \text{Reflected wave} \\
\vec{E}''(\vec{r}, t) &= \vec{E}''_o e^{j(\vec{k}'' \cdot \vec{r} - \omega t)} & \vec{H}''(\vec{r}, t) &= \sqrt{\frac{\sigma + j\omega\xi}{j\omega\mu}} \frac{\vec{k}'' \times \vec{E}''_o e^{j(\vec{k}'' \cdot \vec{r} - \omega t)}}{k''} & \text{Refracted wave}
\end{aligned}$$

Where $\sigma = 0$ for space.

Electromagnetic waves must meet the appropriate boundary conditions at the space/thermal coating boundary (i.e. the normal components of the displacement vector, \mathbf{D} and the magnetic induction vector, \mathbf{B} are continuous and the tangential components of the electric field vector, \mathbf{E} and the magnetic field vector \mathbf{H} are continuous at $z=0$) (reference 2):

$$\begin{aligned}
\vec{D} &= \xi \vec{E} & \vec{D}_o &= \xi_o \vec{E} \\
\vec{B} &= \mu \vec{H} & \vec{B}_o &= \mu_o \vec{H}
\end{aligned}$$

$$[\xi(\vec{E}_o + \vec{E}'_o) - \xi''\vec{E}''_o] \cdot \vec{n} = 0 \quad (9)$$

$$\left[\mu_o \sqrt{\frac{\xi_o}{\mu_o}} \frac{\vec{k} \times \vec{E}_o}{k} + \mu_o \sqrt{\frac{\xi_o}{\mu_o}} \frac{\vec{k}' \times \vec{E}'_o}{k'} - \mu'' \sqrt{\frac{\sigma + j\omega\xi''}{j\omega\mu''}} \frac{\vec{k}'' \times \vec{E}''_o}{k''} \right] \cdot \vec{n} = 0 \quad (10)$$

$$(\vec{E}_o + \vec{E}'_o - \vec{E}''_o) \times \vec{n} = 0 \quad (11)$$

$$\left[\sqrt{\frac{\xi_o}{\mu_o}} \frac{\vec{k} \times \vec{E}_o}{k} + \sqrt{\frac{\xi_o}{\mu_o}} \frac{\vec{k}' \times \vec{E}'_o}{k'} - \sqrt{\frac{\sigma + j\omega\xi''}{j\omega\mu''}} \frac{\vec{k}'' \times \vec{E}''_o}{k''} \right] \times \vec{n} = 0 \quad (12)$$

The first and second boundary condition for the first case give nothing, since the E field is perpendicular to the page and hence \perp to \vec{n} . However, from the third boundary condition we have:

$$E_o + E'_o - E''_o = 0 \quad (13)$$

and the fourth boundary condition gives:

$$\sqrt{\frac{\xi_o}{\mu_o}} \frac{(\vec{k} \times \vec{E}_o) \times \vec{n}}{k} + \sqrt{\frac{\xi_o}{\mu_o}} \frac{(\vec{k}' \times \vec{E}'_o) \times \vec{n}}{k'} - \sqrt{\frac{\sigma + j\omega\xi''}{j\omega\mu''}} \frac{(\vec{k}'' \times \vec{E}''_o) \times \vec{n}}{k''} = 0 \quad (14)$$

By using the appropriate vector identity and substituting E''_o from equation (13) into equation (14), the ratio of the incident electric field, E'_o , to the reflected electric field E_o can be obtained:

$$\frac{E'_o}{E_o} = \frac{\left[\sqrt{\frac{\xi_o}{\mu_o}} \cos(i) - \sqrt{\frac{\sigma + j\omega\xi''}{j\omega\mu''}} \cos(r) \right]}{\left[\sqrt{\frac{\xi_o}{\mu_o}} \cos(i) + \sqrt{\frac{\sigma + j\omega\xi''}{j\omega\mu''}} \cos(r) \right]} \quad (15)$$

To obtain the reflectivity one only needs to multiply the numerator and denominator of this expression by their respective complex conjugates (reference 4). In this case the reflectivity of an electromagnetic wave striking the surface of a thermal control coating with its electric vector perpendicular to the surface normal is:

$$\rho_{\perp} = \frac{\frac{\xi}{\mu} \cos^2(i) - \sqrt{\frac{\xi}{\mu}} \sqrt{2} \sqrt{\frac{\sigma^2 + \omega\xi''^2}{\omega\mu''^2}} + \frac{\xi''}{\mu''} \cos(i) \cos(r) + \sqrt{\frac{\sigma^2 + \omega\xi''^2}{\omega\mu''^2}} \cos^2(r)}{\frac{\xi}{\mu} \cos^2(i) + \sqrt{2} \sqrt{\frac{\xi}{\mu}} \sqrt{\frac{\sigma^2 + \omega\xi''^2}{\omega\mu''^2}} + \frac{\xi''}{\mu''} \cos(i) \cos(r) + \sqrt{\frac{\sigma^2 + \omega\xi''^2}{\omega\mu''^2}} \cos^2(r)}$$

Now for the second case, where the magnetic field, \mathbf{H} , is pointing out of the page (i.e. $\mathbf{H} \perp$ to plane of incidence) the 3rd boundary condition gives:

$$-E_o \cos(i) + E'_o \cos(i) + E''_o \cos(r) = 0 \quad (16)$$

And the forth boundary condition gives:

$$\left[\sqrt{\frac{\xi_o}{\mu_o}} \frac{\vec{k} \times \vec{E}_o}{k} + \sqrt{\frac{\xi_o}{\mu_o}} \frac{\vec{k}' \times \vec{E}'_o}{k'} - \sqrt{\frac{\sigma + j\omega\xi''}{j\omega\mu''}} \frac{\vec{k}'' \times \vec{E}''_o}{k''} \right] \times \vec{n} = 0 \quad (17)$$

Again, using the appropriate vector identity and substituting for E''_o from equation (15) into equation (17), we get the ratio of the incident electric field, E'_o , to the reflected electric field E_o for the parallel case:

$$\frac{E_o}{E'_o} = \frac{-\sqrt{\frac{\xi_o}{\mu_o}} \cos(r) + \sqrt{\frac{\sigma + j\omega\xi''}{j\omega\mu''}} \cos(i)}{\sqrt{\frac{\xi_o}{\mu_o}} \cos(r) + \sqrt{\frac{\sigma + j\omega\xi''}{j\omega\mu''}} \cos(i)} \quad (18)$$

The reflectivity for an electromagnetic wave striking the surface of a thermal control coating with its electric vector parallel to the surface normal is then just the numerator and denominator of this expression multiplied by their respective complex conjugates:

$$\rho_{\parallel} = \frac{\sqrt{\frac{\sigma^2 + \omega\xi^{\prime\prime 2}}{\omega\mu^{\prime\prime 2}} \cos^2(i) - \sqrt{2} \sqrt{\frac{\xi}{\mu}} \sqrt{\frac{\sigma^2 + \omega\xi^{\prime\prime 2}}{\omega\mu^{\prime\prime 2}} + \frac{\xi^{\prime\prime}}{\mu}} \cos(i) \cos(r) + \frac{\xi}{\mu} \cos^2(r)}{\sqrt{\frac{\sigma^2 + \omega\xi^{\prime\prime 2}}{\omega\mu^{\prime\prime 2}} \cos^2(i) + \sqrt{2} \sqrt{\frac{\xi}{\mu}} \sqrt{\frac{\sigma^2 + \omega\xi^{\prime\prime 2}}{\omega\mu^{\prime\prime 2}} + \frac{\xi^{\prime\prime}}{\mu}} \cos(i) \cos(r) + \frac{\xi}{\mu} \cos^2(r)} \quad (19)$$

It is however, useful to cast the entire equation in terms of the angle of incident. This can be accomplished by noting that the phase factors must of necessity all be equal at the boundary $z=0$, therefore:

$$(\vec{k} \cdot \vec{x})_{z=0} = (\vec{k}' \cdot \vec{x})_{z=0} = (\vec{k}'' \cdot \vec{x})_{z=0} \quad (20)$$

Where upon inserting the values for k and k''

$$\sqrt{\frac{\xi}{\mu}} \sin(i) = \sqrt{\frac{\omega^2 \xi^{\prime\prime 2} + \sigma^2}{\omega^2 \mu^{\prime\prime 2}}} \sin(r) \quad (21)$$

This can be put in terms of $\cos(r)$ by solving for $\sin(r)$ and using a common trigonometric identity giving:

$$\cos(r) = \sqrt{1 - \frac{\frac{\xi}{\mu} \omega \mu^{\prime\prime}}{\sqrt{\omega^2 \xi^{\prime\prime 2} + \sigma^2}} \sin^2(i)} \quad (22)$$

Then the perpendicular and parallel components of reflectivity in terms of angle of incident become:

$$\rho_{\parallel} = \frac{\sqrt{\frac{\sigma^2 + \omega\xi^{\prime\prime 2}}{\omega\mu^{\prime\prime 2}} \cos^2(i) - \sqrt{2} \sqrt{\frac{\xi}{\mu}} \sqrt{\frac{\sigma^2 + \omega\xi^{\prime\prime 2}}{\omega\mu^{\prime\prime 2}} + \frac{\xi^{\prime\prime}}{\mu}} \cos(i) \sqrt{1 - \frac{\frac{\xi}{\mu} \omega \mu^{\prime\prime}}{\sqrt{\omega^2 \xi^{\prime\prime 2} + \sigma^2}} \sin^2(i)} + \frac{\xi}{\mu} \left[1 - \frac{\frac{\xi}{\mu} \omega \mu^{\prime\prime}}{\sqrt{\omega^2 \xi^{\prime\prime 2} + \sigma^2}} \sin^2(i) \right]}{\sqrt{\frac{\sigma^2 + \omega\xi^{\prime\prime 2}}{\omega\mu^{\prime\prime 2}} \cos^2(i) + \sqrt{2} \sqrt{\frac{\xi}{\mu}} \sqrt{\frac{\sigma^2 + \omega\xi^{\prime\prime 2}}{\omega\mu^{\prime\prime 2}} + \frac{\xi^{\prime\prime}}{\mu}} \cos(i) \sqrt{1 - \frac{\frac{\xi}{\mu} \omega \mu^{\prime\prime}}{\sqrt{\omega^2 \xi^{\prime\prime 2} + \sigma^2}} \sin^2(i)} + \frac{\xi}{\mu} \left[1 - \frac{\frac{\xi}{\mu} \omega \mu^{\prime\prime}}{\sqrt{\omega^2 \xi^{\prime\prime 2} + \sigma^2}} \sin^2(i) \right]} \quad (23)$$

and;

$$\rho_{\perp} = \frac{\frac{\xi}{\mu} \cos^2(i) - \sqrt{\frac{\xi}{\mu}} \sqrt{2} \sqrt{\frac{\sigma^2 + \omega\xi^{\prime\prime 2}}{\omega\mu^{\prime\prime 2}} + \frac{\xi^{\prime\prime}}{\mu}} \cos(i) \sqrt{1 - \frac{\frac{\xi}{\mu} \omega \mu^{\prime\prime}}{\sqrt{\omega^2 \xi^{\prime\prime 2} + \sigma^2}} \sin^2(i)} + \sqrt{\frac{\sigma^2 + \omega\xi^{\prime\prime 2}}{\omega\mu^{\prime\prime 2}}} \left[1 - \frac{\frac{\xi}{\mu} \omega \mu^{\prime\prime}}{\sqrt{\omega^2 \xi^{\prime\prime 2} + \sigma^2}} \sin^2(i) \right]}{\frac{\xi}{\mu} \cos^2(i) + \sqrt{2} \sqrt{\frac{\xi}{\mu}} \sqrt{\frac{\sigma^2 + \omega\xi^{\prime\prime 2}}{\omega\mu^{\prime\prime 2}} + \frac{\xi^{\prime\prime}}{\mu}} \cos(i) \sqrt{1 - \frac{\frac{\xi}{\mu} \omega \mu^{\prime\prime}}{\sqrt{\omega^2 \xi^{\prime\prime 2} + \sigma^2}} \sin^2(i)} + \sqrt{\frac{\sigma^2 + \omega\xi^{\prime\prime 2}}{\omega\mu^{\prime\prime 2}}} \left[1 - \frac{\frac{\xi}{\mu} \omega \mu^{\prime\prime}}{\sqrt{\omega^2 \xi^{\prime\prime 2} + \sigma^2}} \sin^2(i) \right]} \quad (24)$$

Then the total reflectivity as a function of the angle of incident and the fundamental properties of the coating is just the average of the parallel and perpendicular reflectance components:

$$\rho(\mu_o, \xi_o, \sigma, \mu', \xi', \beta) = \frac{\rho_{\parallel} + \rho_{\perp}}{2} \quad (25)$$

(Where β has been used here for angle of incident instead of i , for the sake of conformity)

The absorptance, reflectance and transmittance must of course sum to unity.

$$\alpha + \rho + t = 1 \quad (26)$$

If the material is opaque ($t=0$) and the absorptance is equal to the emittance (as is generally accepted) then the directional emissivity can be found by substituting the reflectance of the coating from (25):

$$\varepsilon'(\mu_o, \xi_o, \sigma, \mu', \xi', \beta) = 1 - \rho'(\mu_o, \xi_o, \sigma, \mu', \xi', \beta) \quad (27)$$

The emittance as a function of angle of incidence can now be determined for any given set of permittivity, conductivity, permeability and wavelength. The index of refraction for the material can also be found using these same values in the equation below:

$$\bar{n} = \sqrt{\frac{\mu\xi}{2} \left[1 + \sqrt{1 + \left(\frac{\sigma}{\omega\xi} \right)^2} \right]} + i \sqrt{\frac{\mu\xi}{2} \left[-1 + \sqrt{1 + \left(\frac{\sigma}{\omega\xi} \right)^2} \right]} \quad (28)$$

Choosing values of conductivity, permeability and permittivity for a dielectric material coating that gives a real index of refraction equal to approximately 1.5, a directional emissivity graph can be plotted for this hypothetical, but somewhat typical, dielectric coating:

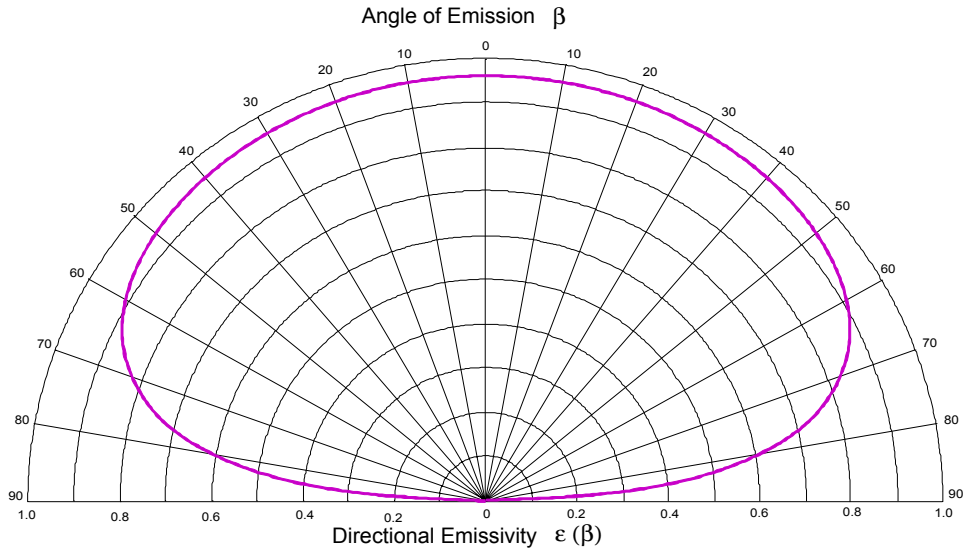


Figure 1.1-2. Directional emissivity curve for a dielectric with an index of refraction of $n=1.5$

This differs from a Lambertian radiator, which would have no change in emissivity as a function of angle. In real materials the emissivity drops considerably at large angles of β as can be seen in the above graph.

When a material is conductive however, such as a metal, the directional emissivity curve has a somewhat different shape than the dielectric case:

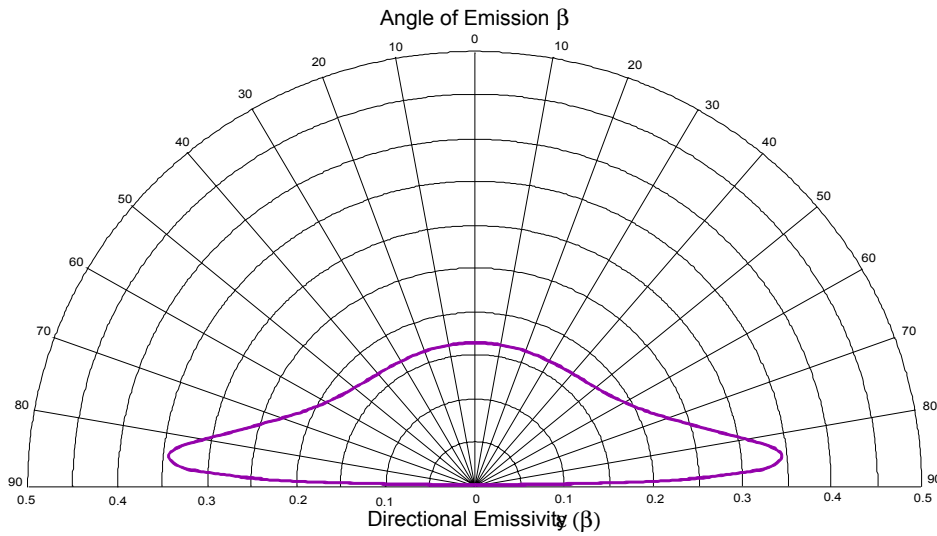


Figure 1.1-3. Directional emissivity curve for a conductor with an index of refraction of $n=5.7+i9.7$

This graph shows that the peak emissivity, rather than occurring at near normal to the material, as in the dielectric case, now occurs at very large angles but still drops to zero as the angle β approaches 90 degrees.

It is often easier to measure the normal emittance of a material than it is to measure the total hemispherical emittance. It is therefore useful to calculate the ratio of these two quantities so that a reasonable conversion can be made when only the normal emittance is unknown. To obtain the total hemispherical emittance, the emittance as a function of angle must be integrated over the entire hemisphere.

$$\epsilon_H = \frac{1}{\pi} \int_0^{2\pi} \int_0^{\pi/2} \epsilon(\beta, \theta) \cos \beta d\omega \quad (29)$$

In this equation, the reference to permittivity, permeability and conductivity have been dropped for simplicity. The angle θ is simply the azimuth angle and it is assumed that the coating's emittance is constant in azimuth.

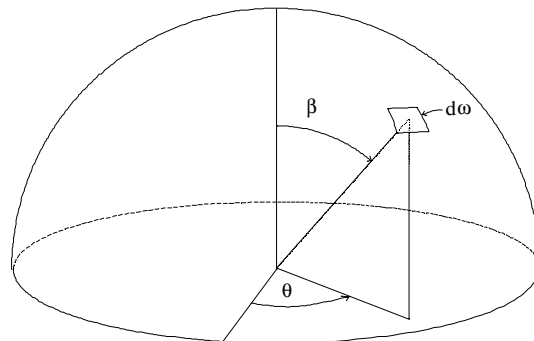


Figure 1.1-4. Hemispherical emittance coordinate system

The ratio of hemispherical emittance to normal emittance is then just:

$$\frac{\epsilon_H}{\epsilon_n} = \frac{\frac{1}{\pi} \int_0^{2\pi} \epsilon(\beta, \theta,) \cos \beta d\omega}{\epsilon(\beta, 0,)} \quad (30)$$

When the values of normal emittance range from 0.4 to 1.0, as would be the case for a dielectric, the following curve results:

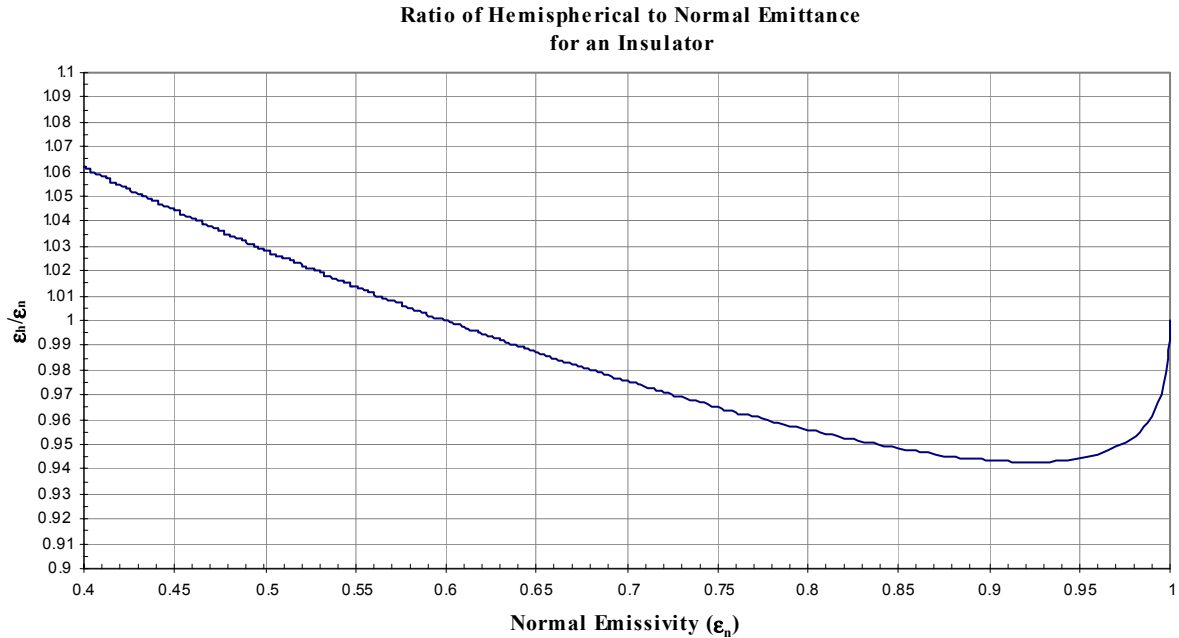


Figure 1.1-5

The shape of this curve is caused by the fact that the emittance at large angles of β changes disproportional relative to the emittance at $\beta = 0$ as the normal emittance decreases from 1 to 0.4. When the index of refraction is equal to 1, the emittance is Lambertian and has the value of 1 at all angles of β . This makes the hemispherical emittance equal to 1 also and consequently the ratio is equal to one. When the index of refraction is a little greater than one, the normal emittance decreases accordingly, but the emittance at large angles of β decreases much more rapidly and very quickly assumes a dependency similar to Figure 1.1-2. Consequently, when integrated to yield the hemispherical emittance, the integrated value is lower than the emittance at $\beta = 0$ and hence the ratio is less than one. When the index of refraction becomes larger, the emittance at larger angle of β decreases less quickly than the emittance at $\beta = 0$ and the emittance curve starts to “morph” into a curve similar to Figure 1.1-3. The relative increase in emittance at larger angles of β causes the integrated emittance to be greater than the emittance at $\beta = 0$ and consequently the ratio is greater than 1 for values of normal emittance less than 0.6.

The case for conductive materials is somewhat different. The ratio of hemispherical to normal emittance is:

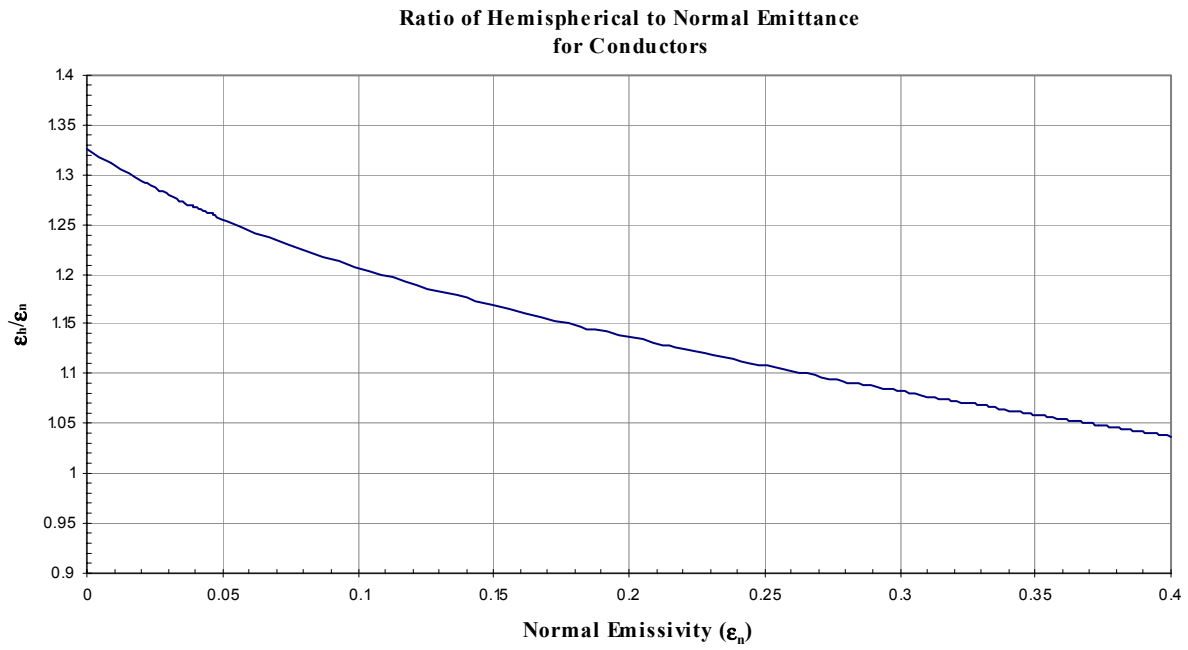


Figure 1.1-6

In the case of metals, the relative increase in emittance at large angles of β simply continues as the normal emittance approaches zero making the ratio rise continuously to $\epsilon_n = 0$.

II. Factors that Affect Emittance

2.1 Change in Emittance with Temperature

The total hemispherical emittance of a thermal control coating often changes with temperature. This is not primarily the result of the intrinsic reflectivity of the coating changing with temperature, but rather it is the intrinsic ability of the coating to emit or absorb energy at different wavelengths that is responsible for the change in coating emittance as the wavelength of peak emission moves to a new wavelength with a change in temperature.

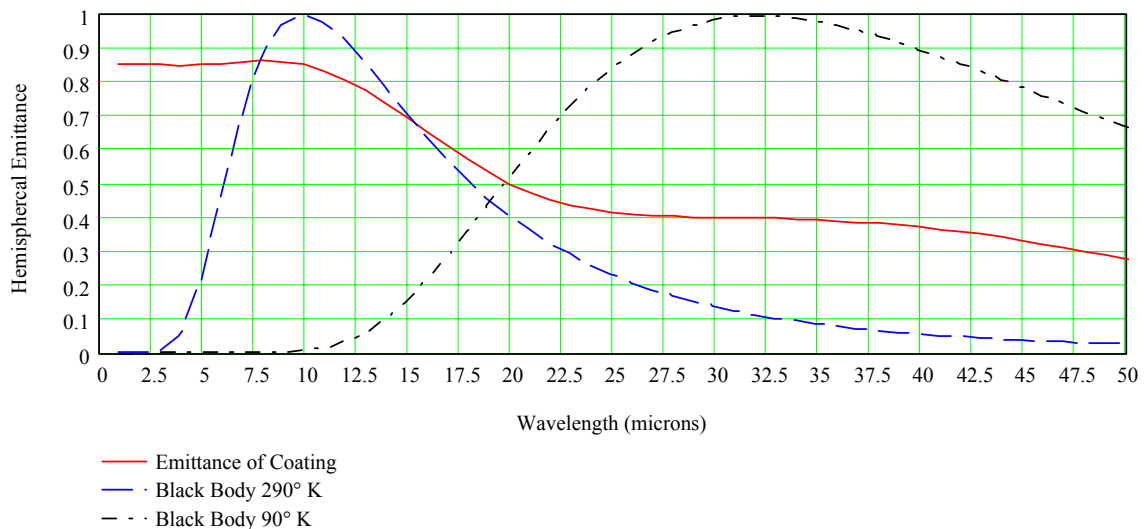


Figure 2.2 Emittance of a Hypothetical Coating and a Black Body

For example, the graph above shows the emittance of a hypothetical coating as a function of wavelength. At a temperature of 290° K the peak of the normalized black body curve is approximately 10 microns. Since the coating has a relatively high emittance in this region, the overall integrated emittance will be correspondingly high. At a temperature of 90° K however, the normalized black body curve peaks at approximately 32 microns and is also much broader. The emittance of the coating is not nearly as high at these wavelengths as it is at 10 microns and therefore the overall integrated emittance will be less at 90° K than at 290° K.

The change in overall reflectivity and consequently total hemispherical emittance can be due to a change in reflectance of the coating with wavelength or it can be due to the fact that the coating is simply thin and therefore possibly transparent at longer wavelengths revealing the underlying substrate. The net reflectivity in this case, is a combination of the reflectivity of the partially transparent coating at long wavelengths and the reflectivity of the underlying substrate (usually aluminum). This would make the effective reflectance of the coating on the substrate greater at long wavelengths and consequently the emittance would decrease with temperature as the peak point of the emission curve moved to longer wavelengths.

If the total reflectivity as a function of wavelength and angle of incidence is known, then the total hemispherical emittance as a function of temperature can easily be found by integrating the total hemispherical reflectance over all angles of azimuth, polar angle and wavelength, weighted to the black body function

$$\varepsilon(T) = \frac{\int_0^{\infty} \left[1 - \int_0^{\frac{\pi}{2}} \int_0^{2\pi} \rho(\theta, \phi, \lambda) \sin(\theta) \cos(\theta) d\theta d\phi \right] G(\lambda, T) d\lambda}{\int_0^{\infty} G(\lambda, T) d\lambda} \quad (31)$$

Where $\rho(\theta, \phi, \lambda)$ is the total reflectivity of the coating as a function of polar angle θ , azimuth angle ϕ , and wavelength λ and $G(\lambda, T)$ is the black body curve as a function of wavelength λ at a given temperature T .

In practice, it is difficult to obtain the reflectance for any given coating over a wide enough wavelength range and at angles of incidence greater than 20 degrees to calculate the total hemispherical emittance as a function of temperature at cryogenic temperatures. It is however, sometimes possible to obtain the reflectance at near normal angles of incidence from 1 to 200 microns. The emittance as a function of temperature can then be calculated if one assumes the coating to be Lambertian (i.e. perfectly diffuse). This assumption can lead to non-trivial errors in the calculated emittance since most coatings may not be Lambertian, especially at longer wavelengths. The inherent error in the reflectance measurement at longer wavelengths is also a cause for increased error in the calculation. The result is an emittance temperature curve with nontrivial error bars.

2.2 The Role of Thickness and Thermal Conductivity of Coatings

Sensors typically affixed to a metallic substrate typically measure spacecraft temperatures. The emittance of the coating at that temperature is then used to calculate heat flow into and out of the coating. The assumption is always that the outer surface of the coating is at the same temperature as the substrate as measured by the sensors.

Background = 2.7°K

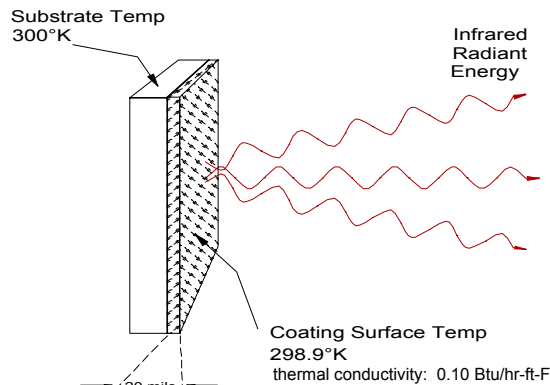


Figure 2.3 Effect of Coating Thermal Conductivity on Effective Emittance of a Coating

When a thermal control coating is used which is very thick and has a very low thermal conductivity, the surface temperature of the coating can be slightly lower or higher than the substrate temperature depending on whether

it has a view of the sun. The effect of this temperature difference between the substrate and surface of the coating is to raise or lower the effective emittance of the coating with respect to the substrate. The effect is generally small and of little consequence. For a coating like Kapton or Teflon, which both have a very low thermal conductivity, the change in effective emittance at 300°K for a 20mil thick coating would be a little more than 0.01, with a corresponding change in temperature of approximately 1°K. If the coating is even thicker the effect will be greater and will increase linearly with coating thickness. When the emittance is measured by a calorimetric technique, the calculated emittance is really an effective emittance with the thermal conductivity of the coating and the associated temperature difference taken into account. Temperatures calculated based on this method will give accurate results, provided that the thickness of the coating on the spacecraft is the same as the calorimetric test case. If instead, the emittance is calculated based on the surface spectral reflectance, then the calculated temperature for very thick coatings may be slightly different than predicted.

2.3 Non-Grey Effects

When the total hemispherical emittance is calculated based on the total hemispherical wavelength dependent reflectance, the result is a single number that does not contain any information about how the infrared energy is emitted or absorbed as a function of wavelength. It is certainly possible for two different coatings to have the same total hemispherical emittance and absorptance at a given temperature, but radiate the infrared energy in different portions of the infrared spectrum. For example, suppose coating A & B have the following total hemispherical reflectance curves over the wavelength range 1 – 40 microns:

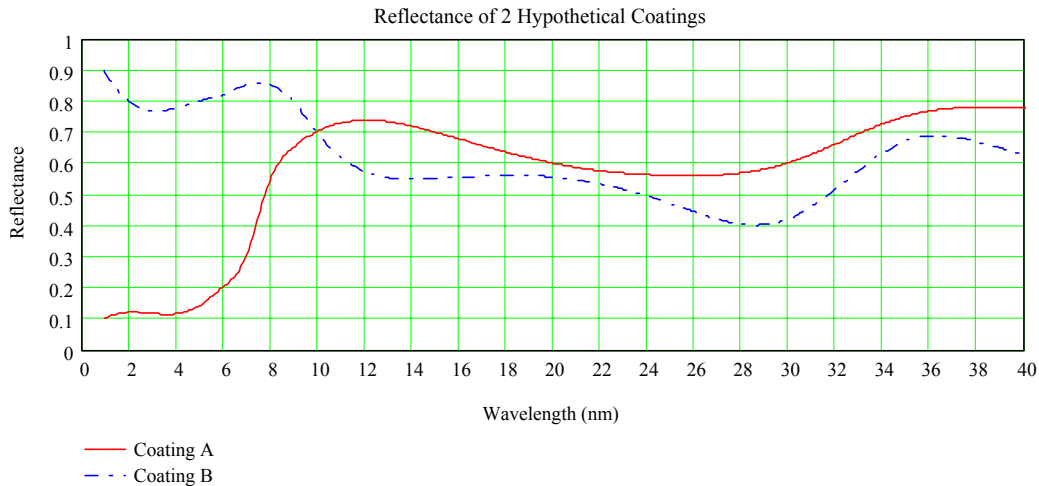


Figure 2.4 Reflectance of two hypothetical coatings

The total hemispherical emittance & absorptance at 290°K can then be found by:

$$\epsilon(T) = \frac{\int_{\lambda_1}^{\lambda_2} [1 - R(\lambda)] G(\lambda, T) d\lambda}{\int_{\lambda_1}^{\lambda_2} G(\lambda, T) d\lambda} \quad (32)$$

where $G(\lambda, T)$ is the black body function:
$$G(\lambda, T) = \frac{8\pi hc}{\lambda^5 e^{\frac{hc}{\lambda kT}} - 1} \quad (33)$$

$R(\lambda)$ is the total hemispherical reflectance function of the coating and

$T=290^{\circ}\text{K}$	$h=6.626 \times 10^{-34} \text{J} \cdot \text{s}$	$\lambda_1=1 \mu\text{m}$
$k=1.381 \times 10^{-23} \text{J} \cdot \text{K}^{-1}$	$c=2.998 \times 10^8 \text{m/s}$	$\lambda_2=200 \mu\text{m}$

The result is that both coatings have an emittance at 290°K of 0.37. Their infrared emission curves (found by multiplying the black body curve at 290°K , $G(\lambda, T)$, by 1 minus the reflectance curve) are however very different. As can be seen in Figure 2.5 below, Coating A has a peak infrared emission at 7 microns while Coating B has a peak infrared emission at 12 microns, even though both coatings have the same emittance/absorptance at 290°K .

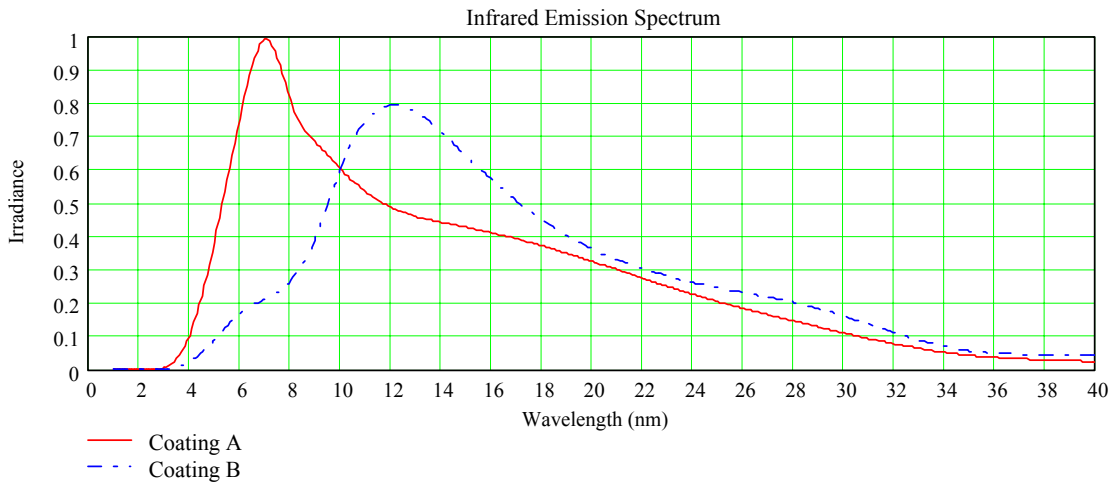


Figure 2.5 Infrared Emission Spectrum of Hypothetical Coatings A & B

This can create a problem when attempting to calculate the equilibrium temperature of objects if the calculation is based simply on the integrated total hemispherical emittance without regard to how the infrared energy is emitted or absorbed as a function of wavelength. It is possible for a coating to radiate heat to a second coating in an area of the infrared spectrum for which the receiving coating has little inherent ability to absorb the infrared energy while the integrated emittance/absorptance value would give no hint of this problem. Most thermal calculations are however, based on the total integrated emittance for the given coatings involved and as such may not be as accurate as one would like under certain conditions. The a priori assumption for most thermal calculations is that the coatings involved are gray, which is to say that their reflectivity's and hence their emittance's do not vary with wavelength. If the coatings are grey or at least reasonably so, there is usually not a problem, however when coatings are non-grey, problems can develop. For example, suppose two coatings, C & D, have the following reflectance curves throughout the 1-200 micron portion of the infrared spectrum:

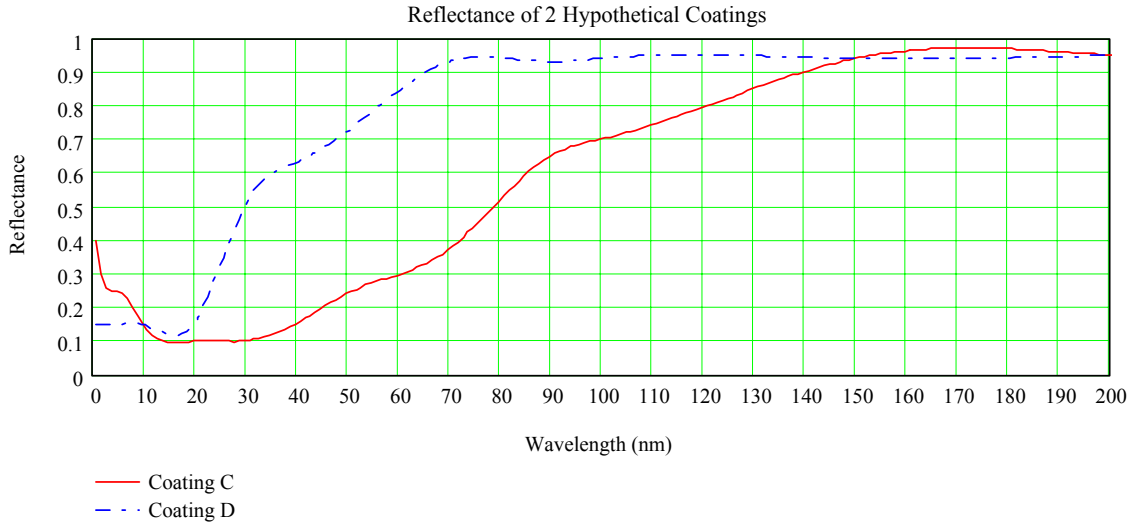


Figure 2.6 Reflectance of Hypothetical Coatings C & D

The total hemispherical emittance as a function of temperature for each coating can be found by using equation 32. The result shows how the emittance varies for each coating which are not too dissimilar from many coatings in use today.

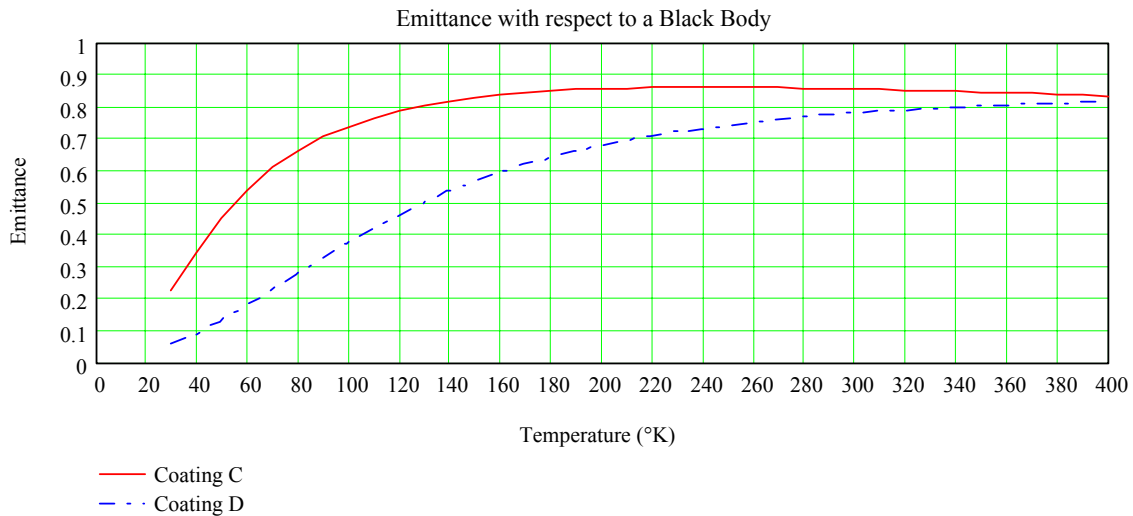


Figure 2.7 Hemispherical Emittance of Coating C & D

If the infrared emission spectrum at 50°K is calculated by multiplying the black body curve, $G(\lambda, 50^\circ\text{K})$, by 1 minus the reflectance curve the following energy emission curves result. The peak infrared emission and hence absorptance for Coating C occurs at about 54 microns, while the peak emission and absorptance for Coating D occurs at about 46 microns. This implies that the coatings are non-grey and an error can occur if this is not taken into account in the equilibrium temperature calculation.

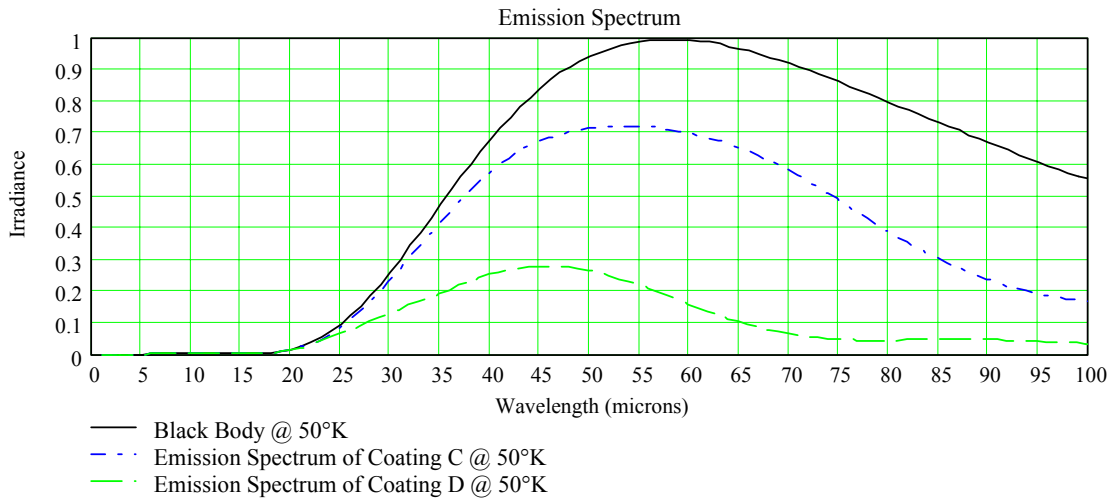


Figure 2.8 Emission Spectrum of Coating C & D

To illustrate the point, suppose Coating C has its temperature fixed at 50°K and radiates to Coating D, which is placed 0.8 meters away, and Coating C and is allowed to come to equilibrium. For simplicity it is assumed that no heat is emitted from the edges or the backside of Coating D, that the area is 1m², and the surrounding background temperature is zero.

Background = 0.0°K

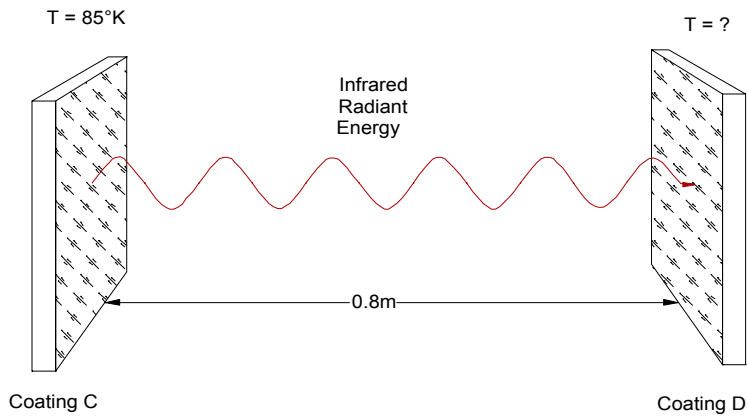


Figure 2.9 Thermal Radiation from Coating C to D

The equilibrium temperature for this test case can be found by the following equation, which accounts for how each coating radiates and absorbs energy as a function of wavelength and also for multiple reflections.

$$T = \left[\frac{\int_{1 \times 10^6}^{2 \times 10^3} \frac{[1-R_d(\lambda)][1-R_c(\lambda)] \cdot F_{12} \cdot G(\lambda, T_c)}{1-R_c(\lambda) \cdot R_d(\lambda) \cdot F_{12} \cdot F_{21}} d\lambda + \int_{1 \times 10^6}^{2 \times 10^3} \frac{[1-R_d^2(\lambda)][R_c(\lambda)] \cdot F_{12} \cdot F_{21} \cdot G(\lambda, T_d)}{1-R_c(\lambda) \cdot R_d(\lambda) \cdot F_{12} \cdot F_{21}} d\lambda}{\varepsilon_d(T_d) \sigma} \right]^{1/4} \quad (34)$$

Where F is the angle factor (also known as configuration factor) for two parallel plates, taken from Jacob (reference 5):

$$F_{12} = \frac{1}{\pi} \left[\frac{1}{B \cdot C} \ln \left(\frac{1+B^2+C^2+B^2C^2}{1+B^2+C^2} \right) - \frac{2}{B} a \tan(C) \right. \\ \left. + \frac{2}{C} \sqrt{1+C^2} \cdot a \tan \left(\frac{B}{\sqrt{1+C^2}} \right) - \frac{2}{C} \cdot a \tan(B) + \frac{2}{B} \sqrt{1+B^2} \cdot a \tan \left(\frac{C}{\sqrt{1+B^2}} \right) \right] \quad (35)$$

& $F_{12} = F_{21}$ (Where F_{12} is the angle factor of area 1 when viewed from area 2, or the fraction of energy emitted by area 1 that strikes area 2)

$B = b/a$ and b is the length, a is the separation distance and c is the width.

$C = c/a$

Alternately, if the integrated total hemispherical emittance values are used instead, the equilibrium temperature can be found by the following equation:

$$T_d^4 = \frac{\frac{\varepsilon_d(T_c) \cdot [F_{12} \cdot \varepsilon_c(T_c) \sigma T_c^4]}{1 - [1 - \varepsilon_c(T_c)(1 - \varepsilon_d(T_c) \cdot F_{12} \cdot F_{21})]}}{\left[\varepsilon_d(T_d) \cdot \sigma - \frac{\varepsilon_d(T_d) [(1 - \varepsilon_c(T_d)) \cdot \varepsilon_d(T_d) \cdot F_{12} \cdot F_{21} \cdot \sigma]}{1 - [1 - \varepsilon_c(T_d)(1 - \varepsilon_d(T_d) \cdot F_{12} \cdot F_{21})]} \right]} \quad (36)$$

Where:

T_c = Temperature at Coating C

T_d = Temperature at Coating D

$\varepsilon_c(T_c)$ = emittance of Coating C at the temperature of Coating C

$\varepsilon_c(T_d)$ = emittance of Coating C at the temperature of Coating D

$\varepsilon_d(T_c)$ = emittance of Coating D at the temperature of Coating C

$\varepsilon_d(T_d)$ = emittance of Coating D at the temperature of Coating D

Both of these methods can easily be solved via a simple procedure in MathCad or an equivalent mathematics program. The result is that the equilibrium temperature for Coating D when the non-grey effect is taken into account is 36.79°K where as the calculated equilibrium temperature is only 34.43°K when the total integrated hemispherical emittance values are used in the calculation.

The maximum error in the calculated equilibrium temperature occurs for a distance of 0.8m in this case and as can be seen in the graph below, the maximum error occurs when the radiator plate is at a temperature of about 50°K. For this particular case the calculated temperature would be too low by approximately 2.36°K. Other coatings combinations could produce greater or lesser errors depending on how the emittance of each coating varies as a function of wavelength.

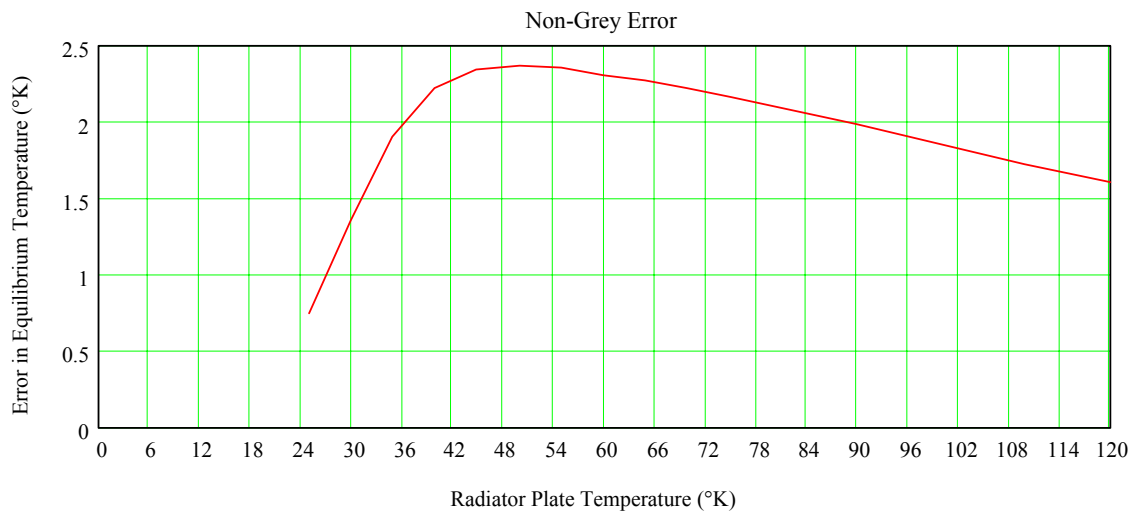


Figure 2.10 Non-Grey Equilibrium Temperature error for coating C

The only way to be sure if a non-grey error is going to present a problem is to measure the total hemispherical reflectance of each of the coatings in question and calculate the temperature based on the reflectance information of each coating over a sufficient wavelength range.

III. Measurement of Thermal Properties

3.1 Solar Absorptance

Electromagnetic theory can, at least in principal, be used to calculate the reflectance of a given coating provided the fundamental properties of permittivity, permeability and conductivity are known. In practice however those properties will rarely, if ever, be known for a coating of interest. It is therefore clear that for many purposes the thermal/optical properties of thermal control coatings must be measured in order to know their value to any precision. The calculation of the solar absorptance however, requires knowledge of the total hemispherical reflectance of the coating. This creates special problems in measurement, since the reflected light for many coatings is a composite of both diffuse and specular reflections as is seen in Figure 3.1-1. The incident energy at a given angle, θ , is separated in reflection into a specular component, r_s at angle θ and a diffuse component, the r_d 's in Figure 3.1-1, which can be at any angle of azimuth β and altitude ϕ .

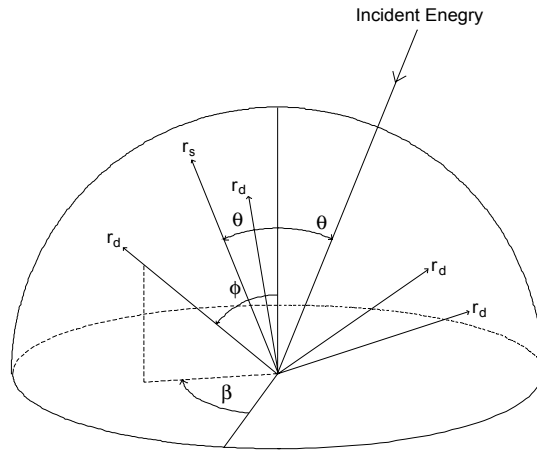


Figure 3.1-1. Directional Total Reflectivity

It is therefore necessary to measure the reflectance by means of an integrating sphere so that both the specular and diffuse components are accounted for or integrated over all angles, β as well as ϕ to obtain the total hemispherical reflectance for a given angle of incidence. For a given angle of incidence (θ) the absorptance is given by (reference 6):

$$\alpha(\theta) = 1 - \rho(\theta) - \tau(\theta) \quad (37)$$

Where ρ and τ are the total reflectance and transmittance respectively for a given angle of incidence θ . If the sample is opaque, as is often the case for a thermal control coating, the transmittance is zero and only the total hemispherical reflectance needs to be measured to calculate the total hemispherical absorptance for a given angle of incidence.

The total directional solar absorptance can be found from the above equation by weighting the total directional reflectance according to the solar spectrum and integrating over the solar spectrum:

$$\rho(\theta) = \frac{\int_0^{\infty} R(\lambda, \theta) S(\lambda) d\lambda}{\int_0^{\infty} S(\lambda) d\lambda} \quad (38)$$

Where $S(\lambda)$ is the solar extraterrestrial spectrum, and $R(\lambda, \theta)$ is the total directional hemispheric reflectance integrated over all angles of β and ϕ for a given angle of incidence θ as in Figure 3.1-1.

A method and procedure for the measurement of reflectance and calculation of solar absorptance is contained in ASTM E903. This standard gives the procedure for both center sample mounted integrating spheres and side sample mounted integrating spheres, see the Figure 3.1-2 below.

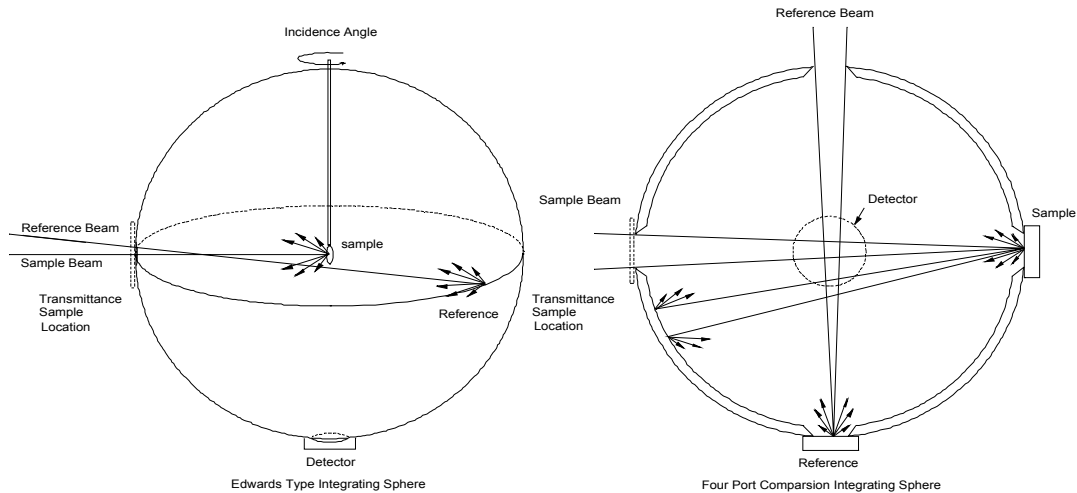


Figure 3.1-2. Two Types of Integrating Spheres

The main advantage of a center sample mounted integrating sphere is that the resulting measurement is absolute. The disadvantage is that a small sample, typically about 1 inch in diameter, is required. A side mounted integrating sphere has the advantage that any size sample to within reason can be accounted as long as the sample is flat, but the integrating sphere coating reflectance must be very nearly 100% and uniform over the measurement wavelength because the reflectance does not cancel out of the equations. The center mounted sample sphere has the additional advantage that it will continue to give accurate results even if the sphere coating is degraded, as long as the degradation/contamination is uniform over the entire surface of the sphere. With a side mounted sphere one must always be on guard against sphere degradation/contamination, as measurement errors will result.

It is also sometimes useful to know the reflectance of a sample as a function of angle of incidence. The center sample mounted integrating sphere can perform this type of measurement while the side mounted integrating sphere is limited to a near normal angle of incidence. The center-mounted sphere has the advantage that the reflectivity of the sphere coating cancels out of the equations leaving the absolute reflectance of the sample. It also has the advantage that the total hemispherical reflectance can be measured as a function of angle of incidence. The total transmittance of samples can also be measured with the integrating sphere as shown in Figure 3.1-2. This measurement includes not only the direct transmittance but also the scatter transmittance as well and can be used in the calculation of the solar absorptance of transparent films.

If it were possible to measure the total hemispheric emittance from zero to infinity then the only error would be the result of the inaccuracy of the reflectance measurement and the error in the solar spectrum data. ASTM E903 states that the typical uncertainty in the calculation of the solar absorptance from the standard solar spectrum and the measured reflectance gives practical error of $\pm 2\%$. This however is for reflectance measurements made over the entire wavelength range. In practice however, the integration of the above equation can only be carried out over the wavelength range of the reflectance measurement instrument, which is typically from 250nm to 2800nm. The ASTM E490 indicates that the energy at air mass zero over that wavelength range is only 97.1% of the total solar spectrum, with most of the residual energy being at the infrared portion of the spectrum at wavelengths greater than 2800nm. Therefore, in addition to the inherent

±2% error in the calculated solar absorptance as suggested by ASTM E903 there is also a potential error of 2.9% due to the infrared solar energy at wavelengths out of the range of the reflectance instrumentation. So the best solar absorptance that can be calculated is (reference 7):

$$\alpha(\theta) = 1 - \frac{\int_{250}^{2800} R(\lambda, \theta) S(\lambda) d\lambda}{\int_{250}^{2800} S(\lambda) d\lambda} \quad (39)$$

Fortunately, the calculated solar absorptance of many spacecraft thermal control coatings would not be greatly altered if the reflectance beyond 2800nm were actually measured.

Reflectance does vary as a function of angle of incidence and this can have an effect on the calculated solar absorptance, but the effect is generally small. The chart below gives the change in calculated solar absorptance as a function of angle of incidence for some common thermal control coatings. Solar absorptances are typically measured at a near normal angle of incidence, typically 10 – 20 degrees, and unless otherwise stated it should be assumed that the stated solar absorptance value was measured at a near normal angle of incidence.

Angle of Incidence	Solar Absorptance			
	Z306	OSR	Kapton 5mil	A276
10	-	0.050	-	-
20	0.952	-	0.43	0.267
30	0.952	-	-	-
40	0.946	-	0.441	0.261
45	-	0.049	-	-
50	0.941	-	-	-
60	0.93	-	0.432	0.250
70	0.903	0.034	-	-
80	0.842	-	-	-

Figure 3.1-3. Solar Absorptance as a Function of Angle of Incidence

The coating thickness can also affect the solar absorptance, particularly white paints. This is primarily due to the fact that most thermal control coatings are rather thin, typically just a few mils thick and hence tend to be semi-transparent when applied thinner than recommended. The chart below shows how solar absorptance can vary for a white silicone coating as a function of coating thickness.

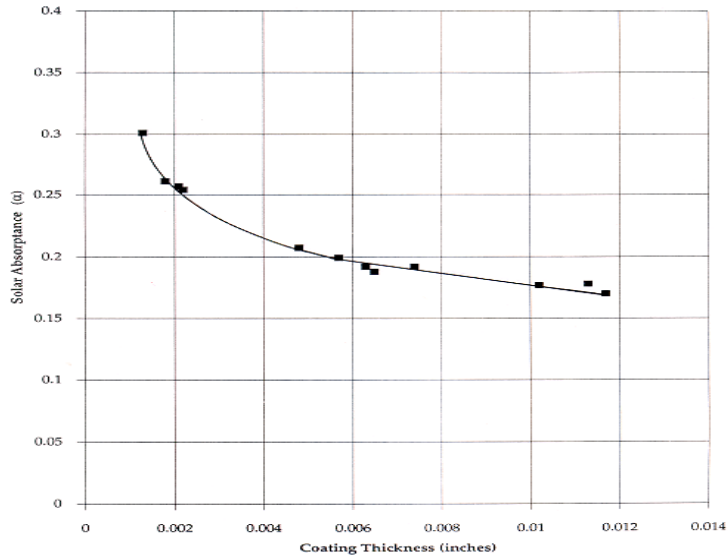


Figure 3.1-4 Solar Absorptance of a White Silicone Paint as a Function of Thickness

From the solar absorptance equation it is clear that the calculated absorptance depends on the solar spectrum. This is different from the terrestrial spectrum due to the absorption of the atmosphere. The graph below shows the difference in an air mass 0 (spectrum of the sun at 1AU with no atmospheric attenuation) and an air mass 1.5 solar spectrum. (spectrum of the sun with atmospheric attenuation as would be observed when the sun is at an elevation of 48.81° above the horizon with the surface normal to the sun), (reference 8).

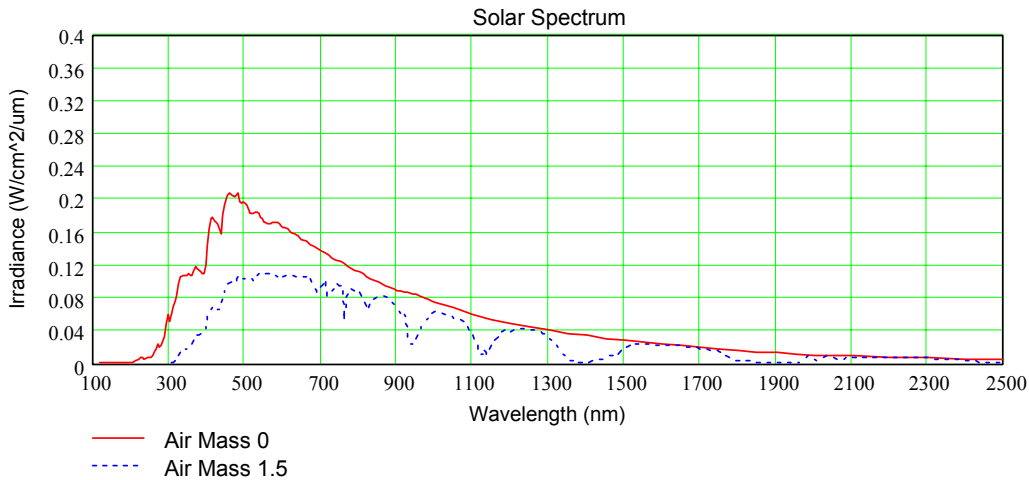


Figure 3.1-5. Comparison of Solar Spectrum (AM0) and Air Mass 1.5 Spectrum

It should be noted that if one were orbiting a different star system, the calculated absorptance for a particular coating would be different. When testing in a vacuum chamber, often a lamp is used to simulate the solar spectrum. For these cases, the spectrum of the simulated solar beam is different than the actual sun and hence the absorptance of some coatings may be different under these circumstances than for an air mass zero solar absorptance. The difference in spectrum for a tungsten lamp and unfiltered Xenon lamp can be seen in Figure 3.1-6 below:

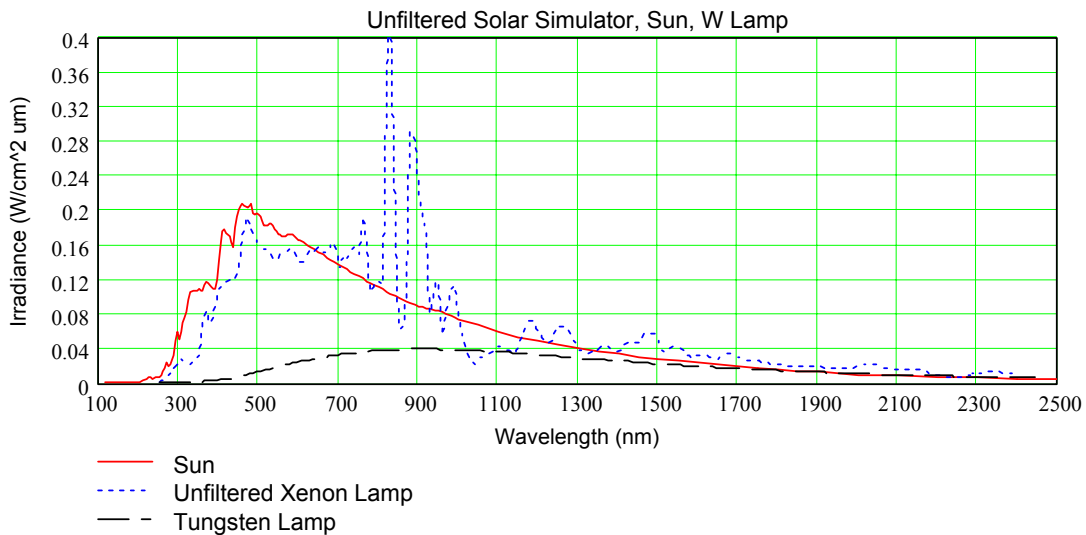


Figure 3.1-6. Comparison of Solar, Unfiltered Xenon Lamp and Tungsten Lamp Spectrum

The difference in spectrum can make a substantial difference in the absorbed energy. The table below gives the calculated solar absorptance for several common thermal control coatings and compares the results with the absorptance calculated for the solar spectrum, an unfiltered Xenon lamp and a tungsten lamp.

Coating	Absorptance		
	Solar Absorptance	Unfiltered Xenon Lamp Absorptance	Tungsten Lamp Absorptance
Kapton 3mil	0.414	0.344	0.186
Kapton 1mil	0.356	0.278	0.132
Gold Plated Aluminum	0.191	0.132	0.046
Aeroglaze A276	0.263	0.237	0.253
Vapor Deposited Aluminum	0.076	0.078	0.059
S13GPLO	0.185	0.149	0.143
Z306	0.96	0.96	0.96
Z93P	0.122	0.087	0.083
Silver Teflon (10mil)	0.089	0.06	0.031
OSR	0.051	0.04	0.031

Figure 3.1-7. Calculated Absorptance with Respect to Three Different Spectrums for some typical Thermal Control Coatings

3.2 Measurement of Emittance

The accurate determination of spacecraft temperatures requires a good knowledge of the hemispherical emittance of the spacecraft coatings involved. There are several methods for determining the emittance of thermal control coatings, by infrared reflectometry, calculation of emittance based on infrared reflectance measurements, by a calorimetric technique for determining the hemispherical emittance as a function of temperature and by a thermal balance method to determining the total hemispherical emittance. Each method has its advantages and potential problems as are discussed below.

3.2.1 Infrared Reflectometry

The simplest method of determining emittance is with a portable infrared reflectometer such as the DB100 or the AzTek Temp 2000. The Gier-Dunkel DB100 has been the main stay in the aerospace industry for this type of measurement for more than 30 years. The DB100 however, is no longer manufactured or serviced. There are however still many DB100's in operation around the country including two at the GSFC. The basic operation of the DB100 consists of two semi-cylindrical rotating cavities. One of the cavities is heated and the other is held at room temperature. As the cavities rotate the sample is alternately irradiated by the infrared energy from the hot and cold cavities. The reflected fluctuating radiant energy from the sample is focused onto an infrared Potassium Bromide (KBr) detector. The resulting electrical signal is then amplified and converted into an infrared reflectance. The effective measurement range of the DB100 is from 4-40 microns and consequently covers approximately 94 % of the energy emitted by a black body at room temperature. The 6% of the spectrum at room temperature not measured by the DB100 is mostly at wavelengths longer than 40 microns.



Figure 3.2-1. Gier-Dunkel DB100

The advantage to the DB100 is that the measurement is fast (just a few seconds) and therefore cheap to perform. The primary disadvantage to using a device like the DB100 is that it gives only a total measurement over the given wavelength range and will be accurate over that wavelength range provided two important caveats are met. First, for this measurement to be valid the reflectance of the sample must be grey, which is to say that the reflectance does not vary over the wavelength range. Second, the reflectance must be Lambertian (reflectance does not vary with angle of incidence). If the reflectivity of the sample varies with wavelength in the infrared, then the sensitivity of the detector as a function of wavelength will play a role in the measurement (the graph below shows typical sensitivity curves for various infrared detectors) (reference 9) and the resulting measured infrared reflectance may not be accurate.

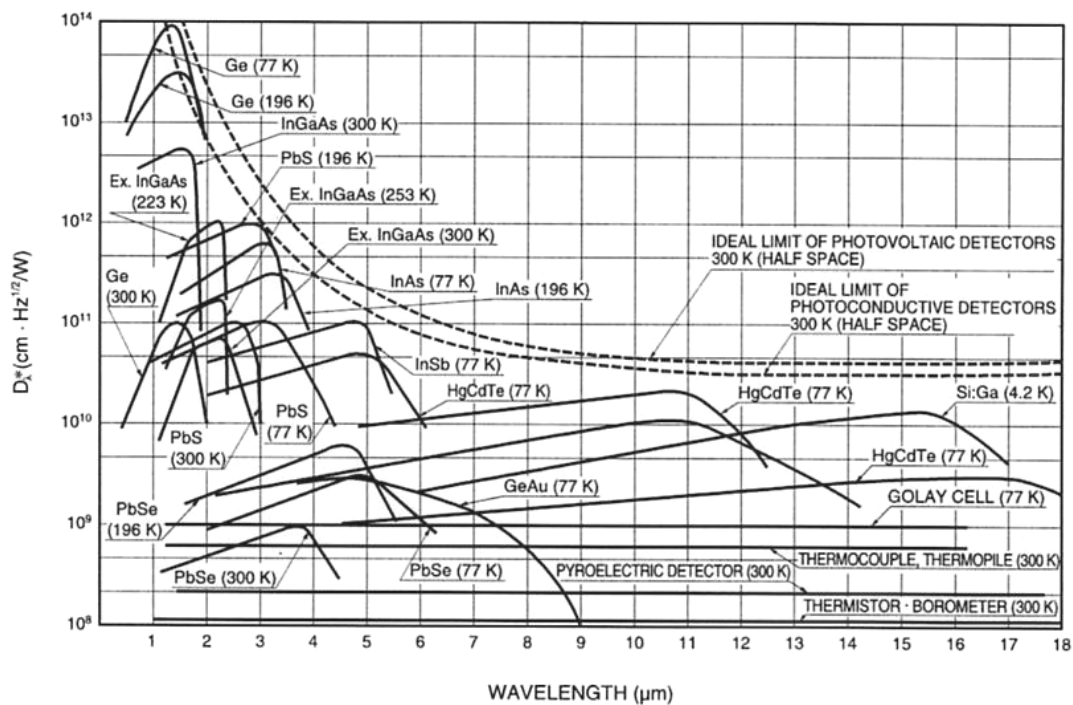


Figure 3.2-2. Spectral Response Characteristics of Various Infrared Detectors (reference 9)

The KBr detector is one that is commonly used in devices like the DB-100 and as can be seen the sensitivity peaks just prior to 400 cm^{-1} and has a near linear response in the NIR and the MIR range.

If the reflectance of the sample is non-Lambertian, then the fact that the DB100 measures the reflectance normally and not as a function of angle of incidence will cause the measured infrared reflectance value to be inaccurate. It should be pointed out however, that assuming the sample to be Lambertian and gray over the 4-40 wavelength range for many samples is not a bad approximation.

The AzTek Temp 2000 has a measurement range of 3-35 microns and can measure normal and hemispherical emittance, both being measured from a normal angle of incidence. The caveats that govern the use of the DB100 also govern the Temp 2000, namely that the sample measured must be gray and Lambertian, any deviation from these requirements will result in a decrease in the accuracy of the measurement.



Figure 3.2-2. AzTek TEMP-2000

3.2.2 Emittance Calculated from Infrared Reflectance Measurements

Another method for determining the hemispherical emittance of thermal control coatings is to calculate it directly from the reflectance vs wavelength curve of the coating. To do this, the total hemispherical reflectance as a function of wavelength and angle of incidence of the sample must be known over a substantial portion of the wavelength range of emission at the planned operating temperature of the coating. If one has access to this information for a particular sample, then the total hemispherical emittance can be calculated from the reflectance curve by the following set of equations:

$$\varepsilon_t(\theta, \phi, \lambda) = 1 - \frac{\int_0^{\pi/2} \int_0^{\pi/2} \int_0^{\infty} \rho(\theta, \phi, \lambda) \frac{8\pi hc}{\lambda^5 (e^{hc/\lambda T_k} - 1)} d\lambda d\phi d\theta}{\int_0^{\infty} \frac{8\pi hc}{\lambda^5 (e^{hc/\lambda T_k} - 1)} d\lambda} \quad (40)$$

$$\varepsilon_h = 2 \int_0^{\pi/2} \varepsilon_t(\theta, \phi, \lambda) \sin(\theta) \cos(\theta) d\theta \quad (41)$$

Where ρ is the reflectance as a function of angle of incidence (θ), circumferential angle (ϕ), and wavelength (γ). The constants, h , c , k and T are Planck's constant, the speed of light, the Stefan-Boltzman constant and the temperature in °K. If a room temperature emittance is calculated and 95% coverage of the spectrum is desired, then it is necessary to have or have measured the reflectance of the desired sample from 4 to 40 microns.

If it is known or assumed as a good approximation that the reflectance is invariant in ϕ and θ , (that is to say Lambertian) then the above equation simplifies to:

$$\varepsilon_h = 2 \int_0^{\pi/2} \left\{ 1 - \frac{\int_0^{\infty} \rho(\lambda) \frac{8\pi hc}{\lambda^5 (e^{hc/\lambda T_k} - 1)} d\lambda}{\int_0^{\infty} \frac{8\pi hc}{\lambda^5 (e^{hc/\lambda T_k} - 1)} d\lambda} \right\} \sin(\theta) \cos(\theta) d\theta \quad (42)$$

Unfortunately, the reflectance data needed to use with this equation is seldom known over a sufficiently wide wavelength range or as a function of angle of incidence to make this method useful over a temperature range other than room temperature. For instance, to cover 95% of the emitted energy at 290 °K the reflectance would have to be measured from 1 to 50 microns. At 80°K it would be necessary to measure the reflectance to 150 microns and for a sample at 30° K it would be necessary to measure the reflectance to approximately 400 microns. Using reflectance data only out to 50 microns for a sample at 80° K would result in only 48% of the energy spectrum covered by the calculation!

It must also be remembered that this method deals with the surface reflectivity of the coating and will not give the apparent emittance as "seen" from the substrate, which is what is often needed by thermal engineers. If the thickness of the sample is substantial and/or the thermal conductivity of the coating is low,

then the surface temperature of the coating can be substantially different from the substrate and hence the coating will appear to have a lower emittance with respect to the substrate than has been calculated by the above method.

3.2.3 Calorimetric Technique for Determining Hemispherical Emittance

The transient calorimetric technique is an accurate but also the most time consuming method of determining total hemispherical emittance as a function of temperature. The technique relies on accurately timing the cool down rate of a block of known specific heat capacity (usually pure aluminum) coated with the material (usually a paint or thin film). Then from knowledge of the specific heat, total area of the sample and cool down rate, the emittance can be calculated. In practice, parasitic heat losses can affect the accuracy of the measurement at cryogenic temperatures and therefore must be minimized or eliminated from the test and taken into account during the calculation. The parasitic heat losses/inputs primarily arise from the heat lost due to the residual gas in the vacuum chamber, heat conducted through and emitted from the temperature sensor leads, heat from the sample being reflected back to the sample from the chamber walls, radiant heat from the outside striking the sample, or heat dissipated by the temperature sensor into the sample substrate.

In this test method it is assumed that the specific heat of the coating itself is small with respect to the aluminum substrate. If this is not true, then the specific heat as a function of temperature must be known for the coating in order for an accurate calculation of the emittance of the coating to be made.

The transient calorimetric technique typically consists of a pure Aluminum block (or ~~A1100 Aluminum~~ as a good substitute) coated with a typical spacecraft coating and suspended via the ~~manganin temperature sensor~~ leads in a black painted liquid helium shroud. During testing, the specimen is first heated to 340°K by solar simulator beam input through ~~Infrasil windows~~. This starting temperature will not only give values for emittance slightly above room temperature, which are sometimes desired, but also allow the room temperature value to be checked by a DB100 or similar such device. Then the input port is covered and the specimen allowed to cool by radiation to the liquid helium shroud in a vacuum of better than 10^{-6} torr. Under the conditions present in the chamber the heat-balance equation is given by:

$$\varepsilon(T)a\sigma T^4 - \varepsilon(T_s)a\sigma T_s^4 = -mC_p \frac{\Delta T}{\Delta t} - m_s C_{p_s} \frac{\Delta T}{\Delta t} - Q_{ll} - Q_{gas} - Q_{sd} \quad (43)$$

Where $\varepsilon(T)$, a , σ , T , T_s , m , C_p , $\Delta T/\Delta t$, m_s , C_{p_s} are the emittance of the sample at a given temperature, sample area, the Stefan-Boltzman constant, sample temperature, shroud temperature, sample mass, specific heat of aluminum, sample cooling rate, mass of the sample coating, specific heat of the sample coating respectively. If the total area of the sample is small with respect to the total area of the chamber, the heat emitted from the sample and subsequently reflected from the chamber wall back to the sample can be neglected. The Q_{sd} term represents the heat supplied to the aluminum block by the silicon diode temperature sensor. This amounts to a few micron watts and represents only a minor correction factor even at 40°K. Q_{ll} represents the heat loss due to conduction and radiation of heat down the manganin wires and Q_{gas} is the heat loss due to the conduction of heat by the residual gas in the chamber.

This method works well as long as the thermal mass of the coating is small with respect to the substrate used and as long as the specific heat of the substrate is known over the entire temperature range of interest to a high degree of accuracy. For this reason it is advantageous to use A1100 Aluminum since its specific heat as a function of temperature is well known. Also, the sample area must be small with respect to the area of the shroud in order to minimize the reflection of heat from the sample back to the sample. The pressure in the chamber must also be kept as low as possible to minimize the conduction of heat from the sample to the shroud wall by residual gasses in the chamber. The actual operating pressure of course depends on the temperature range of interest. For a lower temperature range of -150°C a pressure of 1×10^{-6}

torr is adequate, for lower temperature range an even lower pressure must be maintained to less than 4×10^{-8} torr.

The constraint of time is of course another factor when considering this approach. For a substrate mass of say 25grams, and a typical high emittance paint, the time required for the test can be several days. For a low emittance sample the test time can increase to several weeks!

The diagram below shows the basic schematic concept of the test method.

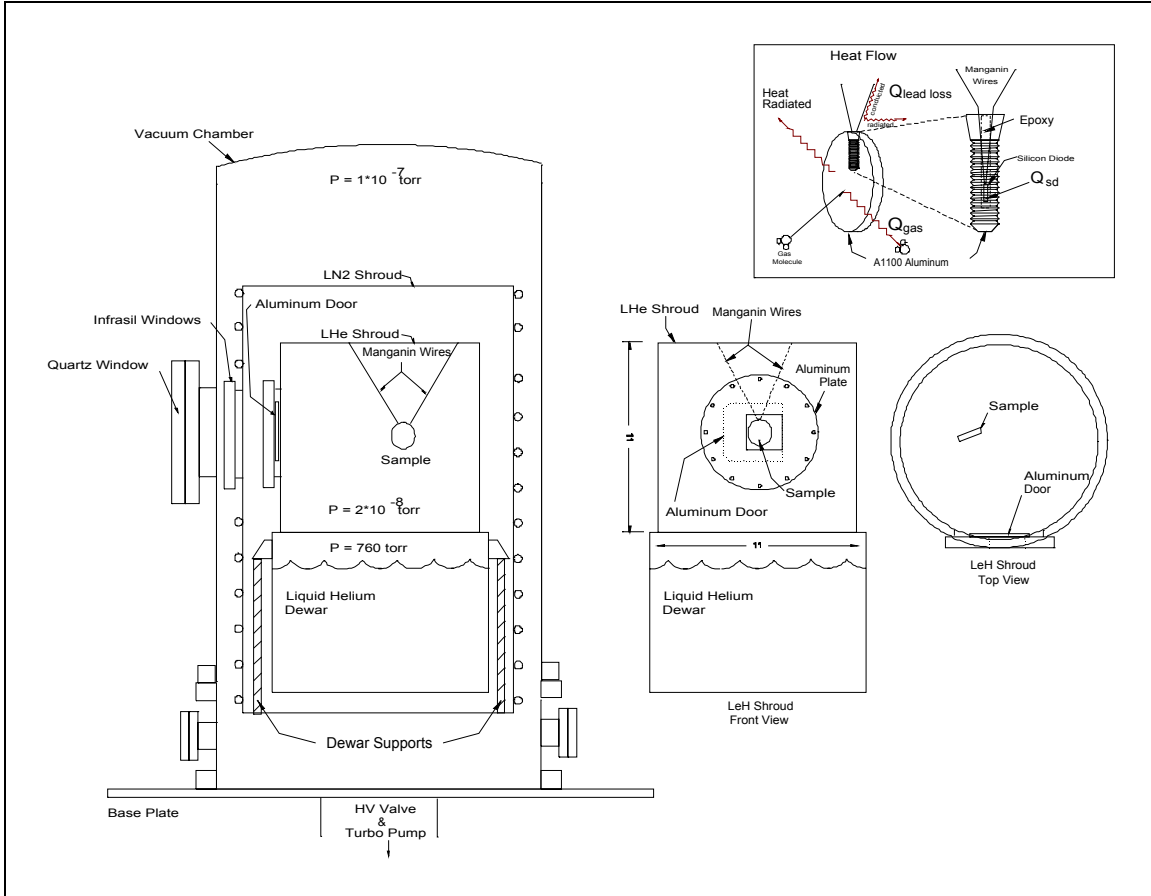


Figure 3.2-3. Emittance by the Calorimetric Technique (a conceptual representation)

3.2.4 Thermal Balance Method for Determining Total Hemispherical Emittance

The fourth method of determining emittance is with a thermal balance test. In this method, a heated sample is suspended inside a cold vacuum shroud with a heater attached to the substrate. With a constant and accurately determined power heat level to the substrate the temperature is allowed to come to equilibrium with the shroud. Then the emittance can then be determined utilizing the following heat balance equation:

$$\epsilon_k a \sigma (T_k - T_{s_k}) = VI - Q_{gas_k} \quad (44)$$

Where T is the temperature of the sample, T_s is the temperature of the shroud, V is the heater voltage, I is the heater current, σ is of course the Stefan-Boltzman constant, a is the sample area and Q_{gas} is the heat lost due to the conduction of heat by the residual gas in the chamber.

The loss due to heat flowing down the temperature sensor leads and the heat wires and heater sensors can for the most part be eliminated by the use of a guard heater. This is a thin heater placed above the sample through which all of the wires coming from the sample must pass. All of the wires must be thermally tied to the guard heater, which is operated at the same temperature as the sample. This effectively eliminates heat flow from the sample to the shroud wall via the heater and thermocouple wires.

Below is a conceptual diagram of the experimental setup.

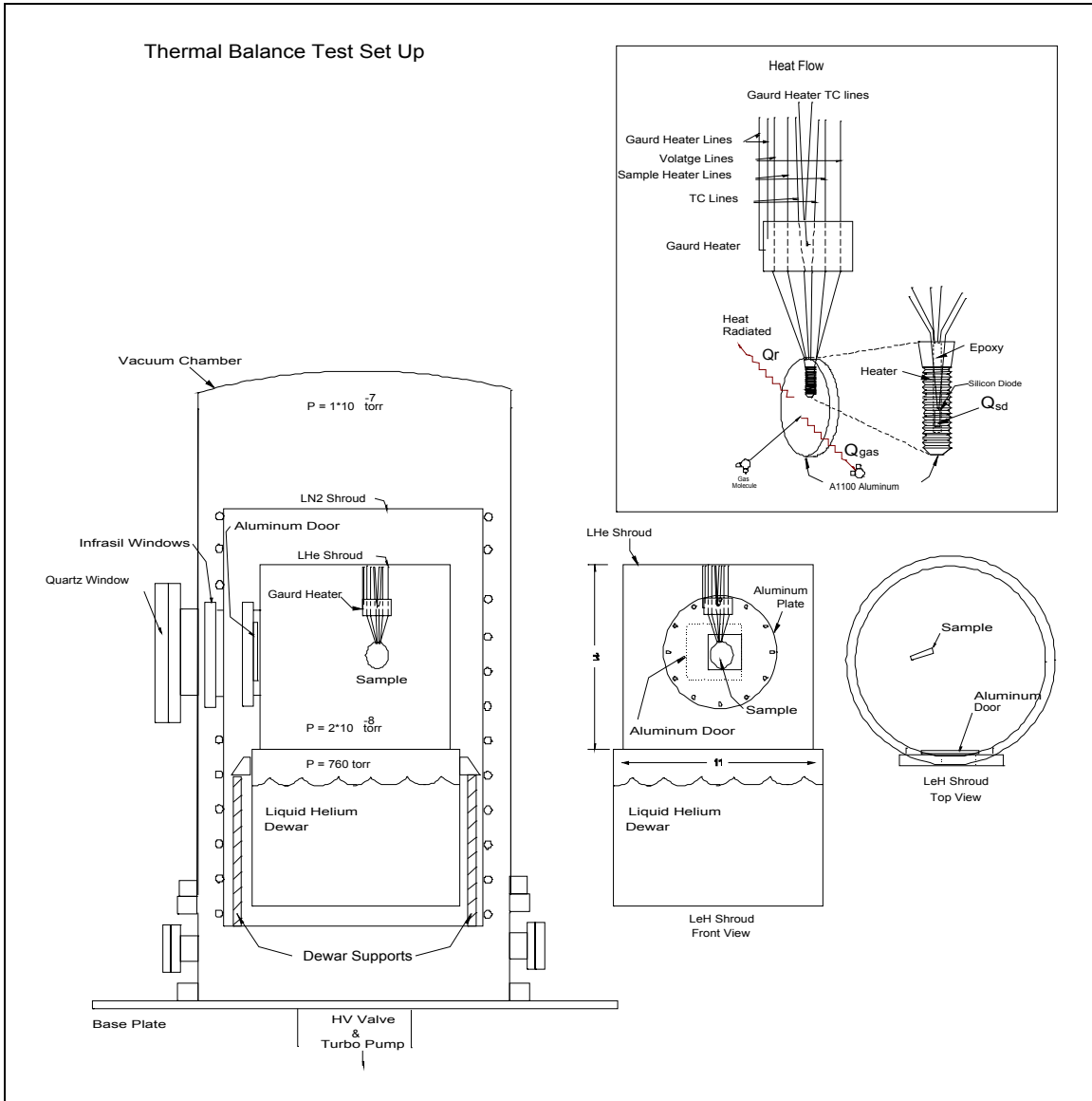


Figure 3.2-4. Emittance by a Thermal Balance Technique, a Conceptual Representation

The thermal balance test method of determining total hemispherical emittance works well, but does have several difficulties associated with it. The sample approaches the equilibrium temperature asymptotically and it can be difficult to judge when the sample has actually reach the equilibrium temperature. Care must also be taken to insure that the temperature of the guard heater is adjusted to the same temperature as the

sample. Adjusting the guard heater temperature can however, affect the sample temperature and this further complicates the judgement of the equilibrium temperature. The guard heater itself must be constructed in such a way that all the wires passing through it, the heater wires, the thermocouple wires and voltage measurement wires, are in good thermal contact with the heater over the test temperature range. This can be a problem if the wires are of different diameter, or have different insulation thicknesses. Lastly, a low emittance coating should be applied to the wire insulation between the sample and the guard heater to minimize the heat radiated to the shroud wall by the wire insulation.

3.2.5 Methods of Increasing Emittance

A high thermal emittance is typically desired for many applications. Achieving a sufficiently high emittance can be a difficult thing to achieve. The typical methods for achieving a high emittance include roughening the surface, increasing the thickness of the coating, and the use of coated honeycomb material. Each has its limitations.

In the first case, increasing the thickness of the coating will increase the emittance, but only up to a maximum value. Beyond a material specific thickness, applying a thicker coating will actually lower the effective emittance. This occurs when the thermal conductivity of the coating is low enough to allow the surface temperature of the coating to fall below the substrate temperature. This will in turn lower the amount of heat radiated to space and consequently the material will appear to have a lower emittance and in fact the effective emittance of the coating will drop. It is in some respects akin to putting a thermal blanket (MLI) over the substrate; although the true emittance of the surface hasn't changed the effective emittance of the coating will appear low and the total heat rejected to space as a consequence will be lower.

Honeycomb works well at increasing the effective emittance of a coating. It must be kept in mind however that the typical cells in a honeycomb sheet are small and numerous. Their small size and number makes abrading the surface in preparation for painting impossible. This means that cleaning the cells is the only method of ensuring good adhesion of the paint to the cell wall. It must be also kept in mind that the cells are concave and therefore any adhesion problem will be exasperated by the concave nature of the honeycomb cells. This will be especially true at cryogenic temperature, where the CTE mismatch between the coating and the honeycomb aluminum combined with the concave nature of the cells can make adhesion difficult. Any loss of adhesion will of course result in a drop in effective emittance of the honeycomb cell.

3.2.6 Considerations and Lessons Learned

When considering emittance there are some important points to keep in mind with spacecraft coatings. First is that coatings are typically thin and since emittance depends to some extent on the thickness of the coating it is important to be sure that the coating has the specified thickness. If your coating is thinner than is typical or specified, the emittance for that coating may not be valid. Also, since some coatings are partially transparent, the emittance to some extent depends on the given substrate. Typically emittances are measured over aluminum since this is the most common spacecraft substrate. If the substrate is other than a metal, then emittance of the coating could be different than expected, especially if the coating is thinner than is typical. It should also be remembered that some paints have several different primers that can be used and the use of a different primer or the lack of a primer can affect the emittance. In conclusion, the thickness and emittance of the coating should always be checked after the coating is applied.

3.3 Electrical Properties

During space flight missions spacecraft can encounter energetic charged particles that can cause differential charging of the spacecraft. This differential charging can result in electrostatic discharges (ESD) between various parts of the spacecraft. This ESD is a source of electromagnetic interference (EMI) which can be coupled to electronic devices. Sensitive ICs can be damaged by several mJ (milli-Joule) of ESD and circuits can be upset with only several nJ (nano-Joule). This charging phenomenon has been blamed for arcing that has caused blown fuses and loss of data transmission on several spacecraft. ESD can also cause electronic parts failure, operational anomalies, degradation of thermal control surfaces, and can also render low energy particle detectors useless.

The principal cause of spacecraft charging is the charged particles trapped by the earth's magnetic field. The differential charging of the relatively thin spacecraft thermal control coatings is due primarily to the low energy charged particles in the Van Allen radiation belts. The penetration depth of the high-energy charged particles is greater than the typical thermal control coatings and therefore these do not contribute much to the surface charging of the coatings. The Van Allen belts, which are responsible for most spacecraft charging, are sometimes modified by magnetic disturbances and the solar cycle but generally exist from approximately 1000 km to 6 Earth radii. In low Earth orbit (below 1000km) spacecraft charging is not much of a concern. The Van Allen belts are generally symmetric in azimuth about the geomagnetic equator and extends to ± 50 degrees above and below it (reference 11 & 12). The actual flux and energy encountered needs to be calculated for each mission based on the spacecraft orbit and time of launch with respect to the solar cycle. The charts below (reference 13) show typical distributions of trapped electrons and protons of varying energies and earth radii

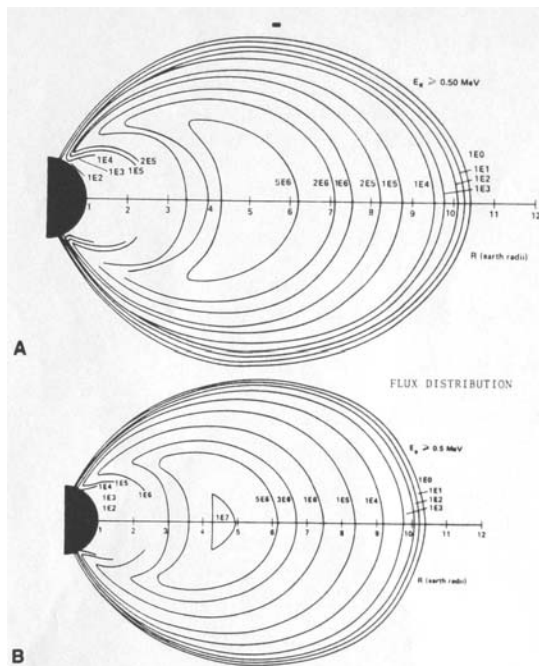


Figure 3.3.1 (A) Distribution of trapped electrons During solar minimum with energy greater than 0.5 MeV. (B) Distribution of electrons with same energy during solar maximum. (reference 13)

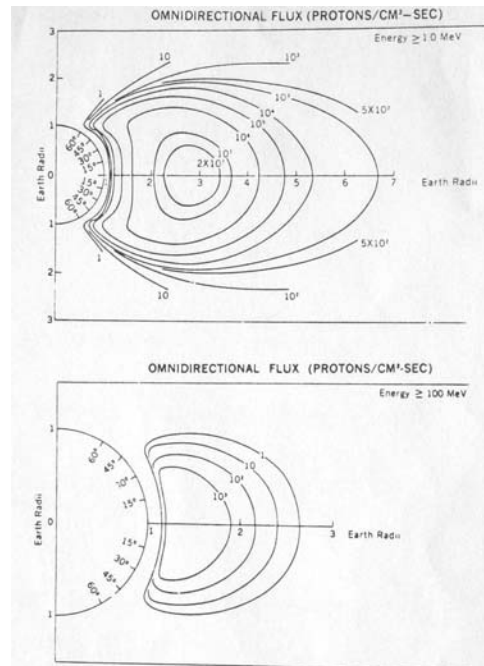


Figure 3.3.2 (A), Distribution of trapped protons with energy greater than 1 MeV. (B), Distribution of trapped protons with energy greater than 100 MeV (reference 13)

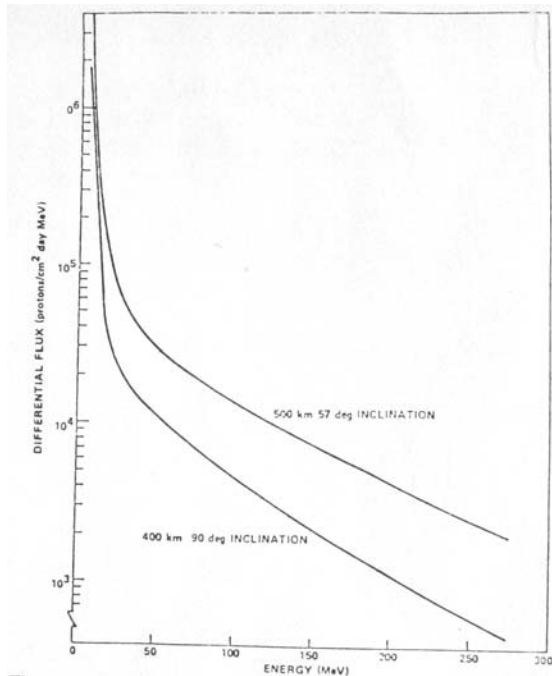


Figure 3.3.3 The radiation due to trapped protons in a 400 km polar orbit and in a 500 km, 57° inclination orbit. (reference 13)

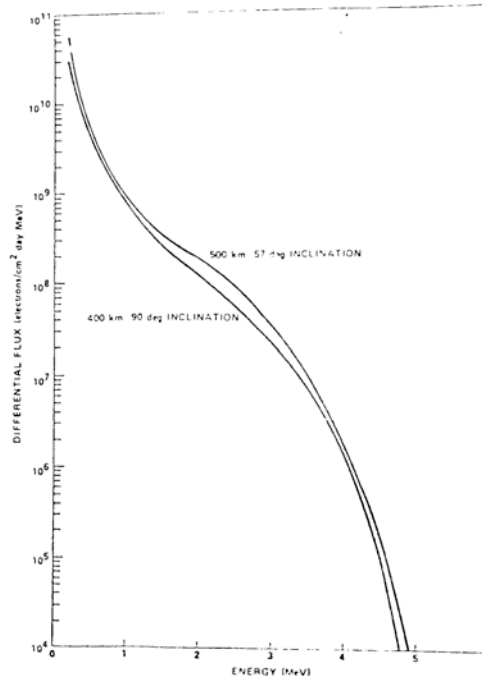


Figure 3.3.4 The radiation due to trapped electrons encountered in a 400 km polar orbit and in a 500 km (reference 13)

Differential spacecraft charging is determined by a number of factors such as photo emission from the coating, temperature of the coating, secondary emission of electrons, contamination of the surface, intensity of radiation, and type of coating. Differential spacecraft charging is primarily the result of low energy electron flux. High-energy electrons penetrate the thin thermal coatings and therefore do not contribute to the differential charging process. Low energy protons do not penetrate the coatings and therefore they tend to lessen the charging caused by the electrons, but they do not eliminate it. This is because proton flux is much less than the electron flux. This may seem paradoxical since space is on the whole charge neutral. The reason the electron flux is greater is not due to the fact that there are more electrons in space than protons. Thermodynamics requires that the electrons and protons be in thermodynamic equilibrium with each other. Since the mass of the electrons is so much less than the mass of protons they must travel faster than the protons in order to reach the same kinetic energy and hence thermal equilibrium. This means that the total number of electrons passing a given point in a fixed amount of time is greater than protons. So the spacecraft receives a much greater electron flux than proton flux.

NASA's preferred reliability practices manual (reference 14) recommends that the energy stored by each nonconductive surface be less than 3mJ, and that ESD (electrostatic discharges) should not be allowed to occur near receivers or antennas operating at less than 8GHz or near sensitive circuits. This implies that the spacecraft must be immune to 3mJ ESD. NASA's NASCAP program will calculate the maximum differential charging on each non-conducting surface if the conductivity of the coatings is known.

The electric field strength within a spacecraft coating can be calculated if the coating thickness and surface voltage are known and is given by:

$$E = V / d \quad (45)$$

Where d is the thickness of the dielectric material. Usually when this electric field strength is greater than $2 \times 10^5 \text{V/cm}$ the risk of ESD is present.

The total ESD energy can be calculated from:

$$W = \frac{1}{2}CV^2 \quad (46)$$

Where C is the capacitance of the nonconductive surface with respect to spacecraft ground.

$$C = \frac{\epsilon_o \epsilon_c A}{d} \quad (47)$$

where d= the thickness of the coating and ϵ_c is the permittivity of the coating and A is the total area of the coating.

To calculate the total energy on each surface of the spacecraft the charge voltage must be known. This too can be calculated if the resistivities of the coatings are known as well as the total charge current impinging on the coating in space. If the resistance is not known, ground-based test must be conducted to determine these parameters. The ESD energy as a function of capacitance and voltage level is displayed in the following diagram taken from NASA's preferred reliability manual:

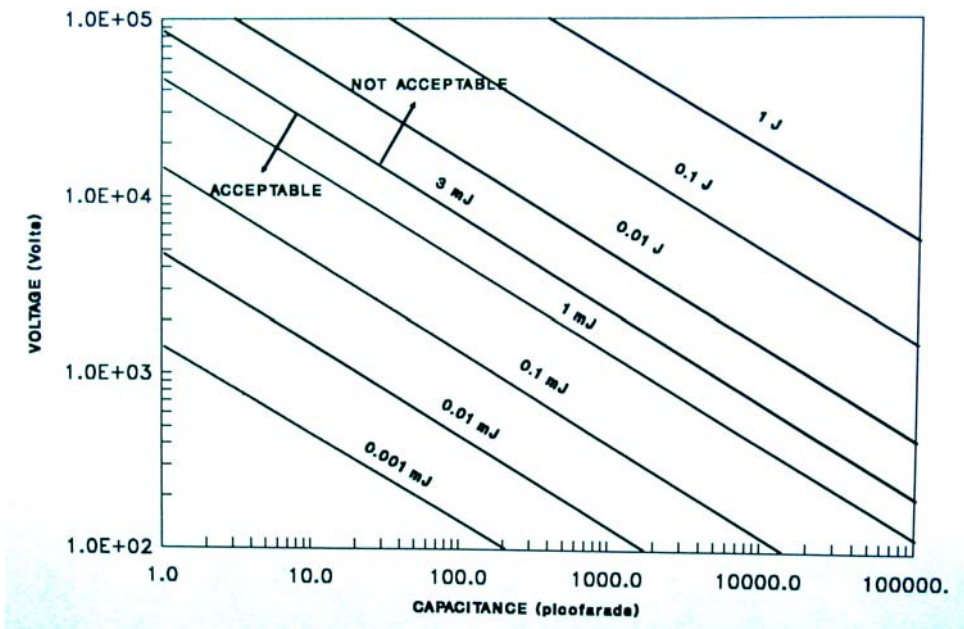


Figure 3.3-1. ESD Energy as a Function of Capacitance and Voltage

Since the current available in the space environment is relatively low, material with a resistivity of 10^9 Ohm-cm are usually considered adequate for effective charge control.

For some missions however it is not unusual for a requirement of not more than 1-volt potential difference to exist between any two parts of the spacecraft. This is far below the 3mJ limit of acceptability to prevent ESD. Under these stringent requirements a more conductive coating is necessary.

When spacecraft charging is of concern two basic cases must be considered in order to measure the conductivity or predict the charging level. The first case deals with a conductive coating on a nonconductive substrate. In this situation charge control is achieved through the inherent sheet conductivity of the coating.

For simplicity, let the conductive coating have conductivity ρ and let it be in an environment with an incoming current density of \mathbf{J} amps/cm²/sec at some angle θ with respect to the surface and let's further assume that the charge is deposited at the surface with no photo or secondary emissions. The maximum voltage will occur at a point furthest from the ground point. In the figure this is just $h/2$ since it is assumed that the entire edge of the coating is grounded.

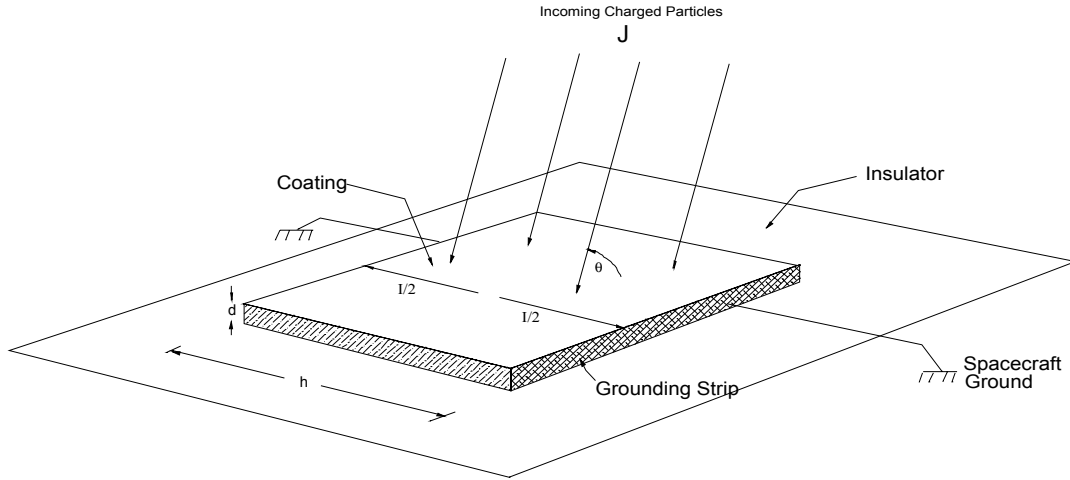


Figure 3.3-2. Spacecraft Coating on an Insulating Substrate

Then the total current incident on the coating is therefore:

$$I = \vec{J} \cdot \vec{A} = Jh^2 \cos(\theta) \quad (48)$$

And the voltage potential from $h/2$ to ground is just:

$$\begin{aligned} \Delta V &= \frac{I}{2} R \\ &= \frac{Jh^2 \cos(\theta)}{2} \left(\frac{\rho}{d} \right) \end{aligned} \quad (49)$$

where ρ/d = the sheet conductivity of the coating in Ω/\square (ohms per square, where the size of the square is not relevant since any size square will result in exactly the same measured resistance). Now depending on the particular orbit, the current density can range from 1×10^{-9} amp/cm² to 1×10^{-8} amp/cm². This implies that in order to have a voltage potential of less than one volt, which is required on some scientific missions, with a typical coating thickness of 2 mils (0.05 cm) and grounded on a 10cm square, the sheet resistivity of the coating would have to be (assuming the maximum current density):

$$\rho \leq 1 \times 10^5 \Omega/\square$$

For the case of a conductive paint on a metallic substrate the charge is not conducted laterally but rather through the thickness of the material to the metallic substrate. The appropriate units for this situation is ($\Omega\cdot m$). The situation is illustrated in the following diagram:

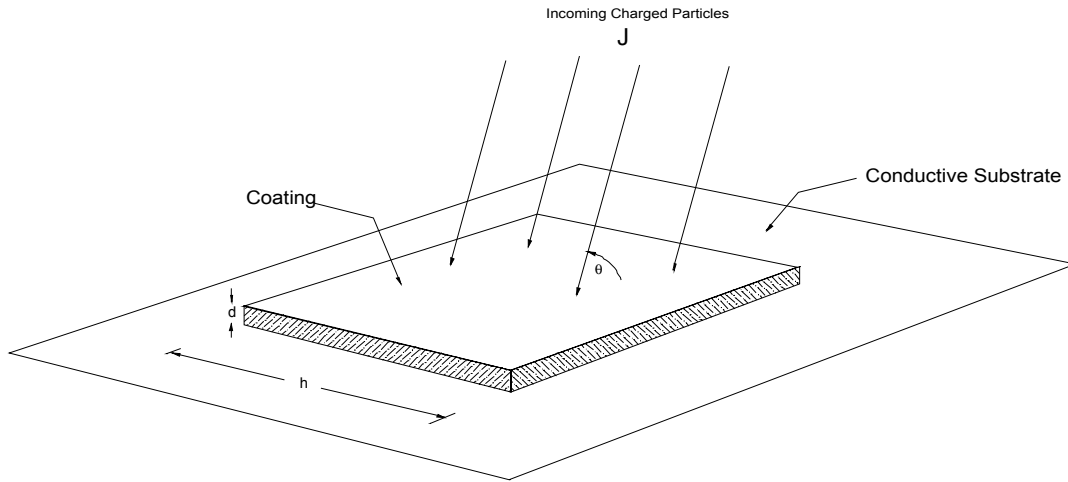


Figure 3.3-3. Spacecraft Coating on a Conductive Substrate

$$\begin{aligned}
 I &= \vec{J} \cdot \vec{A} \\
 &= JA \cos(\theta)
 \end{aligned}
 \tag{50}$$

and the potential voltage from the surface of the coating to ground would be:

$$\begin{aligned}
 \Delta V &= IR \\
 &= I \left(\rho \frac{d}{A} \right) \\
 &= J \rho d \cos(\theta)
 \end{aligned}
 \tag{51}$$

Assuming currents of the same order as last times gives resistances of the order of:

$$\rho = 2 \times 10^9 \Omega\text{-cm}$$

It is important to have the appropriate specification with respect to spacecraft charging, $\Omega/$ refers to sheet conductivity and hence assumes that charge conduction will be laterally along the surface of a coating applied over a nonconductive substrate with grounding at the edges of the coating. $\Omega\text{-cm}$ refers to bulk conductivity and assumes that charge conduction will be through the bulk of the material to an electrically conductive substrate. These two forms of conductivity measurements (bulk and sheet) can not necessarily be converted from one to another. Only if the material is amorphous and homogeneous can the conversion be made. Paints like silicates tend to crack when curing and therefore produce a small scale “mud tilling” effect. In that case there is little if any lateral conductivity and charge conduction is only possible through the substrate to a metallic substrate. In this case a conversion from bulk conductivity to sheet conductivity or vice versa is not valid.

One method for alleviating a high charge with respect to ground on a non-conductive substrate is to coat the substrate with a conductive medium before the application of the thermal control coating as shown in Figure 3.3-4:

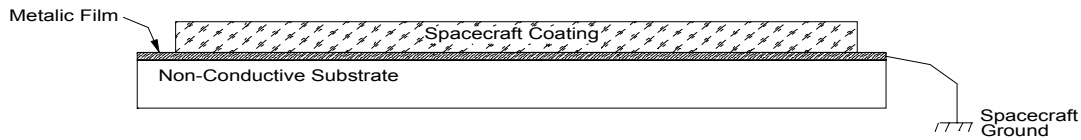


Figure 3.3-4. One Method of Grounding Spacecraft Coating to a non-Conductive Substrate

Another common method of preventing spacecraft charging is to coat the thermal control coating with a very thin layer (typically 200Å) of Indium Tin Oxide. This provides a conductive path for electrons and does not change the emittance of the coatings but does increase the solar absorptance somewhat. One method that has been tried many times that does not typically have any effect on charging is the use of vapor deposited aluminum grids. On a non-conductive surface the grids are intended to carry away any charge build up between the grids. What typically happens is that the space between the grids simply charges to its maximum level and then discharges by small arcs to the grid. This over time tends to vaporize the grid and causes a constant RF noise, while the overall charge of the coating is about the same as it was without the grid.

Finding a coating, which not only satisfies thermal requirements but electrical conductivity requirements as well, is sometimes difficult to fulfill. This is particularly true if a low absorptance high emittance coating is needed for thermal reasons. Since the conductivity of a desired spacecraft coating may not be known, it may be necessary to measure the charging or conductivity of the coating with a ground based test.

If ground based testing of a coating is necessary, the measurement of conductivity for space flight coatings should be performed under as close to actual conditions as is possible in a laboratory. The reason for this is that the conductivity of spacecraft coatings can depend upon a number of factors. First the length of time the coating has been exposed to vacuum can cause outgassing of volatiles and water vapor which can alter the conductivity of the coating. Second, the energy of the electron flux can have a bearing on the extend to which a coating will charge since the conductivity is a function of electron energy. Third, the temperature of the coating can also play a significant role in the charging process. It is therefore necessary to know the operating temperature that the coating will be subjected to on orbit.

The following chart shows typical conductivity changes with temperature for a common thermal control coating. These results were obtained with a mono-energetic electron beam and represent the amount of charge build up on the surface on an electrically conductive paint when exposed to an electron beam at two different temperatures.

Conductive White Paint		
Beam Energy & Current	Surface Charge (volts) @ 1nA/cm² Temp = 20 °C	Surface Charge (volts) @ 1nA/cm² Temp = -127°C
1 KeV	0	-20
2 KeV	10	-20
5 KeV	0	-320
10 KeV	10	-300
20 KeV	10	-280

Figure 3.3-5 Surface Charging of a White Conductive Paint

The incoming charge fluence and energy can also affect the charge build up. With increasing energy the penetration depth of the electron increases and can penetrate the entire coating thickness and thus reduce the charge build up. The chart below for a thin film coating illustrates the point as well as a marked temperature dependence.

Thin Film Coating				
Beam Energy & Current	Surface Charge T = -118°C	Surface Charge T = -51°C	Surface Charge T = 3°C	Surface Charge T = 21°C
5 KeV @ 1nA/cm ²	-200	-170	-60	-45
5KeV @ 10nA/cm ²	-1300	-600	-200	-200
10KeV@ 1nA/cm ²	-975	-500	-170	-170
10KeV@ 10nA/cm ²	-950	-550	-200	-170
20KeV@ 1nA/cm ²	-250	-170	-80	-100
20KeV@ 10nA/cm ²	-35	-50	-50	-30

Figure 3.3-6. Surface Charging of a Thin Film Coating

There are several methods for determining the conductivity of spacecraft coatings. The simplest is the four-point probe method. (Figure 3.3-7). In this method four pointed probes are placed in contact with the surface of the coating and a current is established through the outside points. The voltage is then measured across the inside points and the conductivity of the coating calculated.

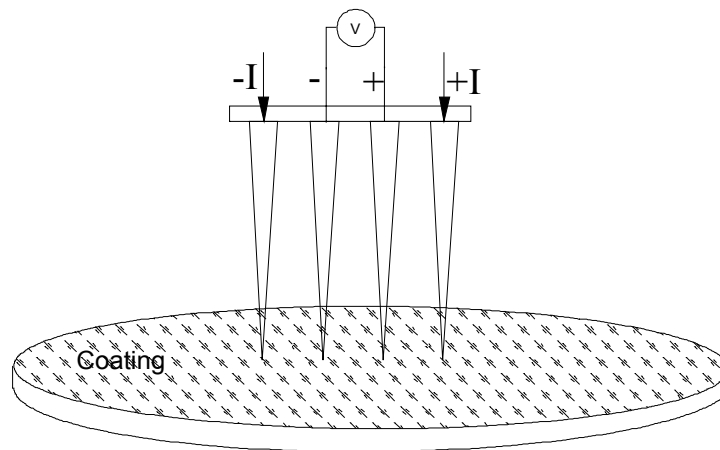


Figure 3.3-7. Four point probe method for determining conductivity

This method works well with metal and vapor deposited coatings. It has its drawbacks for soft coatings and coatings, which may outgas water vapor or other volatiles under vacuum. It has the added disadvantage that electrostatic fields are concentrated at the points of the probes which is different than the uniform electric field that is seen by the coating in space. The other disadvantage is that the electrons in the probes enter the coating at low velocity, typically only about 0.1cm/s (the drift velocity of electrons traveling in electrical wires:) in space the electron speed depends on the energy of the particle. For an electron of 10KeV the velocity of the electron as it strikes the spacecraft coating is on the order of 6×10^7 m/sec. This gives a penetration depth to the electron that is not present in a four-point probe. The last problem with the four-point probe or any similar type of measurement is that there are no secondary electrons emitted as can happen with a 10 or 20KeV electron beam.

A better method, but not necessarily the best, is to utilize an electron flood gun in a vacuum chamber to “illuminate” the coating with a low energy electron beam and then measure the charge build up with a noncontacting probe that sweeps over the surface a few millimeters above the surface. See schematic diagram in Figure 3.3-8 below.

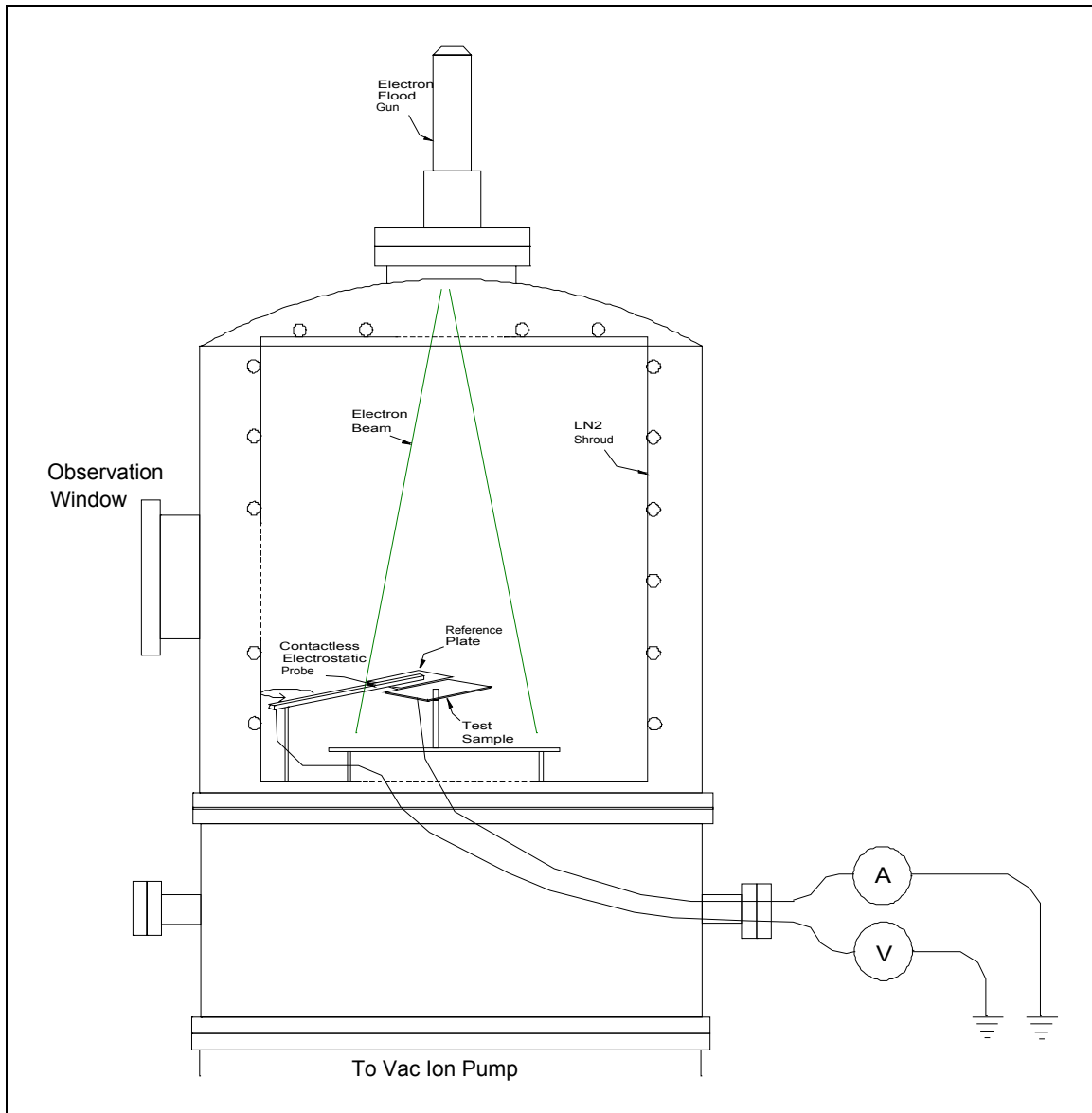


Figure 3.3-8. Electrostatic Charge Facility Conceptual Diagram

The main disadvantage of this method is that it still does not simulate the actual conditions of space, specifically, the electron beam energy is mono-energetic and in space the coating will see an entire spectrum of electron energies. Secondly, and probably more importantly is the fact that during the scanning of the surface by the electrostatic probe, the probe shields the surface from the electron beam thus creating an electron shadow on the surface. For coatings that have a very long discharge time this is not a problem, however for coatings that tend to discharge quickly the blocking of the beam cause the area under the probe to discharge, thus the probe may measure a charge build up less than there actually is when in reality there may be a charge on the surface when it isn't shielded by the probe. In practice, the probe has a very wide field of view and so will measure at least some of the charge that rests outside of the electron shadow cause by its presence.

Two things that have gotten little attention in the past are degradation with respect to spacecraft charging and coating glow. Degradation of the surface of spacecraft thermal control coatings by UV, particulate radiation or by molecular contamination can change the electrical properties of the coating and can cause the coating to charge to an unacceptable level. This fact must be taken into account. Currently little data exists which would

give any indication how electrical conductivity changes with respect to various degradation environments. Coating glow can happen for certain coatings when incoming electrons of sufficient energy cause the surface to luminesce. This can be easily seen during an electron gun illumination. This glow can be quite bright at times and may need to be considered during future missions.

References

1. Siegel, Robert , Howell, John R., Thermal Radiation Heat Transfer volume 1, The Blackbody, Electromagnetic and Material Properties, National Aeronautics and Space Administration, Washington DC, 1968
2. Jackson, J.D., Classical Electrodynamics, Second Edition, John Wiley Company, New York, 1975
3. Davis, Harry F., Snider, Arthur David, Introduction to Vector Analysis, fourth edition, Allyn and Bacon Inc. , Boston, 1979
4. Complex Variables and Applications third edition, Ruel V. Churchill, James W. Brown and Roger F. Verhey, McGraw-Hill, New York, 1976
5. Handbook of Heat Transfer Vol 1 & II, Max Jacob, John Wiley and Sons, New York, 1957
6. Edwards, D.K., J.T. Gier, K.E. Nelson, and R.D. Roddick, "Integrating Sphere for Imperfectly Diffuse Samples," Applied Optics, 51, November 1961
7. Henninger, John H., Solar Absorptance and Thermal Emittance of Some Common Spacecraft Thermal-Control Coatings, NASA Reference Publication 1121, National Aeronautics and Space Administration, Goddard Space Flight Center, Greenbelt Maryland, April 1984
8. 2000 ASTM Standard Extraterrestrial Spectrum Reference E-490-00
9. Characteristics and use of Infrared Detectors, Technical Information SD-12, Hamamatsu
10. Total Emittance Measurement Portable, Temp 200A, Operations Manual, AZ Technology, Huntsville, Al, August 2002
11. Introduction to the Space Environment second edition, Thomas F. Tascione, Krieger Publishing Company, Makabar Florida, 1994
12. Introduction to Space Physics, edited by Margaret G. Kivelson and Christopher T. Russell, Cambridge University Press, New York, 1995
13. Space and Planetary Environment Criteria. Guidelines for Use in Space Vehicle Development, R.E. Smith and G.S. West, 1982, NASA Technical Memorandum 82478.
14. Surface Charging / ESD Analysis, Preferred Reliability Practices, Practice No. PD-AP-1301, NASA,

IV. Thermal Coatings Data

The emittance and solar absorptance listed in the following tables were measured in compliance with ASTM E408-71 and ASTM E903-82 respectively. These measurements have been compiled over several decades at GSFC by John Henninger (reference 7), Lonny Kauder, Wanda Peters, Amani Ginyard, Monali Joshi & Blake Miller.

4.1 Black Coatings

	α_s	ϵ_n
Anodize Black	0.88	0.88
Carbon Black Paint NS-7	0.96	0.88
Catalac Black Paint	0.96	0.88
Chemglaze Black Paint Z306	0.96	0.91
Aeroglaze 306/Kevlar Composite	0.96	0.91
CTL15 Black Gloss Paint	0.95	0.87
Deep Sky Black	0.91-0.95	0.94
Delrin Black Plastic	0.96	0.87
Ebanol C Black	0.97	0.73
Ebanol C Black – 384 ESH UV	0.97	0.75
E-Glass Fabric 5276	0.74	0.91
GSFC MS-94	0.96	0.89
GSFC NSB69-82	0.97	0.90
Aeroglaze H322	0.96	0.86
Aeroglaze L-300	0.95	0.84
Martin Black Velvet	0.91	0.94
MH21S/LO Black Paint	0.98	---
NSB6982	0.97	0.91
Paladin Black Lacquer	0.95	0.75
Polyethylene Black Plastic	0.93	0.92
PT401 Gloss Black Paint	0.95	0.85
Pyromark 1200 Black Paint	0.95	0.83
Tedlar Black Plastic	0.94	0.90
Vel-Black	0.99	0.95

4.2 White & Color Coatings

	α_s	ϵ_n
Astro-Quartz	0.06	---
Astro-Quartz with 900 C bake out	0.03	---
Aeroglaze A971 yellow paint	0.43	0.89
AZ4301	0.19	---
Beta Cloth/VDA Sheldahl	0.38	0.85
Beta Cloth/VDA Chemfab 500 no silicone	0.45	0.90
Beta Cloth Glass/Al	0.29	0.91
Barium Sulfate with Polyvinyl Alcohol	0.06	0.88
Biphenyl-White Solid	0.23	0.86
Catalac White Paint	0.24	0.90
Dupont Lucite Acrylic Lacquer	0.35	0.90
Dow Corning White Paint	0.19	0.88
Gortex Expanded Teflon/VDA (VDA side)	0.54	0.54
Gortex Expanded Teflon/VDA (Teflon side)	0.43	0.43
GSFC White Paint NS43C	0.20	0.92
GSFC White Paint NS44-B	0.34	0.91
GSFC White Paint MS74	0.17	0.92
Aeroglaze A276	0.26	0.88
Aeroglaze A276/K1100 composite 1500ESH	0.53	0.89
Tedlar White Plastic	0.39	0.87
S13GLO	0.20	0.90
S13GPLO/Kevlar Composite	0.21	0.90
TOR-RC Triton Systems	0.18	0.82
COR-RC Triton Systems	0.28	0.71
YB71 white paint	0.18	0.90
Z93	0.16	0.92
Zinc Orthotitanate with Potassium Silicate	0.13	0.92
Zinc Oxide with Sodium Silicate	0.15	0.92
Zirconium Oxide with 650 Glass Resin	0.23	0.88

4.3 Conductive Paints

	α_s	ϵ_n
Electrodag	0.90	0.68
GSFC NS43G	0.26	0.90
NS43G/Hincom	0.18	0.92
GSFC Green NS53-B	0.52	0.87
GSFC Green NS43-E	0.57	0.89
GSFC White NS43C	0.20	0.92
GSFC Green NS55-F	0.57	0.91
GSFC Green NS-79	0.57	0.91
Z93SC55	0.14	0.94

4.4 Anodized Aluminum Coatings

	α_s	ϵ_n
Black	0.65	0.82
Black	0.86	0.86
Black Anoblack	0.94	0.89
Black		
0.0001mils	0.51	0.75
0.0005mils	0.60	0.82
0.001mils	0.67	0.84
Black Anodize with sealer		
0.001mils	0.71	0.84
0.002mils	0.70	0.86
1.5 mils	0.73	0.86
Blue	0.67	0.87
Blue	0.53	0.82
Brown	0.73	0.86
Chromic	0.44	0.56
Clear	0.27	0.76
Clear	0.35	0.84
Clear/ 7075 Aluminum	0.68	0.82
Clear		
0.0001mils	0.32	0.75
0.0005mils	0.37	0.81
0.001mils	0.44	0.85
Clear Type 2 Class 1	0.43	0.67
Clear with sealer		
0.001mils	0.50	0.84
0.002mils	0.70	0.86
1.5mils	0.59	0.87
Green	0.66	0.88
Gold	0.48	0.82
Gold		
0.0001mils	0.40	0.74
0.0005mils	0.46	0.81
0.001mils	0.52	0.82
Hard Anodize		
Aluminum 7075-T6	0.83	0.87
Aluminum 6061-T6	0.90	0.86
Aluminum 2024-T6	0.76	0.90
Plain	0.26	0.04
Red	0.57	0.88
Sulphuric	0.42	0.87
Yellow	0.47	0.87
Blue Anodized Titanium Foil	0.70	0.13

4.5 Metals and Conversion Coatings

	α_s	ϵ_n
Alodyne Aluminum 2024	0.42	0.10
Alodyne Aluminum 6061-T2	0.44	0.14
Aluminum Polished	0.14	0.03
Alzac A-2	0.88	0.88
Alzac A-5	0.18	---
Alodine Beryllium	0.68 - 0.76	0.06 - 0.15
Beryllium Copper Oxidized	0.83 - 0.87	0.09
Beryllium		
Lathe finish	0.51	0.05
Lap finish	0.71	0.12
Wire finish	0.77	0.28
Milled finish	0.52	0.07
Black Chrome	0.96	0.62
Black Copper	0.98	0.63
Black Irridite	0.62	0.17
Black Nickel	0.91	0.66
Black Nickel/ZK60Mg	0.78 - 0.80	0.56 - 0.61
Black Nickel/Magnesium	0.92	0.74
Black Nickel/Titanium	0.91	0.77
Buffed Aluminum	0.16	0.03
Buffed Copper	0.30	0.03
Constantan- Metal Strip	0.37	0.09
Copper Foil Tape		
Plain	0.32	0.02
Sanded	0.26	0.04
Tarnished	0.55	0.04
Dow 7 on Polished Magnesium	---	0.49
Dow 7 on Sanded Magnesium	---	0.65
Dow 9 on Magnesium	---	0.87
Dow 23 on Magnesium	0.62	0.67
Ebanol C Black	0.97	0.77
Electroplated Gold	0.23	0.03
Electrolytic Gold	0.20	0.02
Electroless Nickel	0.39	0.07
Gold Plated Beryllium Mirror	0.21	0.03
Irridite Aluminum	---	0.11
Irridite Aluminum	0.24	0.04
Inconel X Foil	0.52	0.10
Kannigen-Nickel Alloy	0.45	0.08
Mu metal	---	0.09
Plain Beryllium Copper	0.31	0.03
Platinum Foil	0.33	0.04
Stainless Steel		
Polished	0.42	0.11
Machined	0.47	0.14
Sandblasted	0.58	0.38
Machine Rolled	0.39	0.11
Boom-Polished	0.44	0.10
1-mil 304 Foil	0.40	0.05
Tantalum Foil	0.40	0.05
TiN/Titanium	0.52	0.11
Titanium Anodized	0.84 - 0.86	0.44 - 0.48
Tiodize Titanium TinFin400	0.74	0.73
Tiodize Titanium TinFin200	0.74	0.23
Tungsten Polished	0.44	0.03

4.6 Vapor Deposited Coatings *

	α_s	ϵ_n
Aluminum	0.08	0.02
Aluminum on Black Kapton	0.12	0.03
Aluminum on Fiberglass	0.15	0.07
Aluminum on Stainless Steel	0.08	0.02
Aluminum on Lacquer	0.08	0.02
Aluminum on abraded Lacquer	0.33	0.07
Chromium	0.56	0.17
Chromium on 5-mil Kapton	0.57	0.24
Germanium	0.52	0.09
Gold	0.19	0.02
Iron Oxide	0.85	0.56
Molybdenum	0.56	0.21
Nickel	0.38	0.04
Rhodium	0.18	0.03
Silver	0.04	0.02
Titanium	0.52	0.12
Tungsten	0.60	0.27

* on glass substrates except where noted

4.7 Solar Cells & OSRs

Spacecraft	α_s	ϵ_n
ACE	0.71	---
AE	0.78	0.82
AMSAT	0.82	0.85
ATN Black	0.77	0.80
ATN Blue	0.86	0.85
ATS-F	0.85	0.85
COMSAT	0.82	0.85
DE	0.77	0.81
EUVE	0.85	0.85
ETS/GOES	0.82	0.80
FAME	0.94	0.85
GOES	0.91	0.81
GPS-Conductive Coating	0.81	0.80
HELIOS	0.80	0.82
IME-Conductive Coating	0.75	0.79
IMP-H	0.78	0.82
IMP-I	0.78	0.81
ISEE-Conductive Coating	0.91	0.79
IUE	0.86	0.84
OA0	0.85	0.81
OCLI OSR 3mil ceria doped borosilicate with ITO	0.10	---
OSR	0.06	0.80
PAC	0.77	0.81
Silicon Wafer	0.57 – 0.60	0.56
SMS-B	0.81	0.80
Spanish INTASAT	0.86	0.86
SSS	0.79	0.82
ST5	0.91	0.83
TOPHAT	0.89	0.91
TRW Solar Cell	0.86	0.82

4.8 Composite Coatings

	α_s	ϵ_n
Aluminum Composite Coating on 3 mil Kapton	0.14	0.67
Aluminum Composite over Aluminum Foil	0.09	0.72
Aluminum Oxide (Al_2O_3) – (12 λ /4) on Buffed Aluminum		
Initial	0.13	0.23
2560 ESH UV + P ⁺	0.13	0.23
Aluminum Oxide (Al_2O_3) – (12 λ /4) on Fused Silica	0.12	0.24
Silver Beryllium Copper (AgBeCu)	0.19	0.03
Kapton Overcoating	0.31	0.57
Parylene C Overcoating	0.22	0.34
Teflon Overcoating	0.12	0.38
GSFC Dark Mirror Coating SiO-Cr-Al	0.86	0.04
GSFC Composite SiOx- Al_2O_3 -Ag	0.07	0.68
Helios Second Surface Mirror/Silver Backing		
Initial	0.07	0.79
24 Hours at 5 Suns	0.07	0.80
48 Hours at 11 Suns + P ⁺	0.08	0.79
Inconel with Teflon Overcoating – 1 mil	0.55	0.46
SiOx /VDA/0.5mil Kapton	0.19	0.14
Vespel Polyimide SP1	0.89	0.90
M46J/RS-3 Composite Substrate	0.91	0.73
M55J/954-3	0.92	0.80
M40 Graphite Composite	0.94	
GSFC Spectrally Selective Composite Coating	0.13	0.68
Silver Composite (Al_2O_3 /Ag/0.33mil Kapton)	0.73	0.25
Silver Aluminum Oxide (Ag/ Al_2O_3 /1mil Kapton	0.07	0.32 – 0.44
Teflon Impregnated Anodized Titanium	0.75	0.26
Uplix-S 0.5 mil with 10,000 \AA Al_2O_3	0.08	0.25
Uplix-S 1.0 mil with 10,000 \AA Al_2O_3	0.08	0.23

4.9 Films and Tapes

	α_s	ϵ_n
Aclar Film (Aluminum Backing)		
1 mil	0.12	0.45
2 mil	0.11	0.62
5 mil	0.11	0.73
Black Kapton	0.93	0.85
Germanium Black Kapton	0.55	0.84
Germanium Black Kapton reinforced	0.50	0.85
Kapton Film (Aluminum Backing)		
0.08 mil	0.23	0.24
0.15 mil	0.25	0.34
0.25 mil	0.31	0.45
0.50 mil	0.34	0.55
1.0 Mil	0.38	0.67
1.5 mil	0.40	0.71
2.0 mil	0.41	0.75
3.0 mil	0.45	0.82
5.0 mil	0.46	0.86
Kapton Film (Chromium-Silicon Oxide-Aluminum Backing (Green))		
1.0 mil	0.79	0.78
Kapton Film (Aluminum-Aluminum Oxide Overcoating) 1 mil		
Initial	0.12	0.20
1800 ESH UV	0.12	0.20
Kapton Film (Aluminum-Silicon Oxide Overcoating)		
Initial	0.11	0.33
2400 ESH UV	0.22	0.33
Kapton Film (Silver-Aluminum Oxide Overcoating)		
Initial	0.08	0.19
24000 ESH UV	0.08	0.21
Kapton Film (Aluminum-Silicon Oxide Overcoating)		
Initial	0.12	0.18
4000 ESH UV	0.28	0.24
Kapton 3mil (ITO/VDA/Kapton)	0.09	0.02
Kapton 3mil (ITO/Kapton/VDA)	0.43	0.82
Kimfoil Polycarbonate Film (Aluminum Backing)		
0.08 mil	0.19	0.23
0.20 mil	0.20	0.30
0.24 mil	0.17	0.28
Mylar Film		
Aluminum Backing		
0.15 mil	0.14	0.28
0.25 mil	0.15	0.34
3.0 mil	0.17	0.76
5.0 mil	0.19	0.77
Skylab Sail		
Initial	0.15	0.35
1900 ESH UV	0.19	0.36
Skylab Parasol Fabric (Orange)		
Initial	0.51	0.86
2400 ESH UV	0.65	0.86
Tedlar (Gold Backing)		
0.5 mil	0.30	0.49
1.0 mil	0.26	0.58
Polyester Film Yellow Tape IP8102YE	0.52	0.82
Sumitomo Bakelite	0.17	0.82
Tedlar 1.5 mil overcoat SiOx	0.21	0.63

4.9 Films and Tapes (continued)

	α_s	ϵ_n
Teflon		
Aluminum Backing	0.08	0.66
2 mil	0.13	0.81
5 mil	0.13	0.87
10 mil		
	0.09	0.80
ATO/5mil Teflon/Ag/Niobium		
Gold Backing	0.24	0.43
0.5 mil	0.22	0.52
1.0 mil	0.22	0.81
5 mil	0.23	0.82
10 mil		
Silver Backing	0.08	0.68
2 mil	0.08	0.81
5 mil	0.09	0.88
10 mil		
Tefzel (Gold Backing)	0.29	0.47
0.05 mil	0.26	0.61
1.0 mil		
Tapes	0.95	0.90
235-3M Black	0.20	0.03
425-3M Aluminum Foil	0.22	0.03
1170-3M Electrical Tape	0.15	0.59
850-3M Mylar-Aluminum Backing	0.09	0.03
7361-Mystic Aluminized Kapton	0.14	0.03
7452-Mystic Aluminum Foil	0.21	0.03
7800-Mystic Aluminum Foil	0.19	0.03
Y9360-3M Aluminized Mylar	0.23	0.02
3M Gold Tape	0.26	0.04
3M Gold Tape	0.40	0.89
ITO/FEP type A/Inconel/Y966 Courtaulds	0.11	0.79
Tedlar 3M838	0.87 – 0.90	0.86

V. Total Hemispherical Reflectance Curves for Selected Thermal Control Coatings

The reflectance measurements contained in the following pages represents a compilation of reflectance measurements of commonly used thermal control coatings compiled at GSFC over a period of 20 years. The data was compiled using a variety of instruments, including a Beckman DK2, Perkin-Elmer Lamda-9, AZ-Tek LPSR 200 & 300 and was collected by John Henninger, Lonny Kauder, Wanda Peters, Amani Ginyard, Monali Joshi, & Blake Miller . The accuracy of the reflectance measurements is generally ± 0.02 .

3M 1170 Electrical Tape

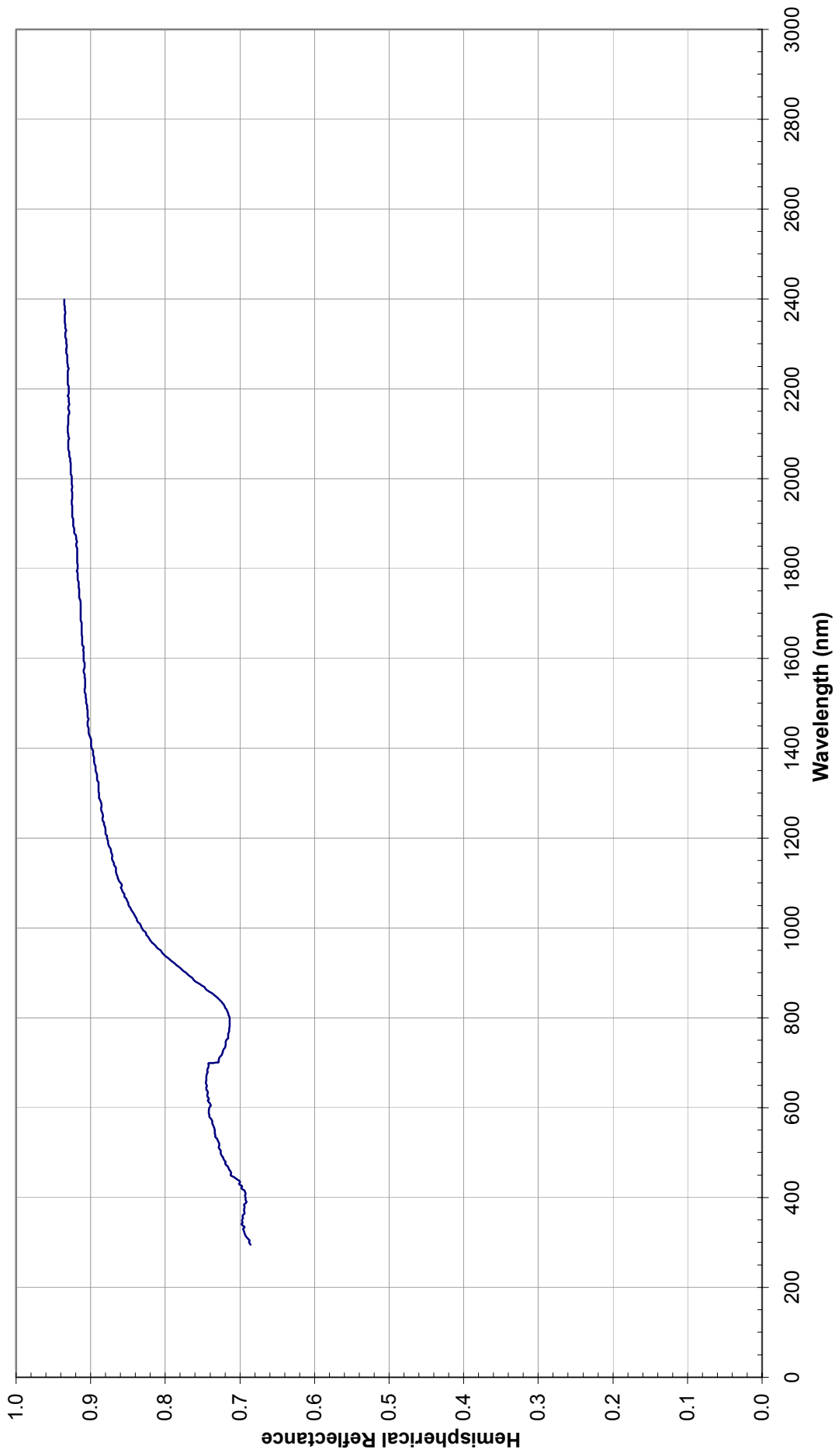


Figure 5.1

Aeroglaze A276 White Paint

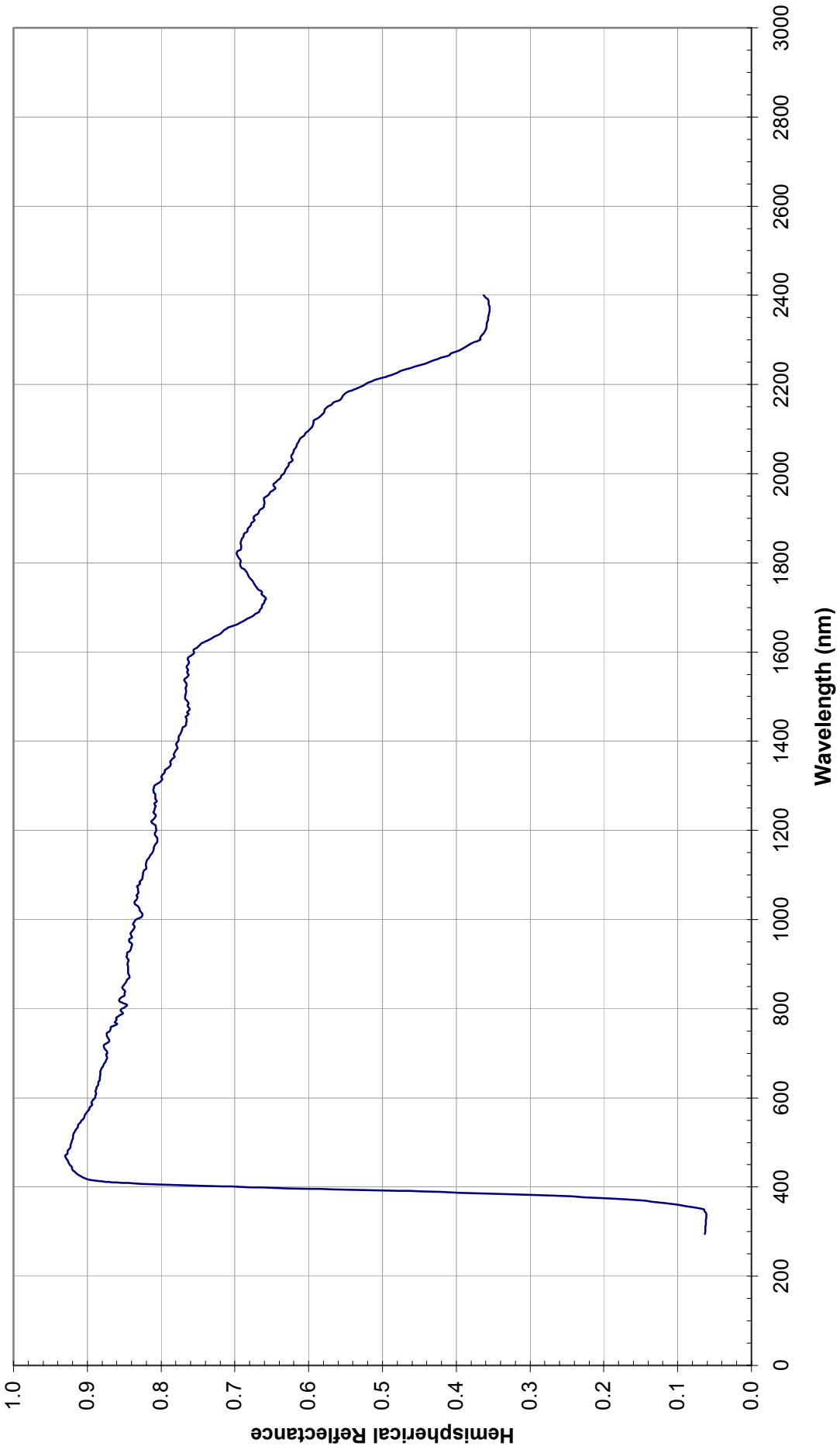


Figure 5.2

Aeroglaze A971 Yellow Paint

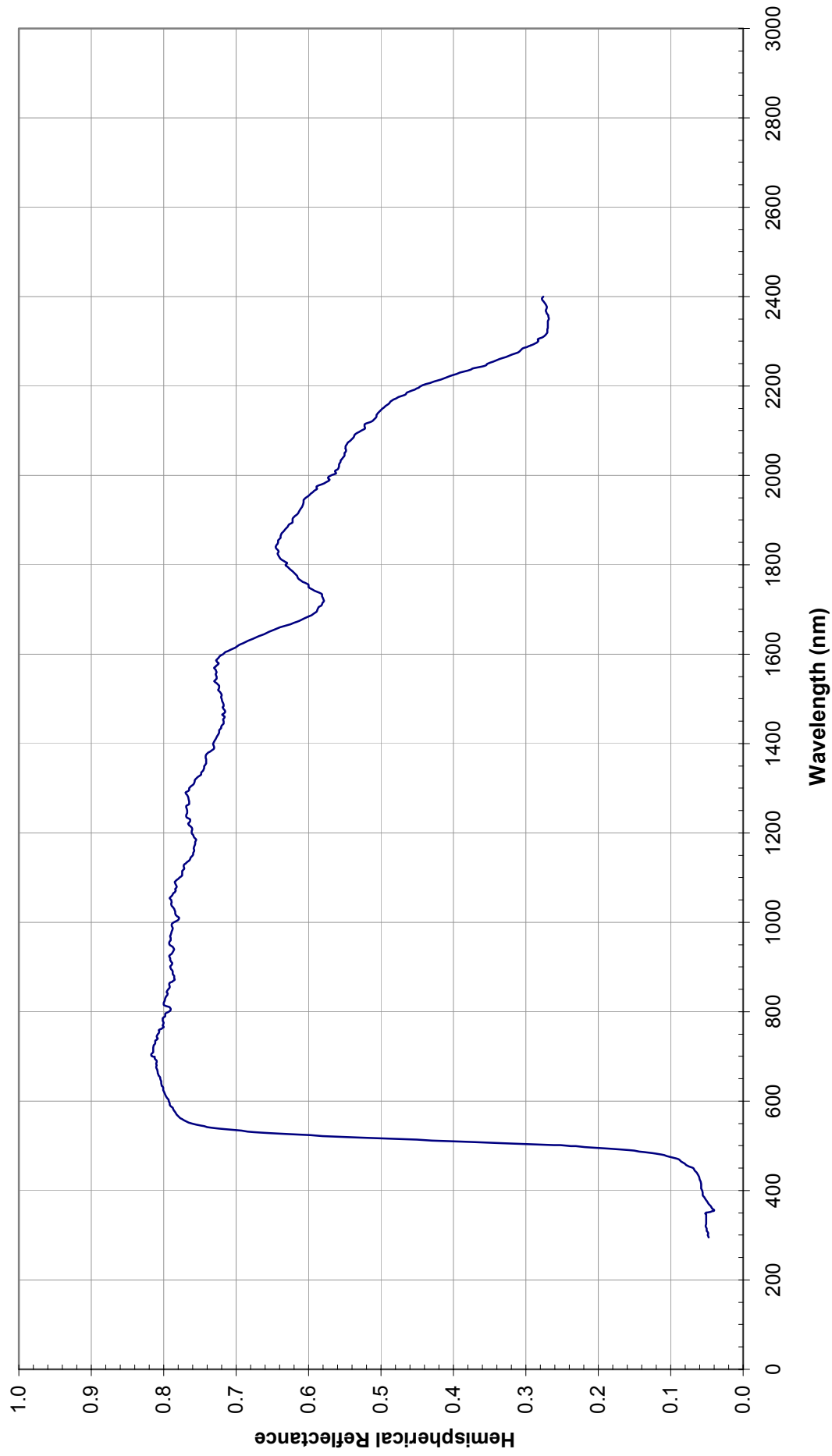


Figure 5.3

Aeroglaze Z306

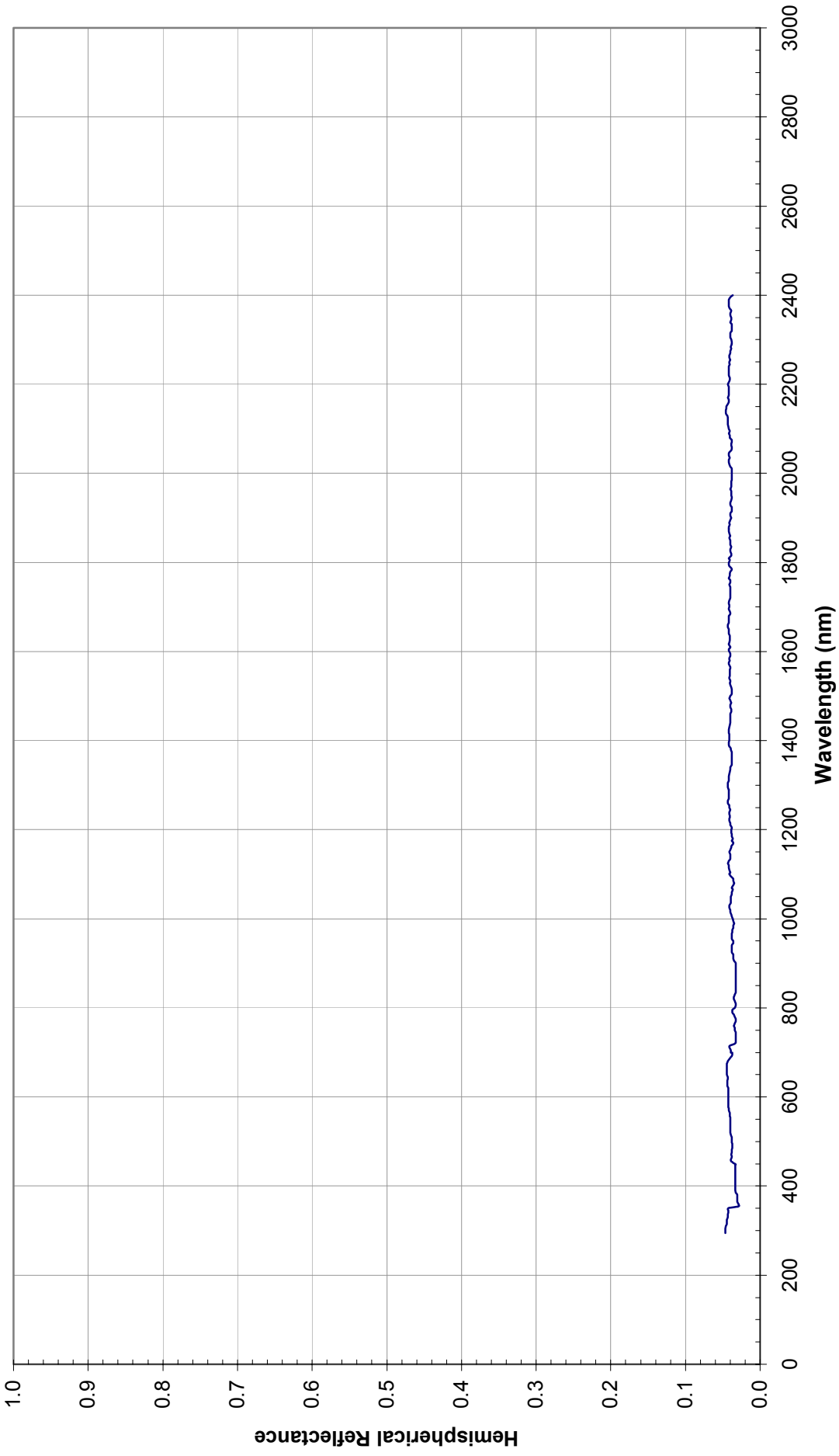


Figure 5.4

Alodyne Aluminum

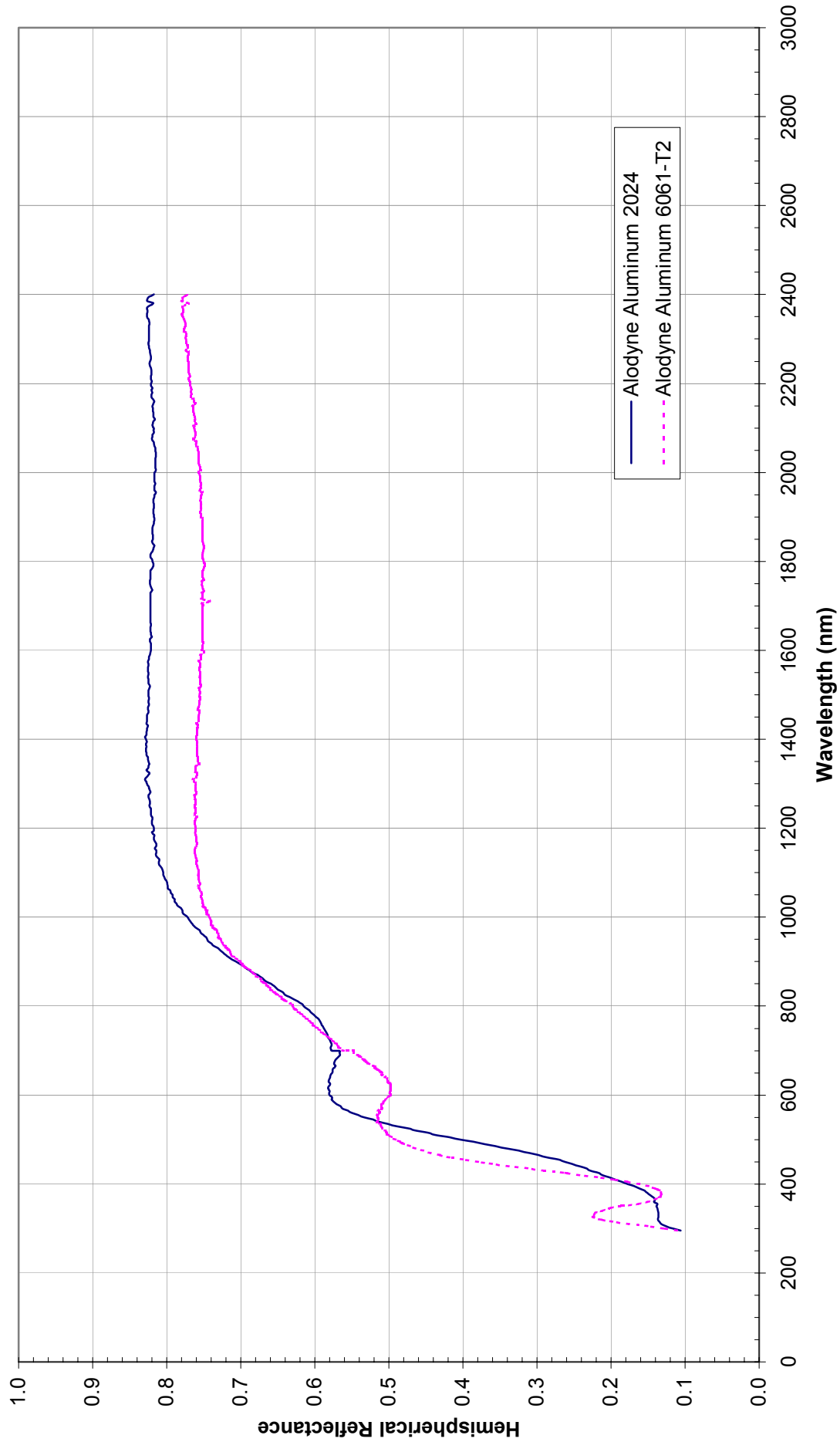


Figure 5.5

Clear Anodized Aluminum

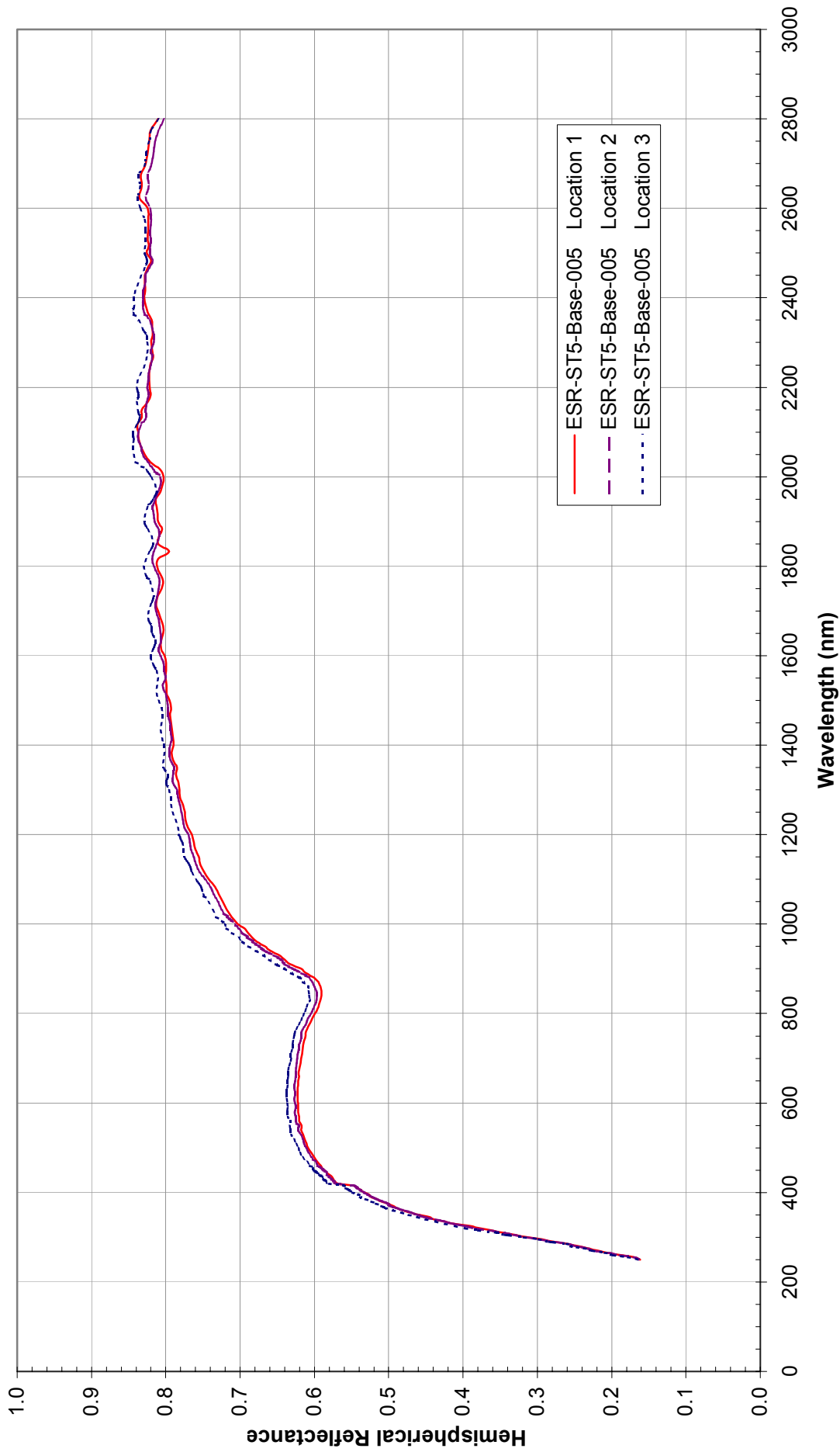


Figure 5.6

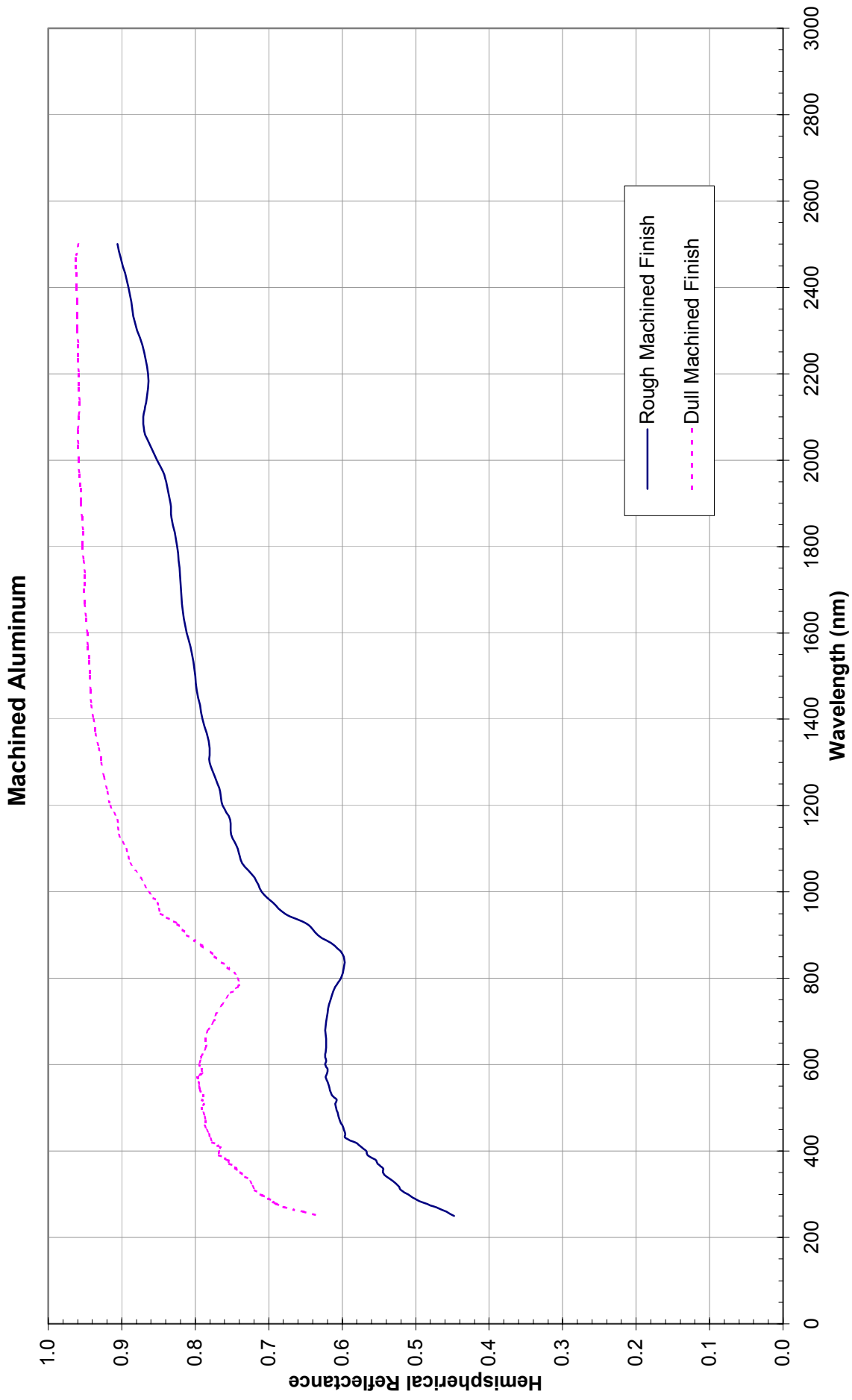


Figure 5.7

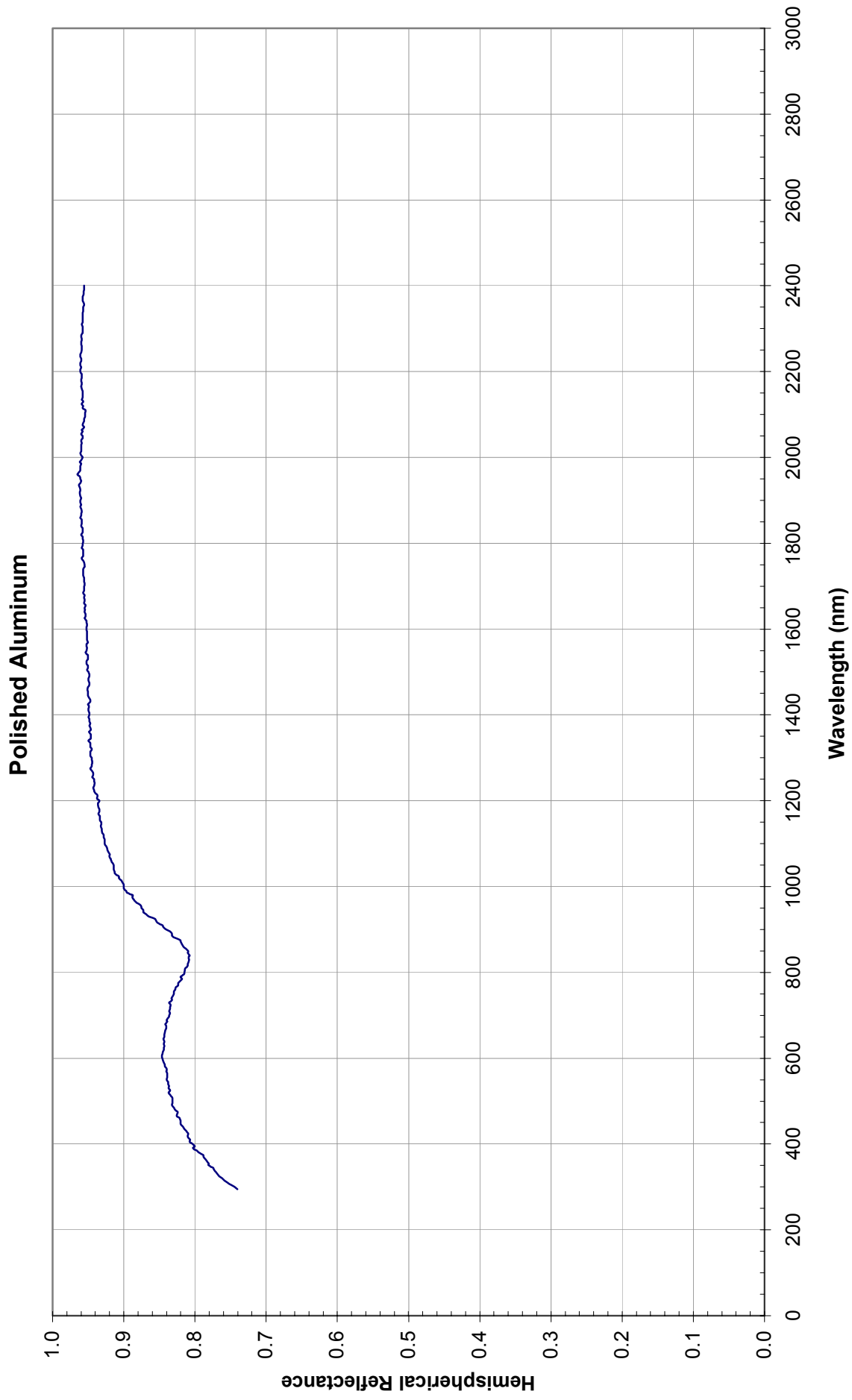


Figure 5.8

Astro-Quartz

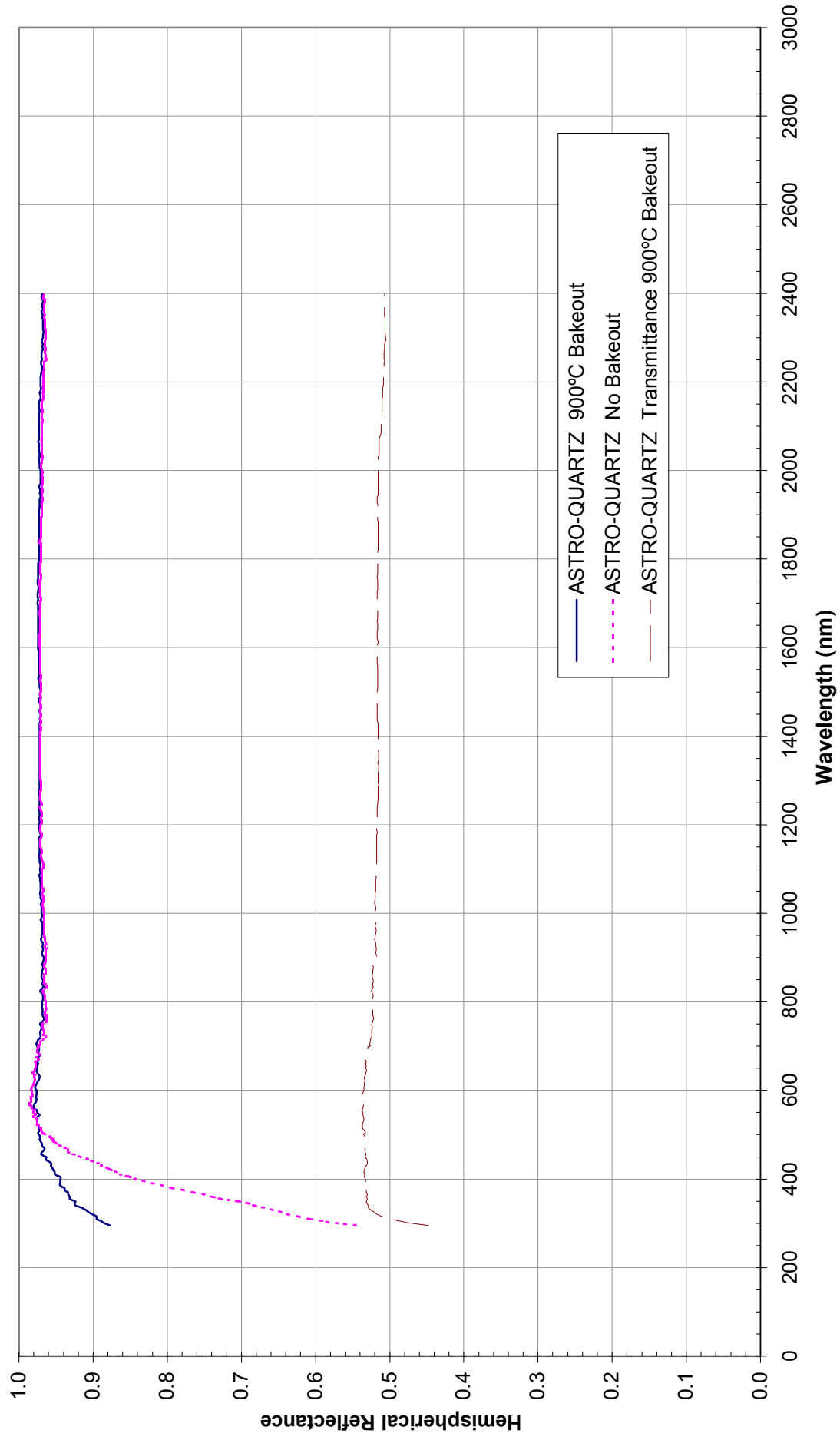


Figure 5.9

Comparison of Thick AZ93 White Paint with Z93P White Paint

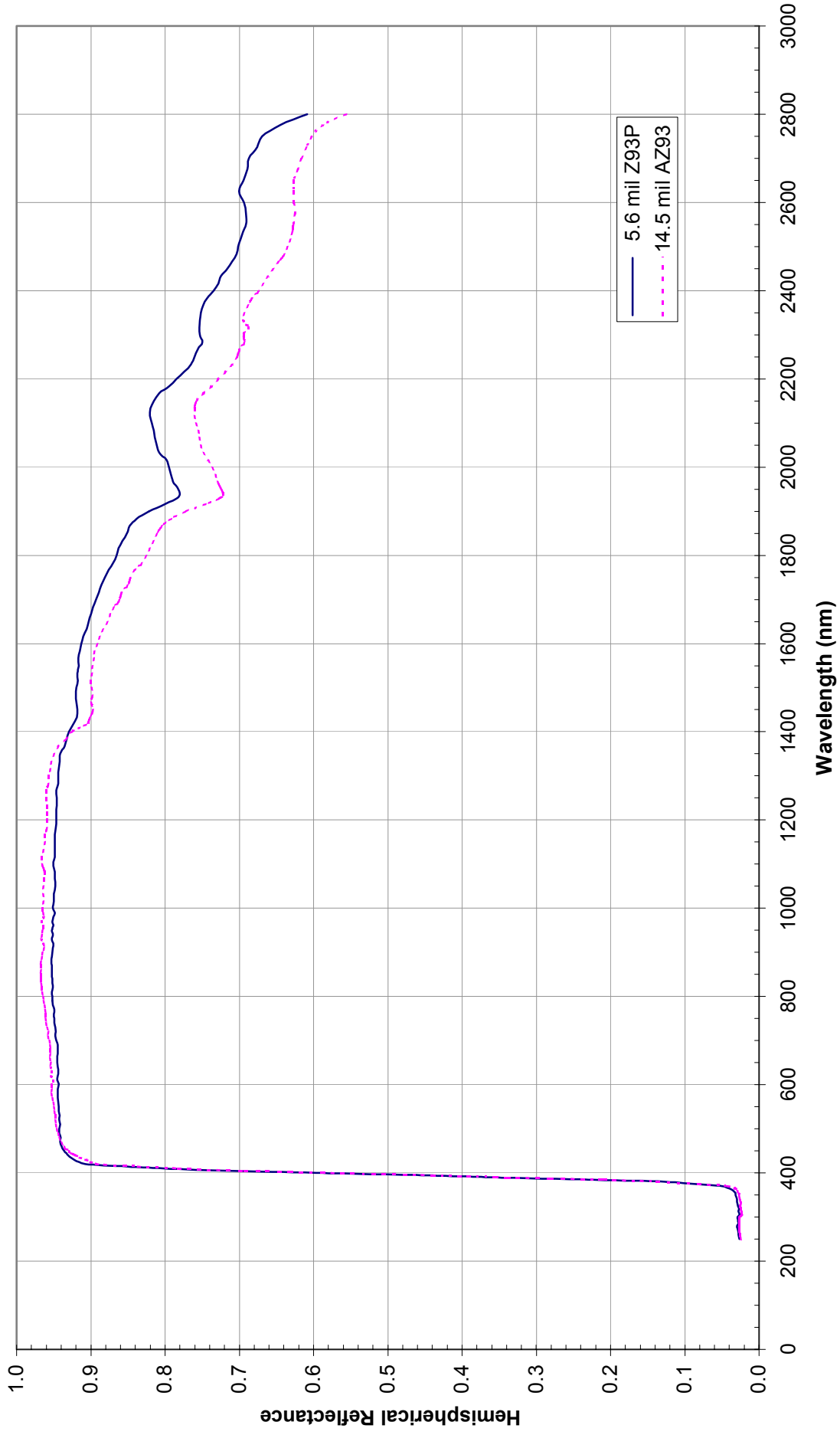


Figure 5.10

Un-coated BeCu

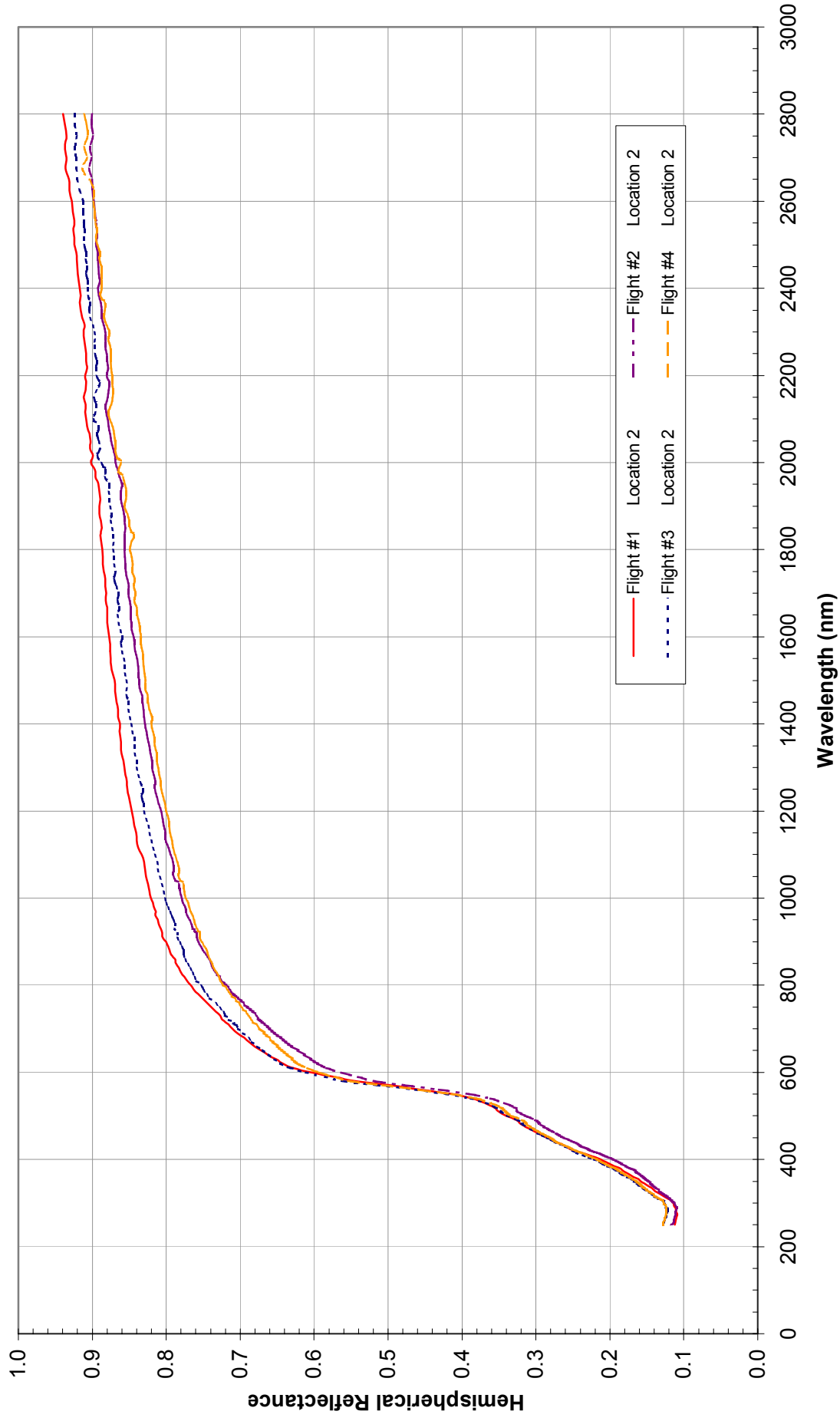


Figure 5.11

100CB Black Kapton

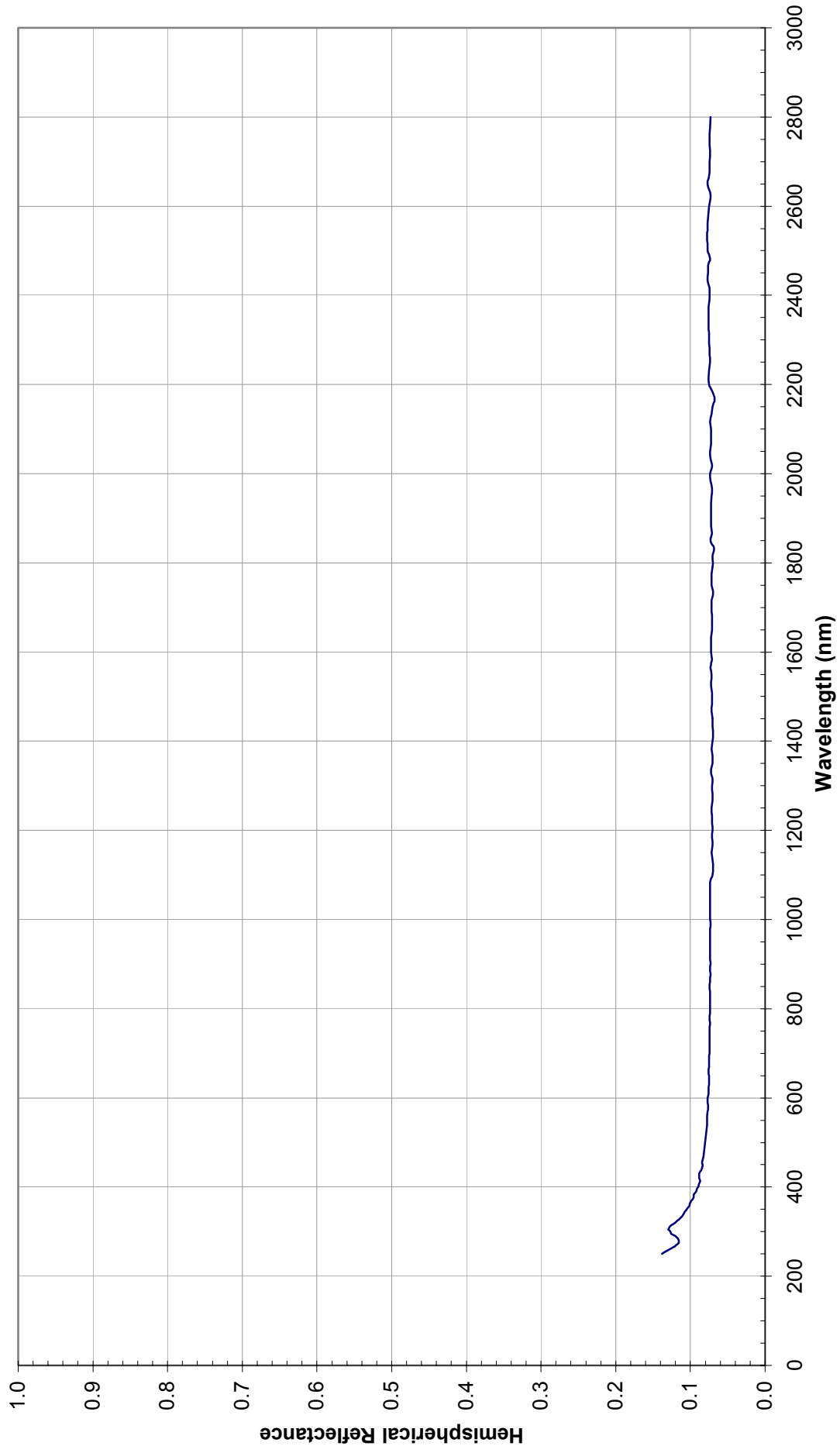


Figure 5.12

Black Kapton 100XC Film

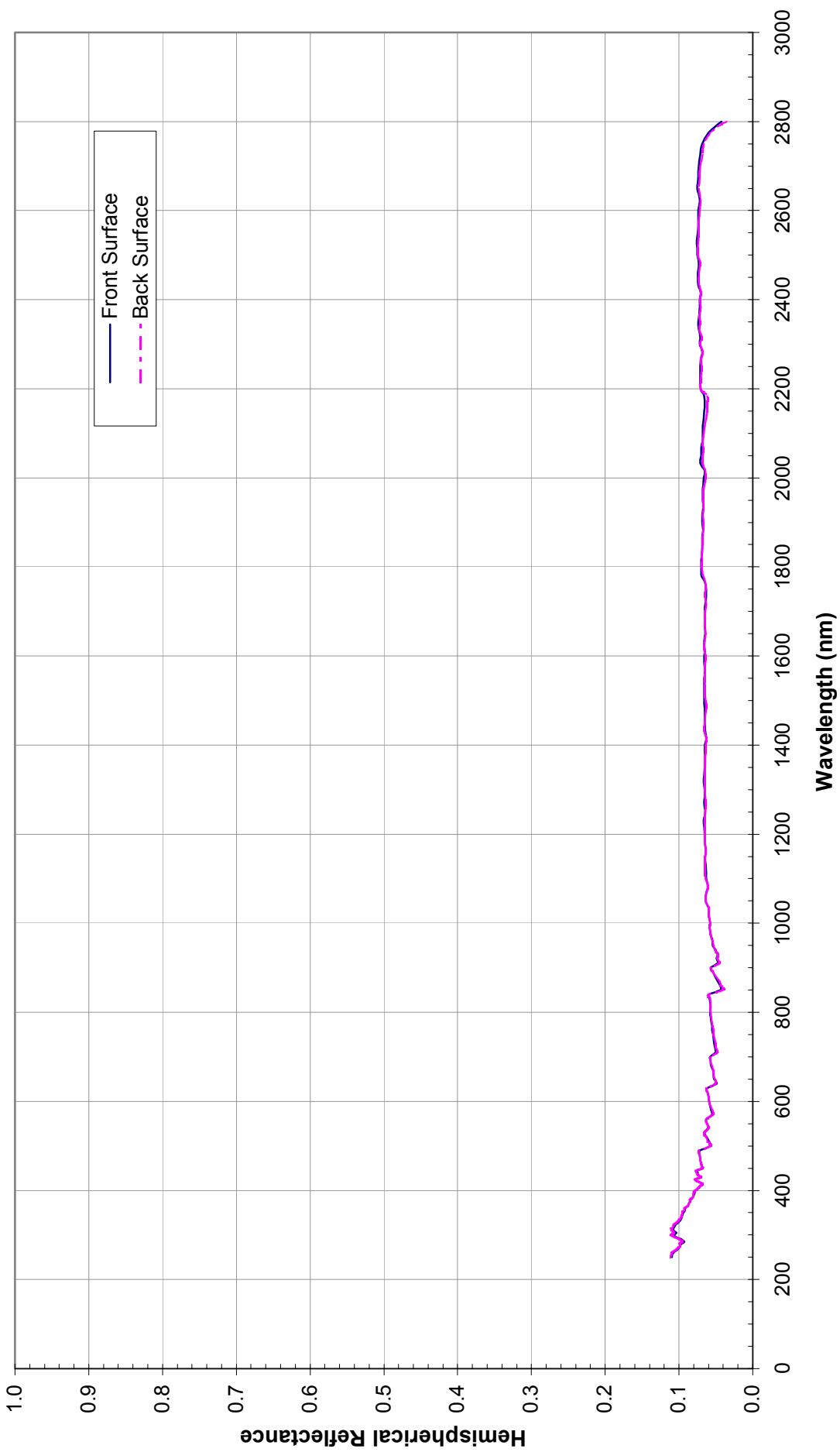


Figure 5.13

Black Nickel on Aluminum

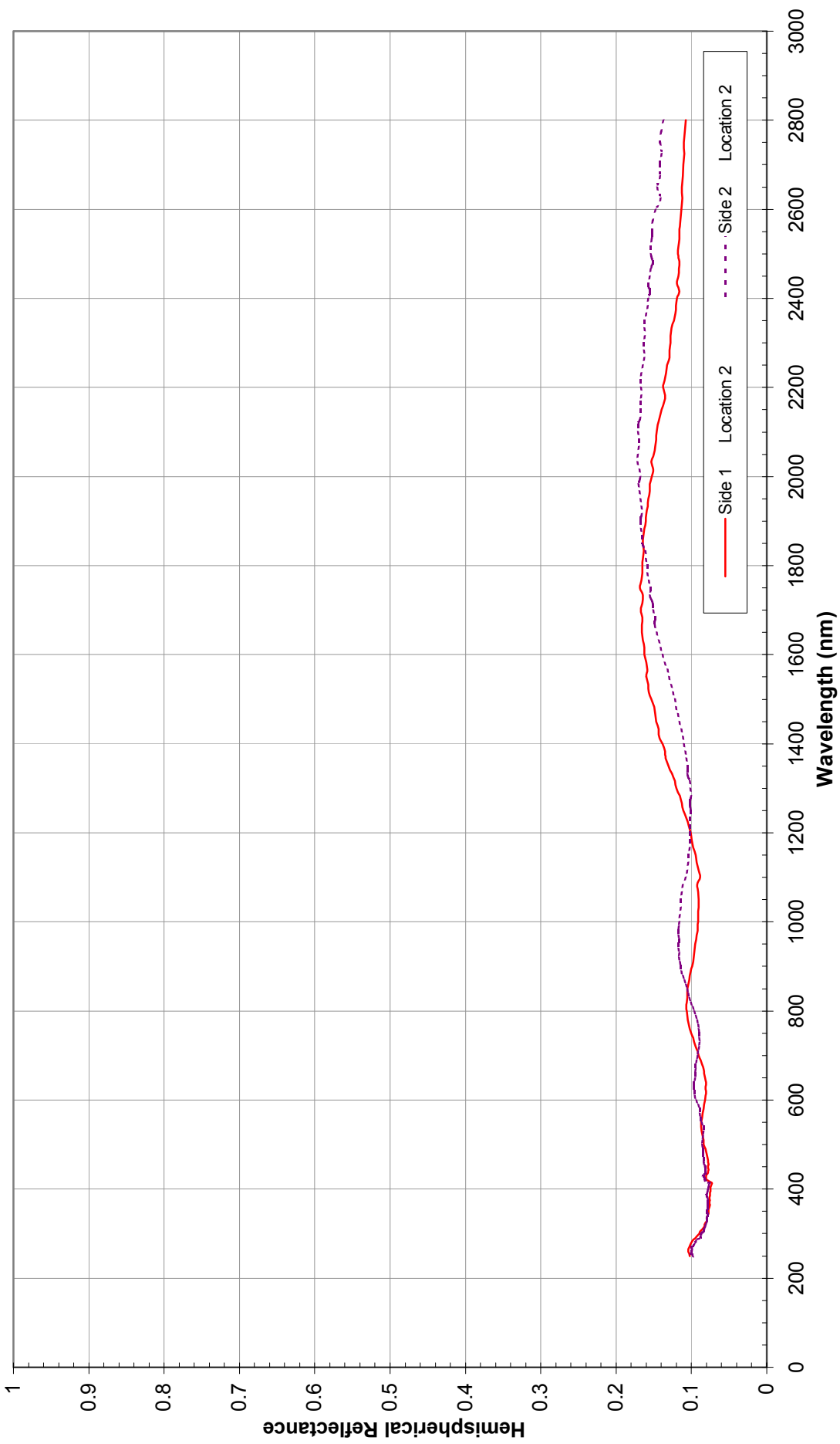


Figure 5.14

275 D-E Germanium Black Kapton "XC230"/AL
Manufactured By DUNMORE

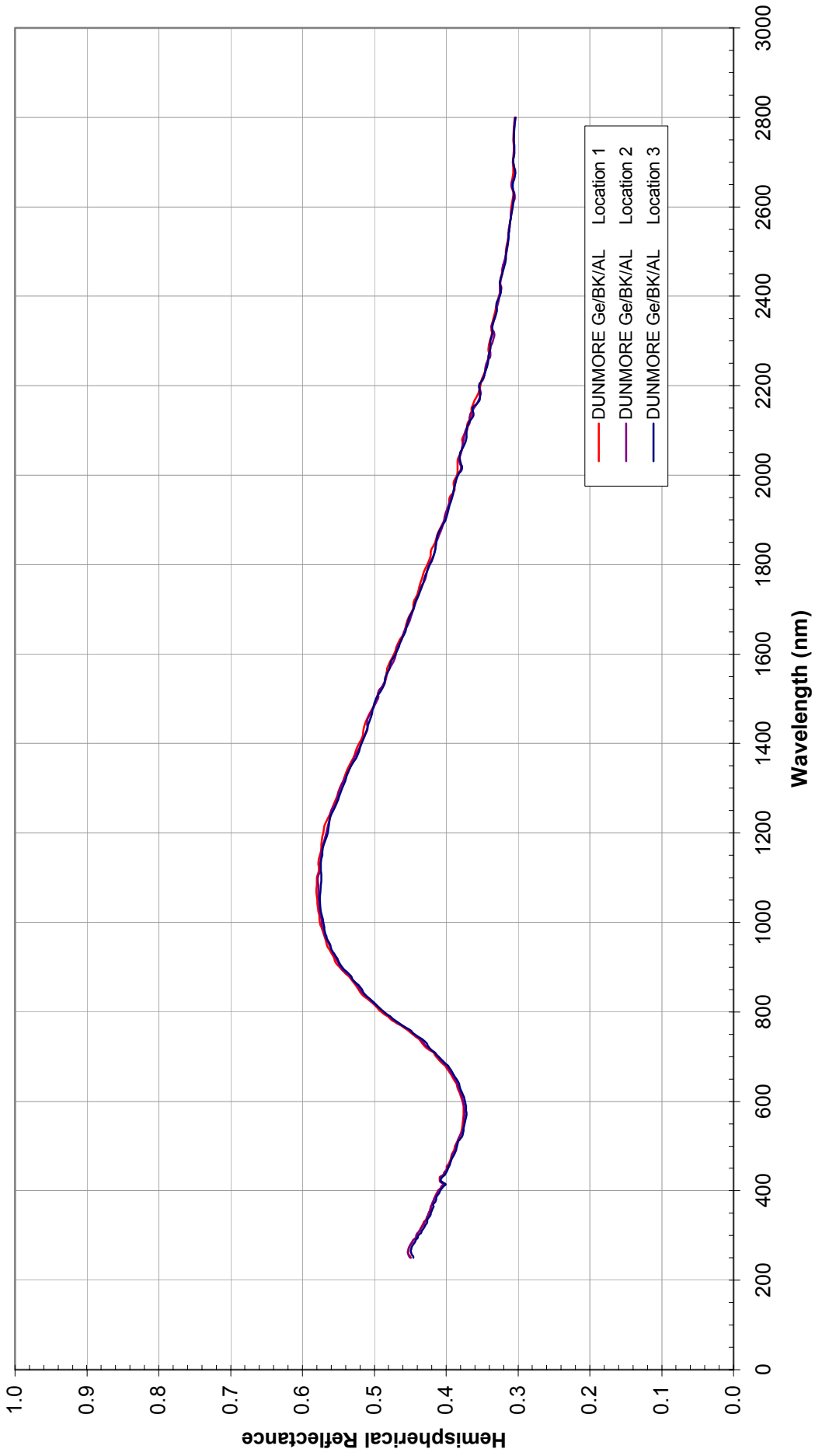


Figure 5.15

KN-90GW Reinforced Germanium Coated Black Kapton Film Manufactured By ORCON

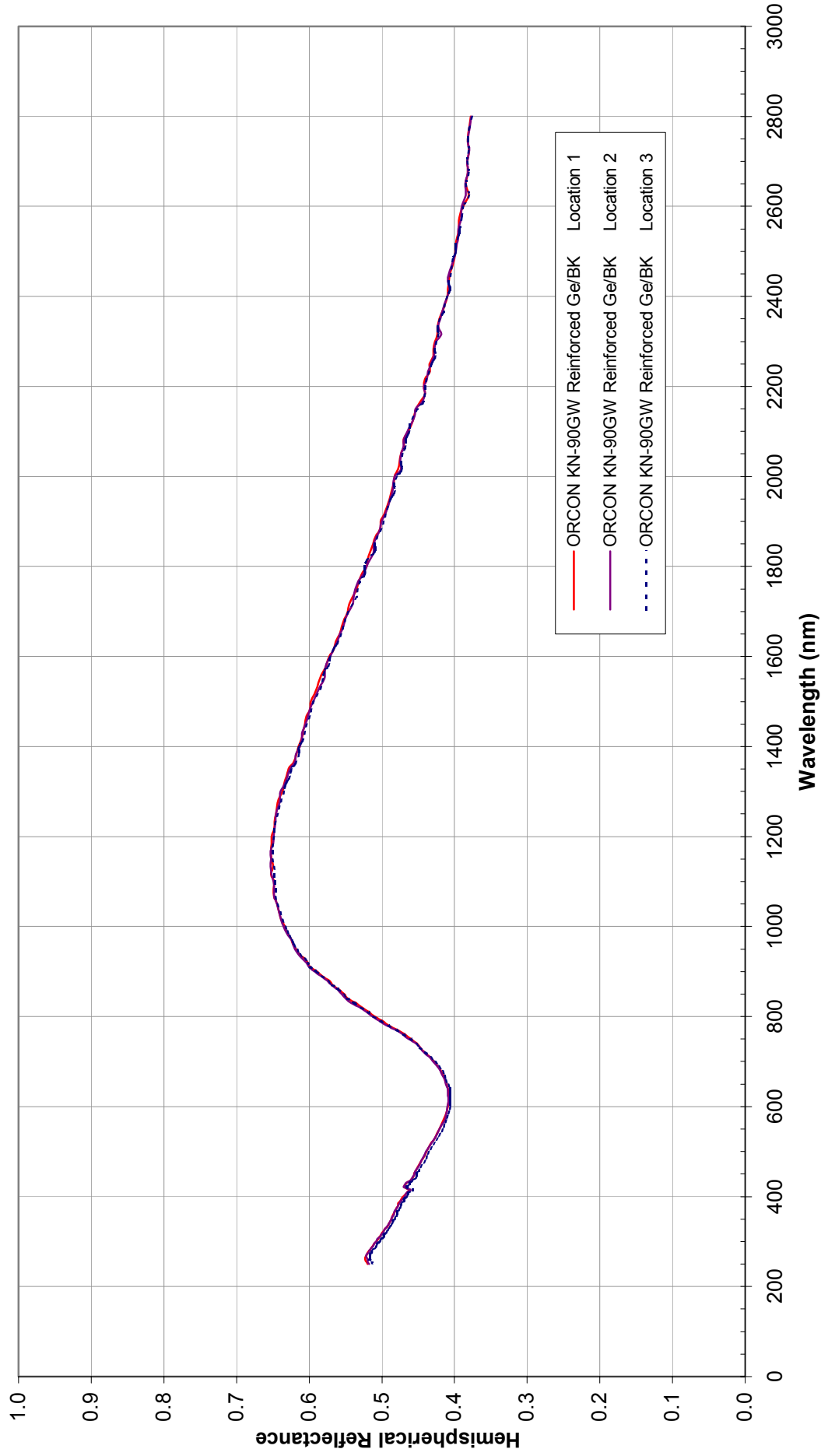


Figure 5.16

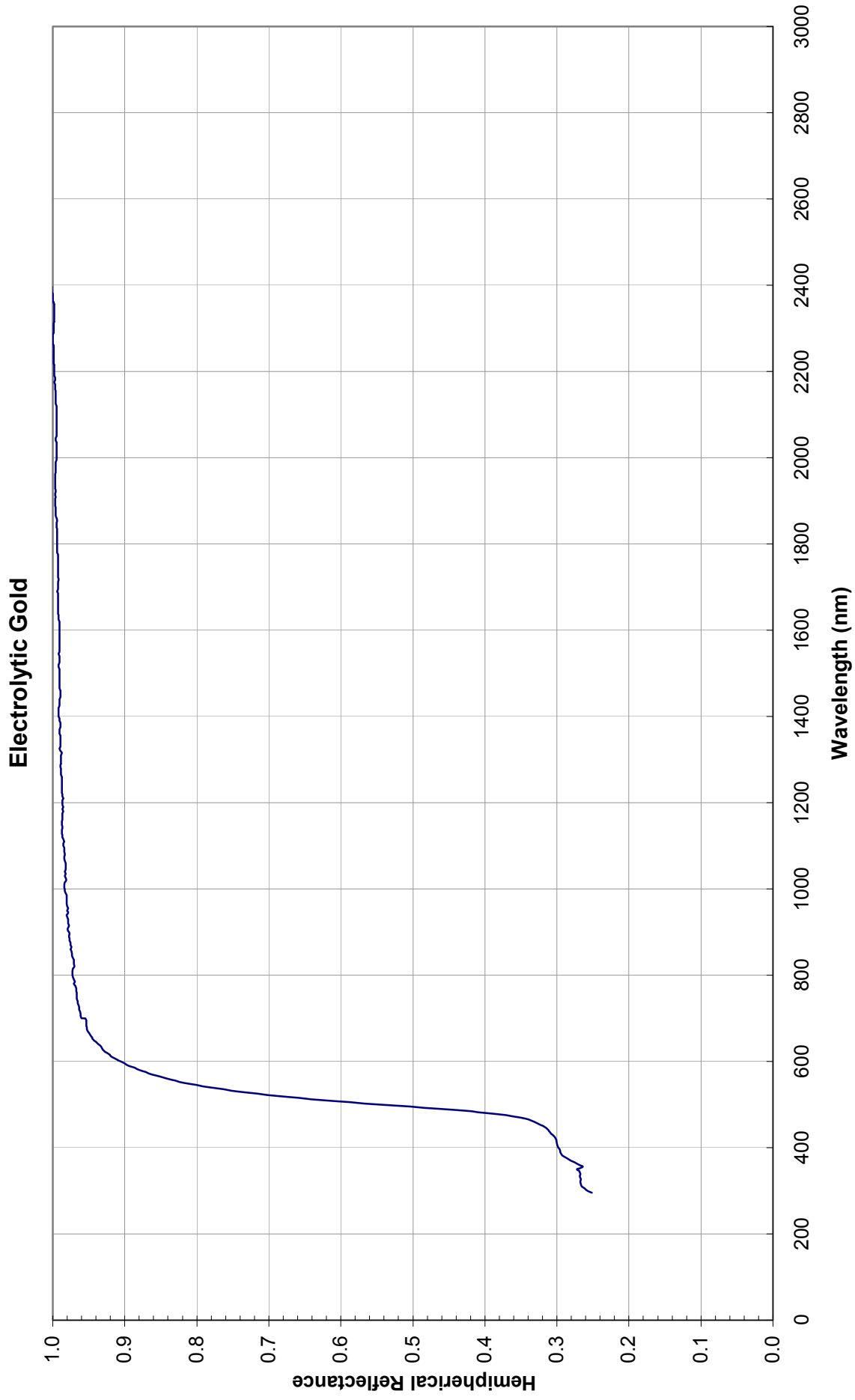


Figure 5.17

**GSFC Dark Mirror Coating
(20 degree angle of incidence)**

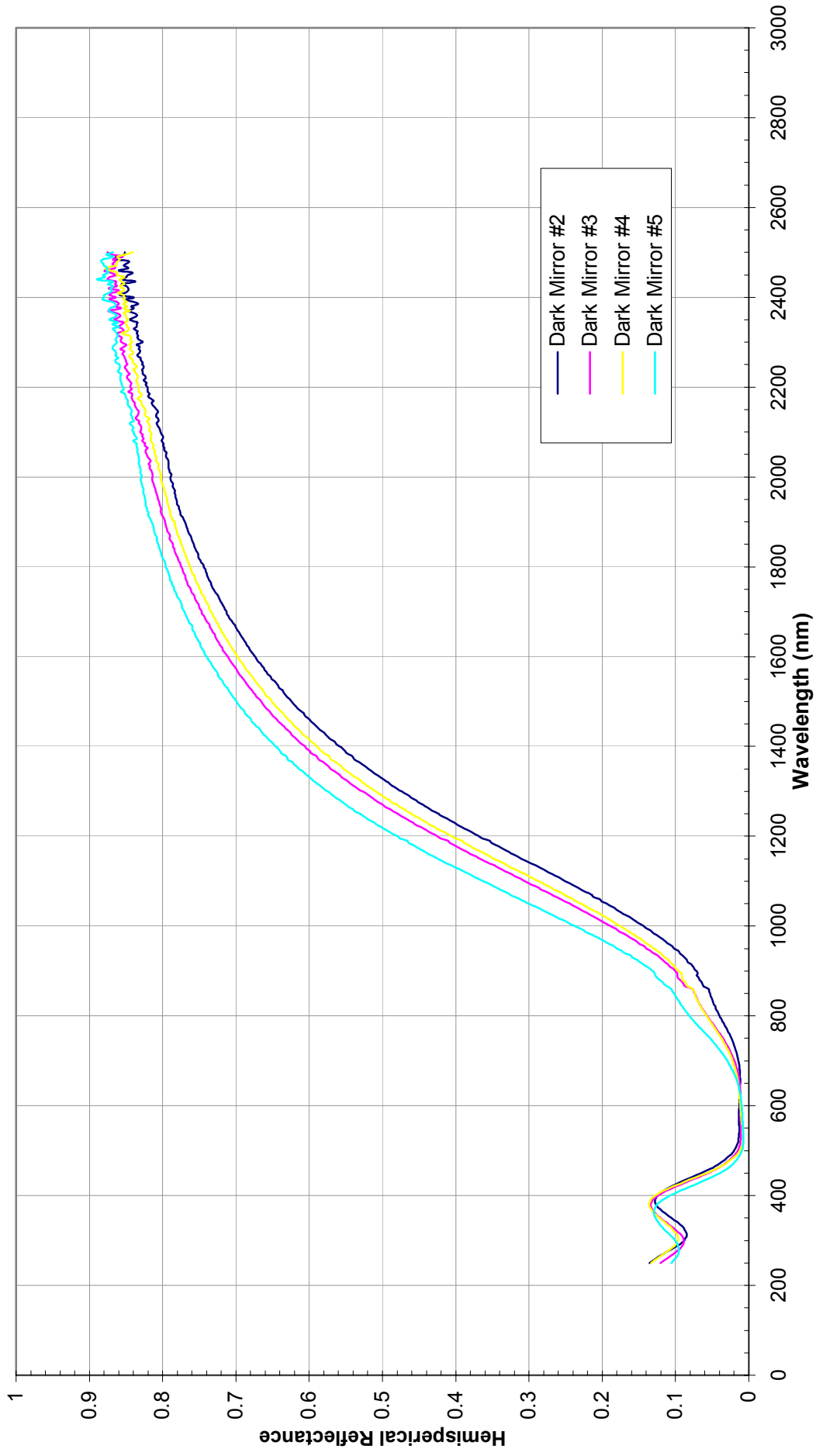


Figure 5.18

GSFC Dark Mirror Coating (45 degree angle of incidence)

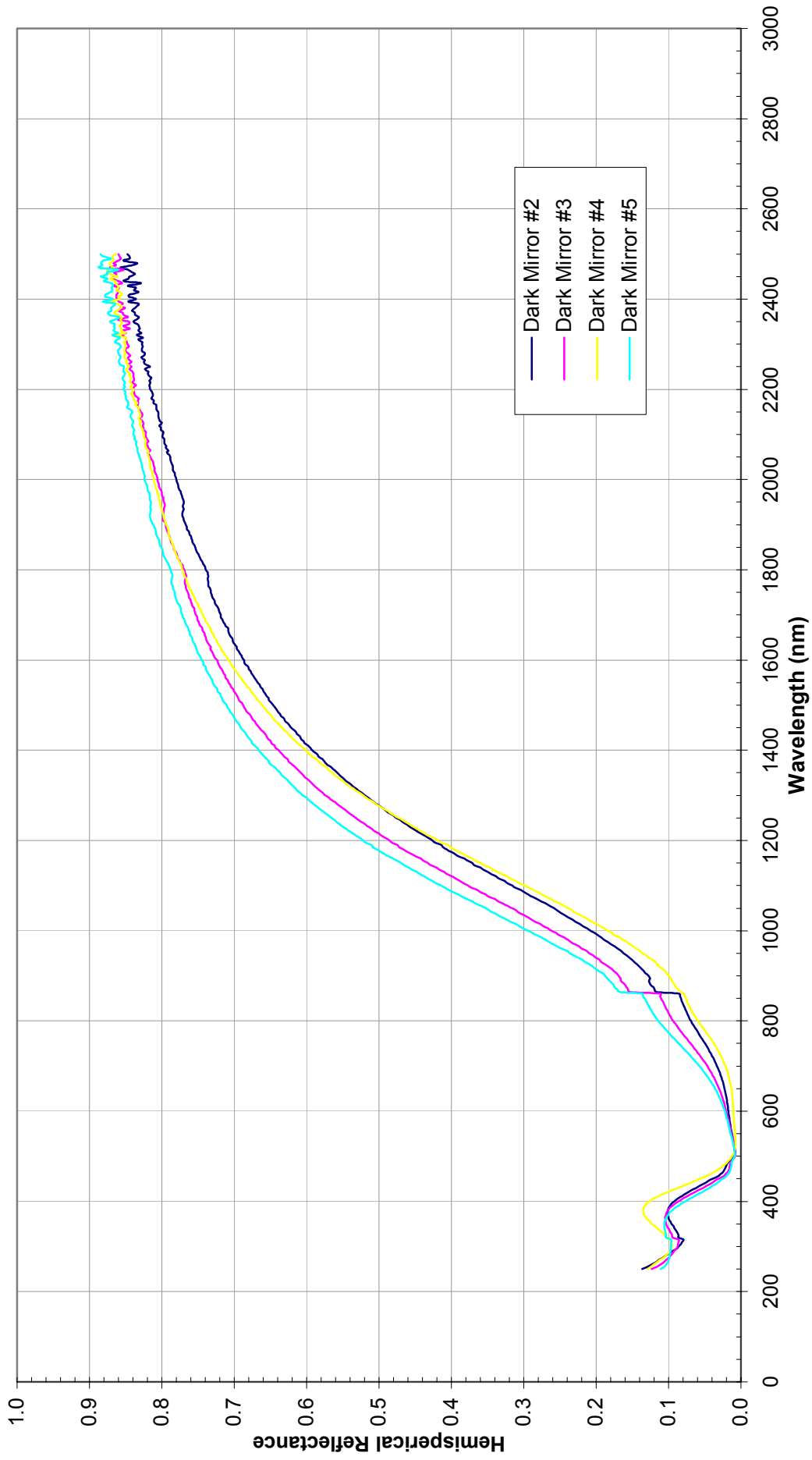


Figure 5.19

ITO Kapton

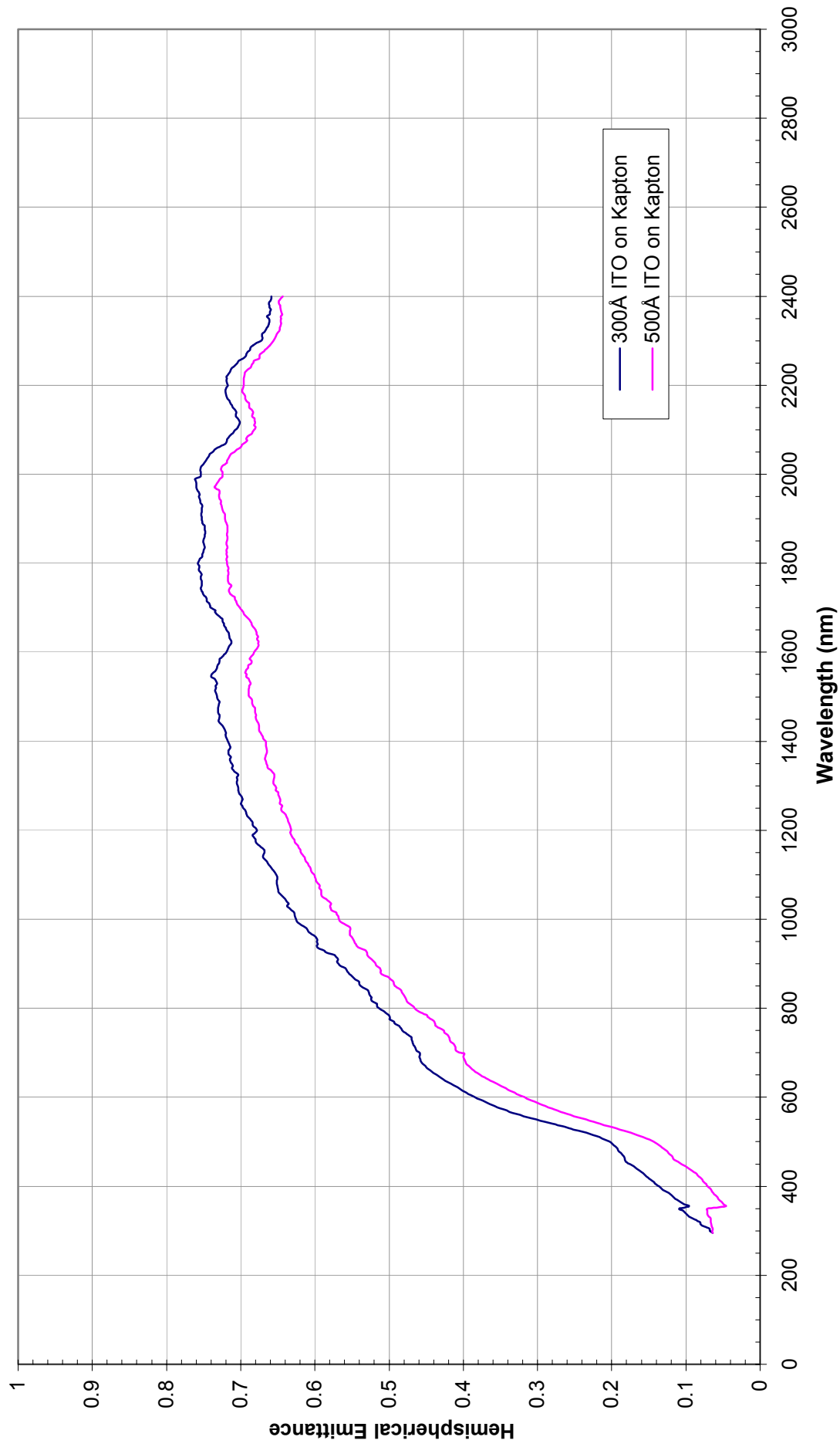


Figure 5.20

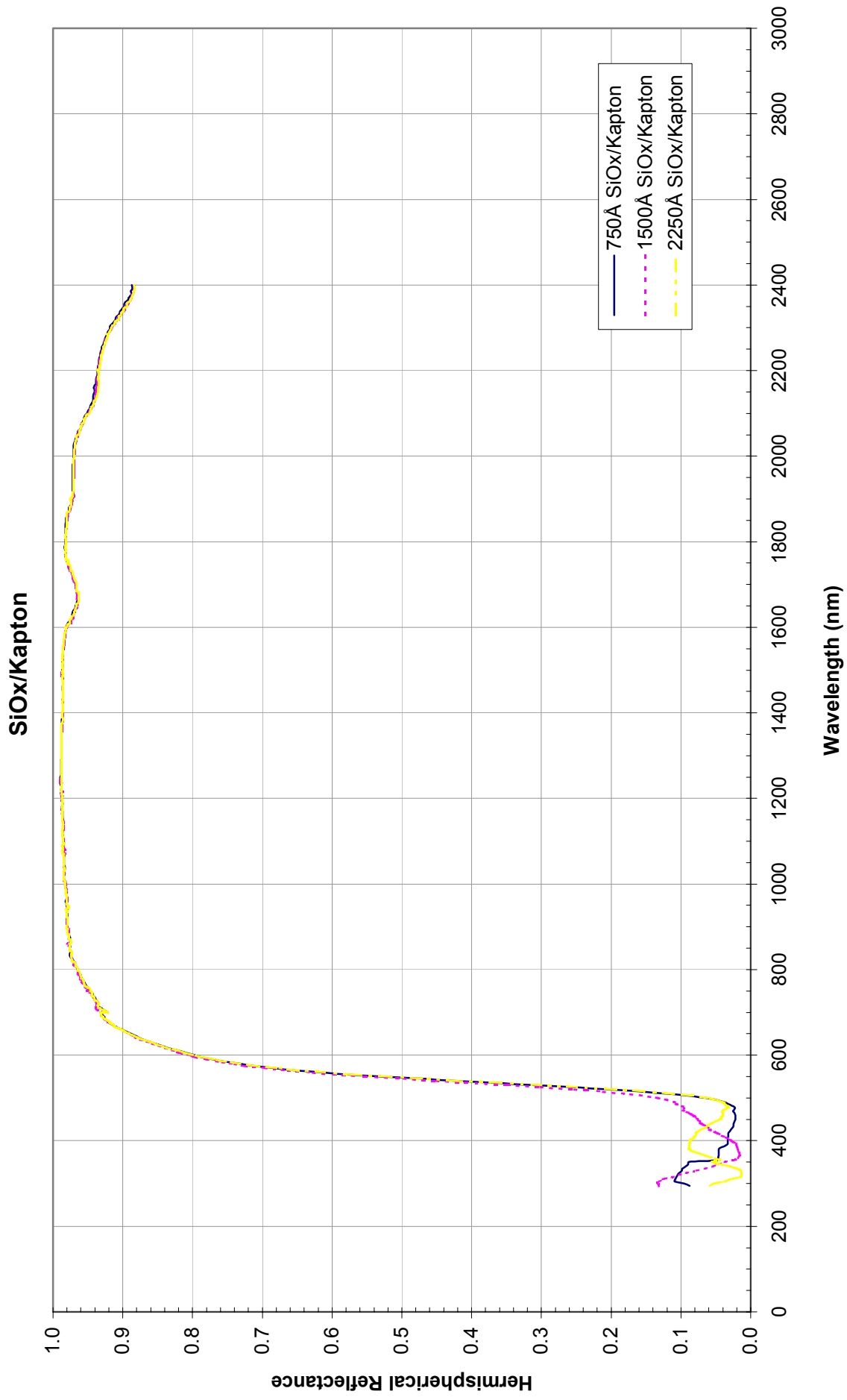


Figure 5.21

1500 Å SiOx/ Kapton/VDA

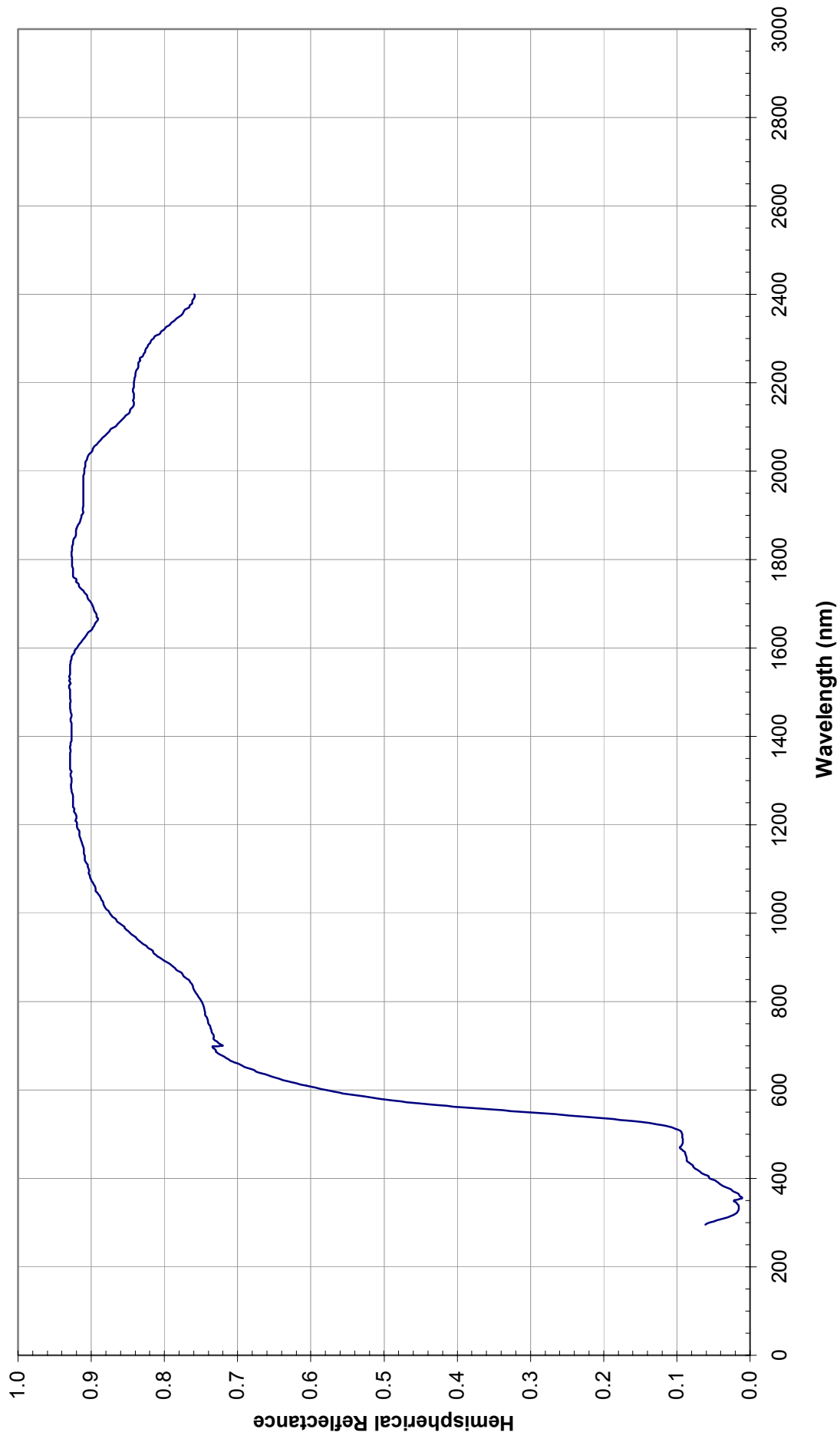


Figure 5.22

1500Å SiO_x/ VDA / Kapton

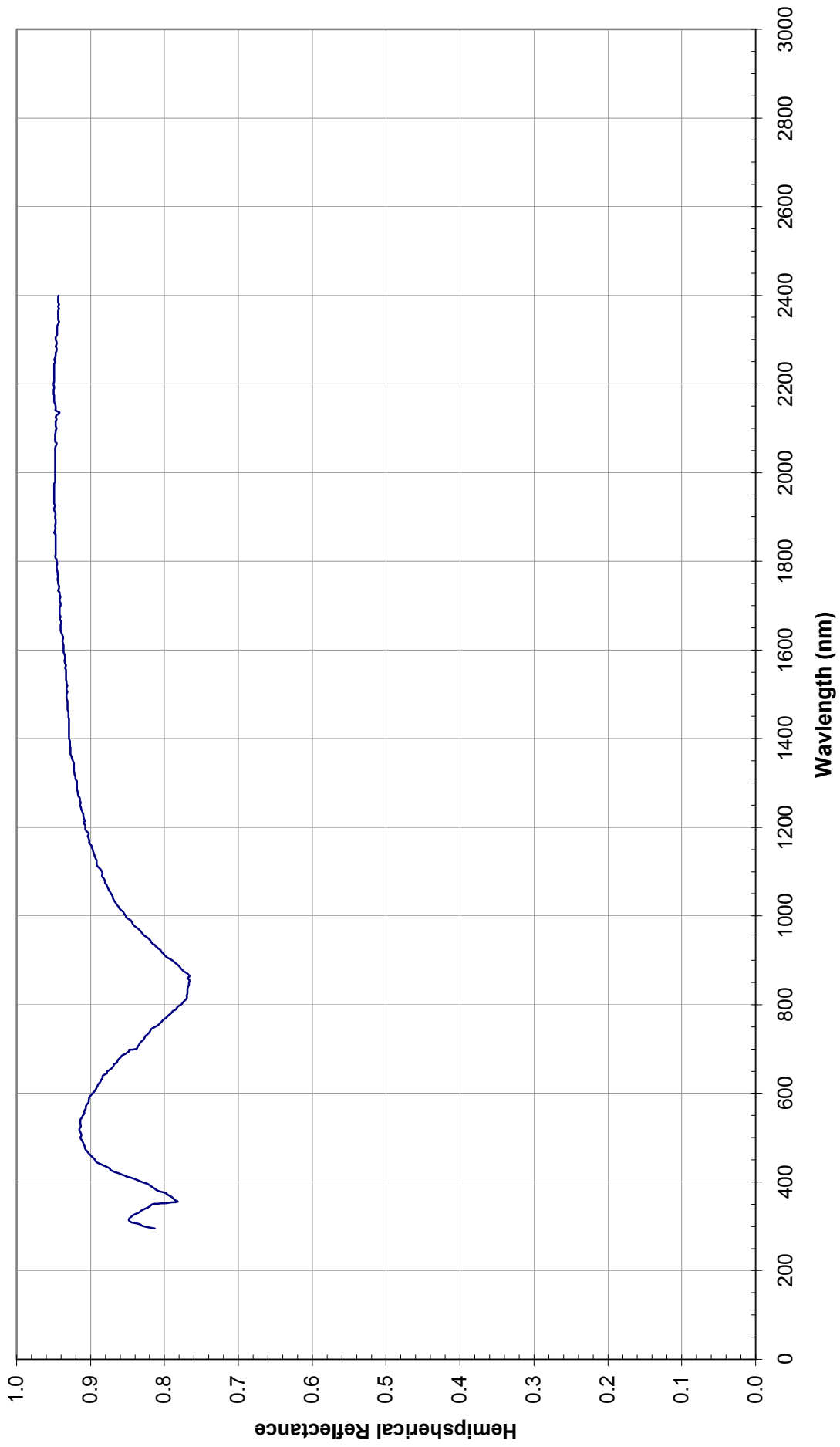


Figure 5.23

**IR Window Transmittance
UV, Vis, Near IR**

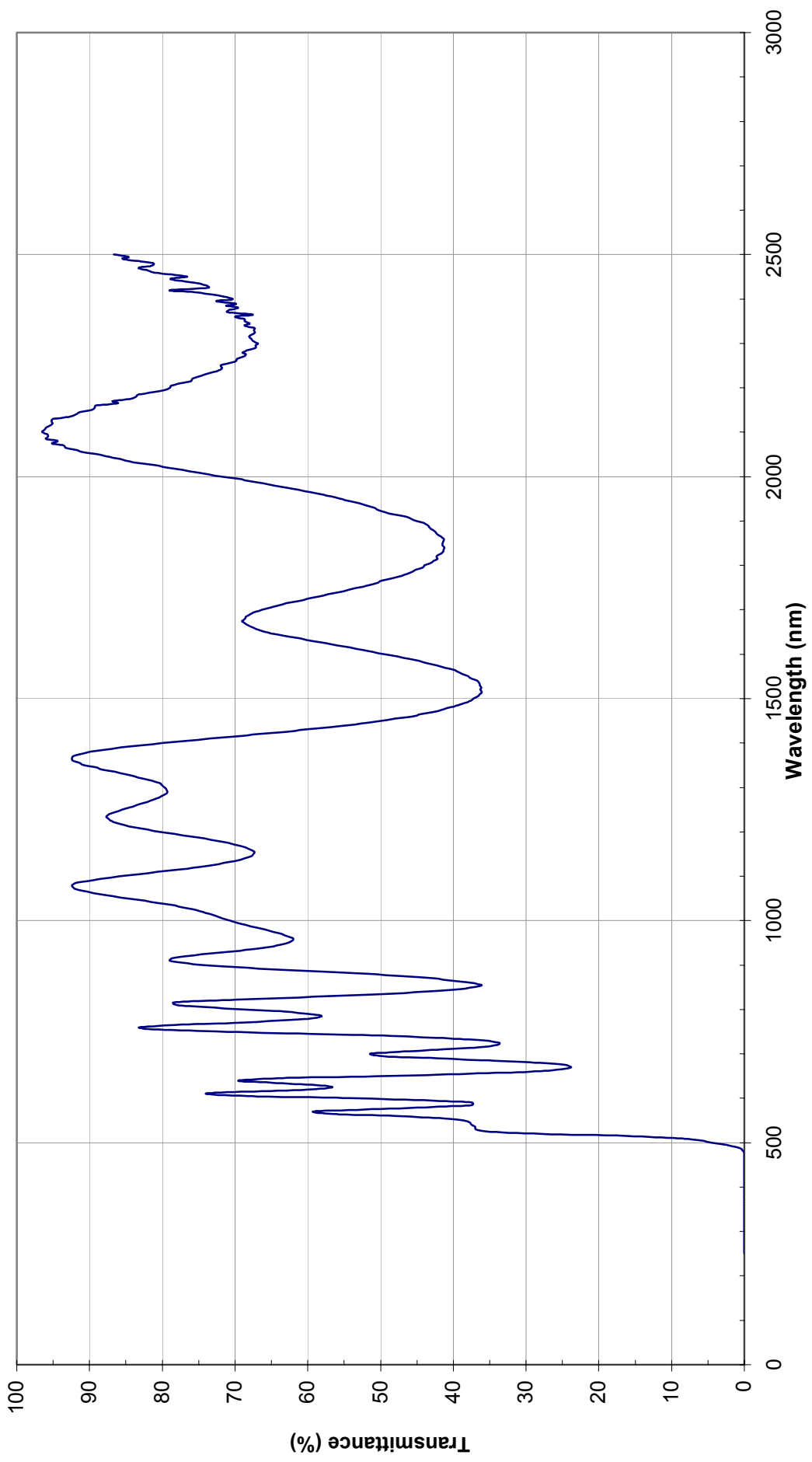


Figure 5.24

IR Window Transmittance
IR region

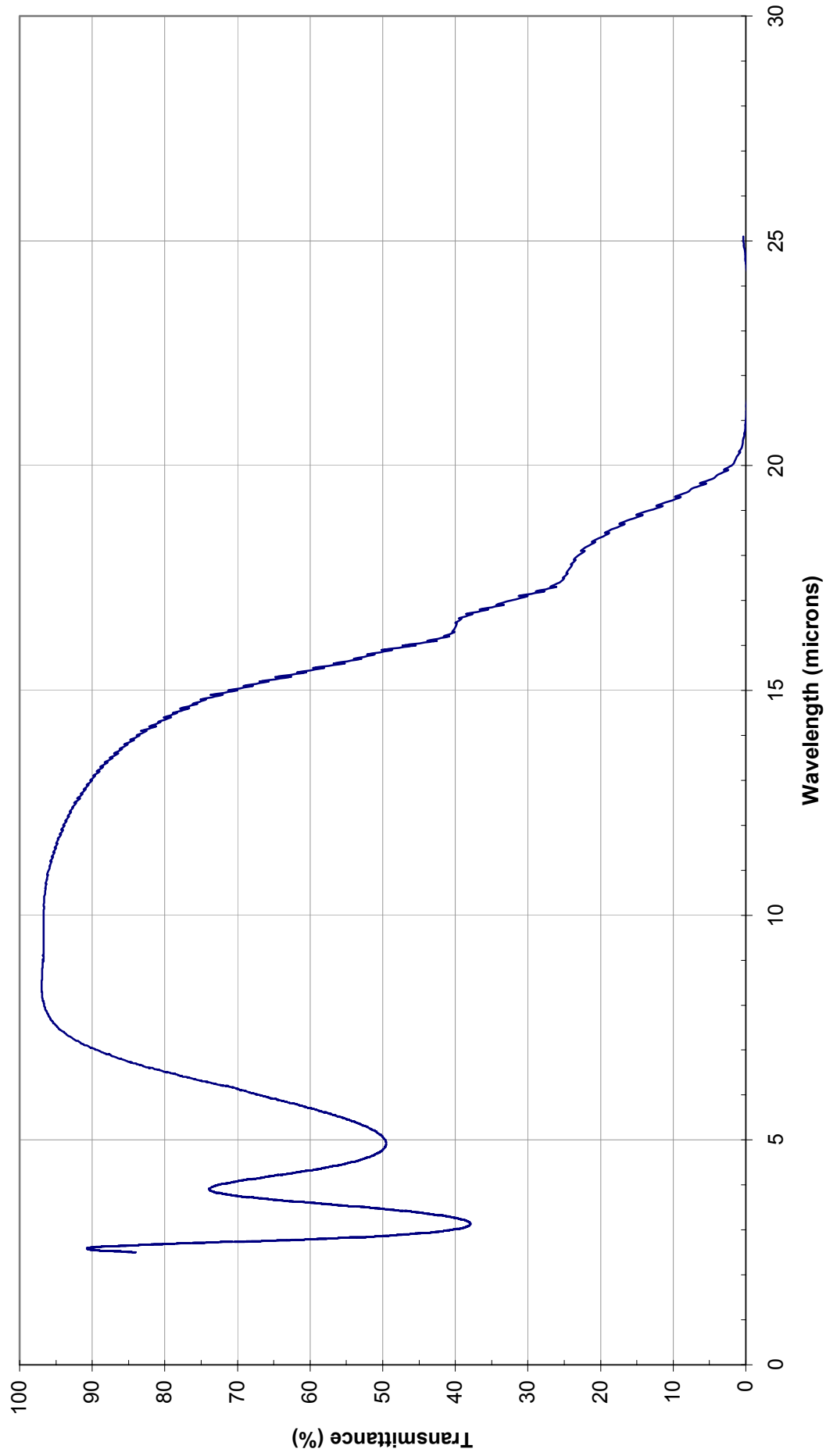


Figure 5.25

MS74

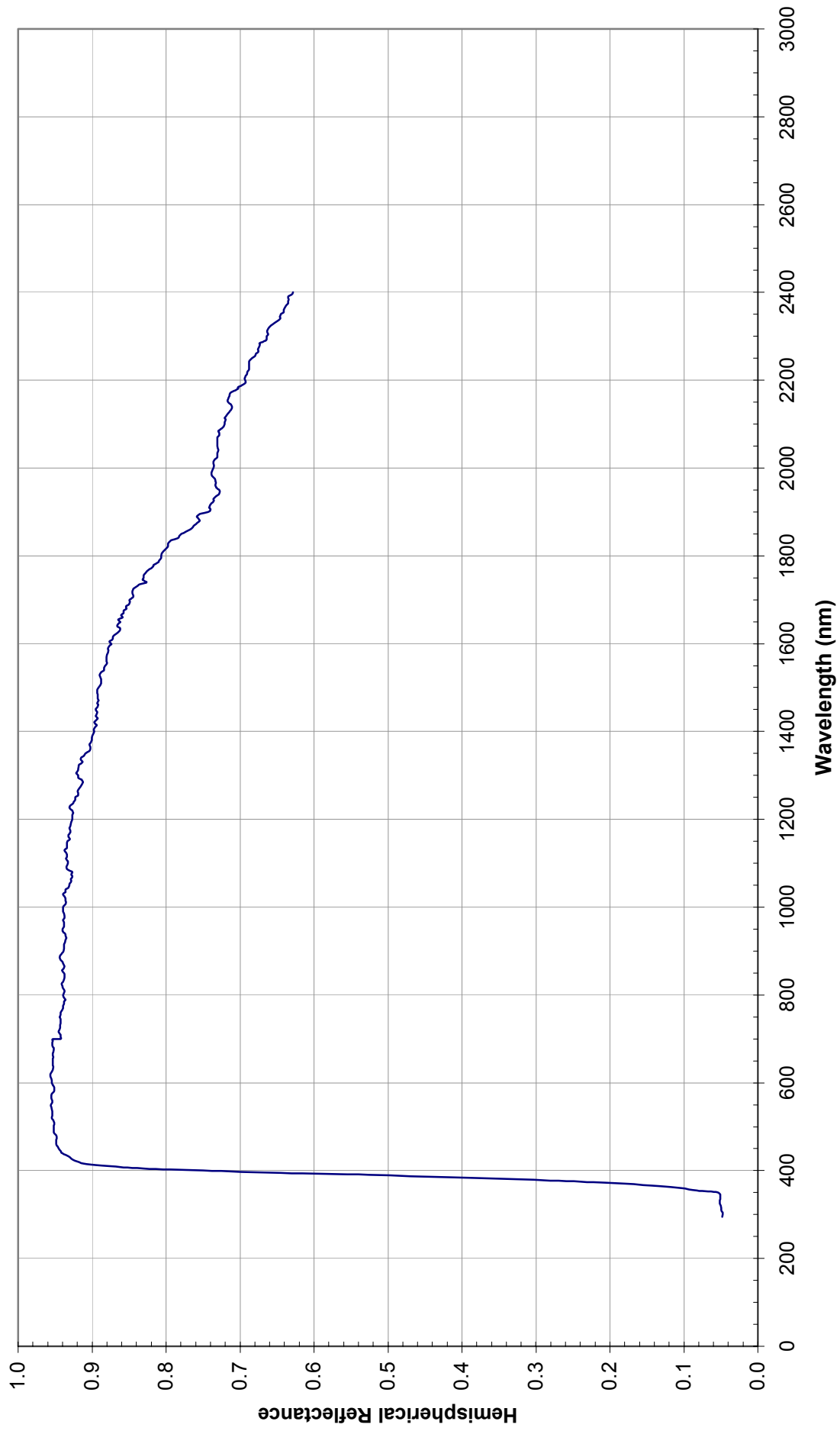


Figure 5.26

GSFC MSA94B

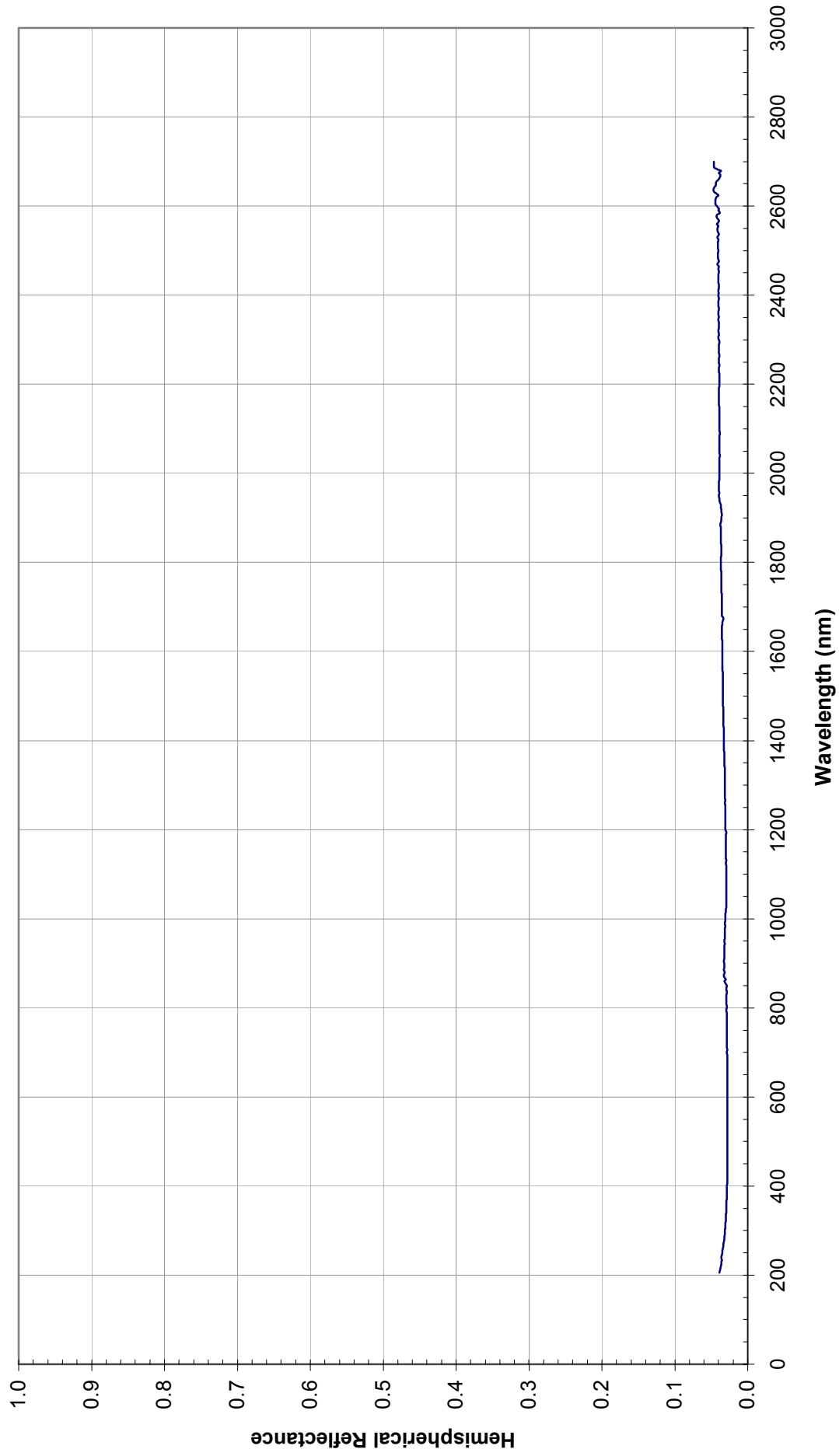


Figure 5.27

NS43G

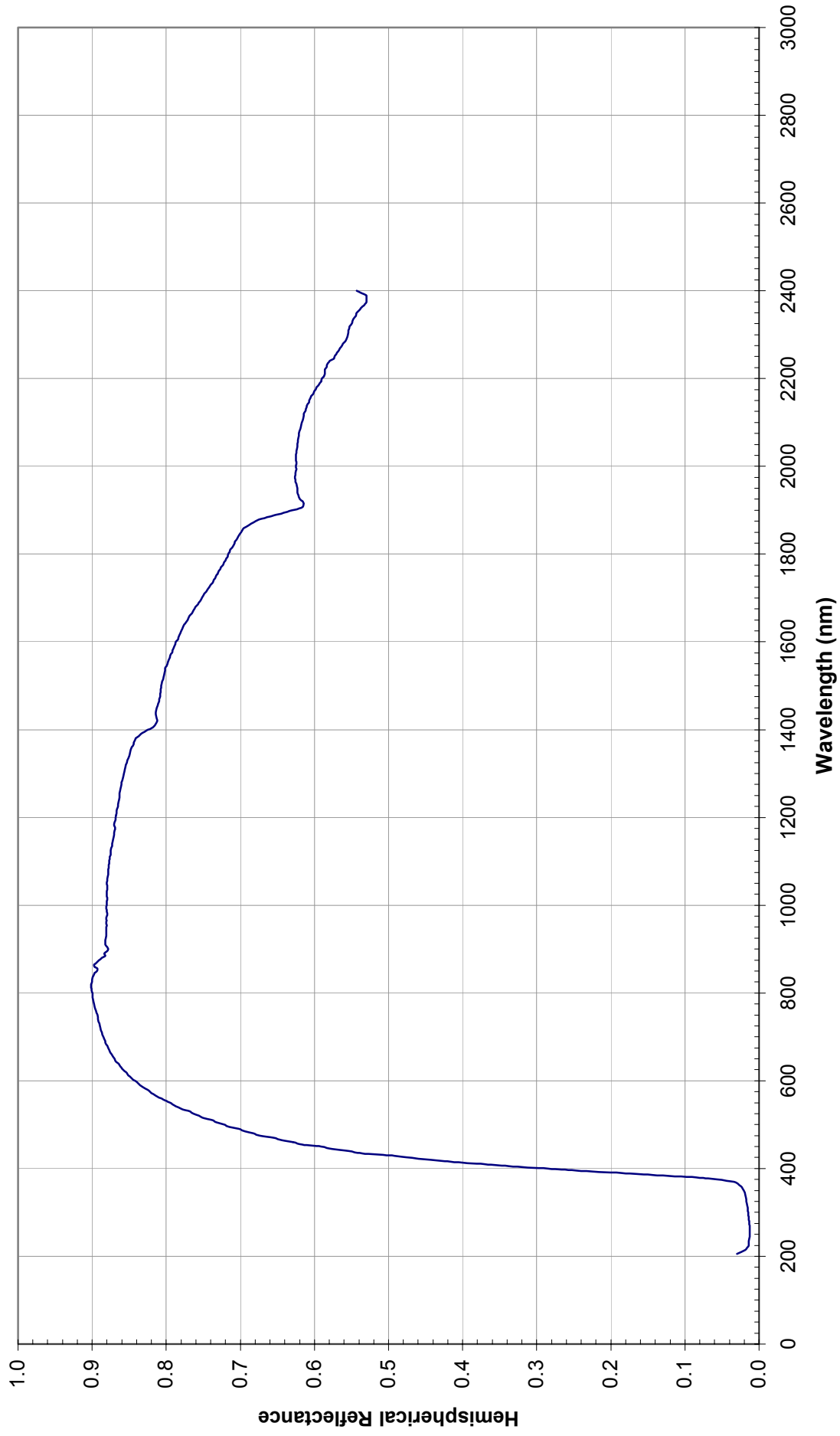


Figure 5.28

GSFC NSB69-82

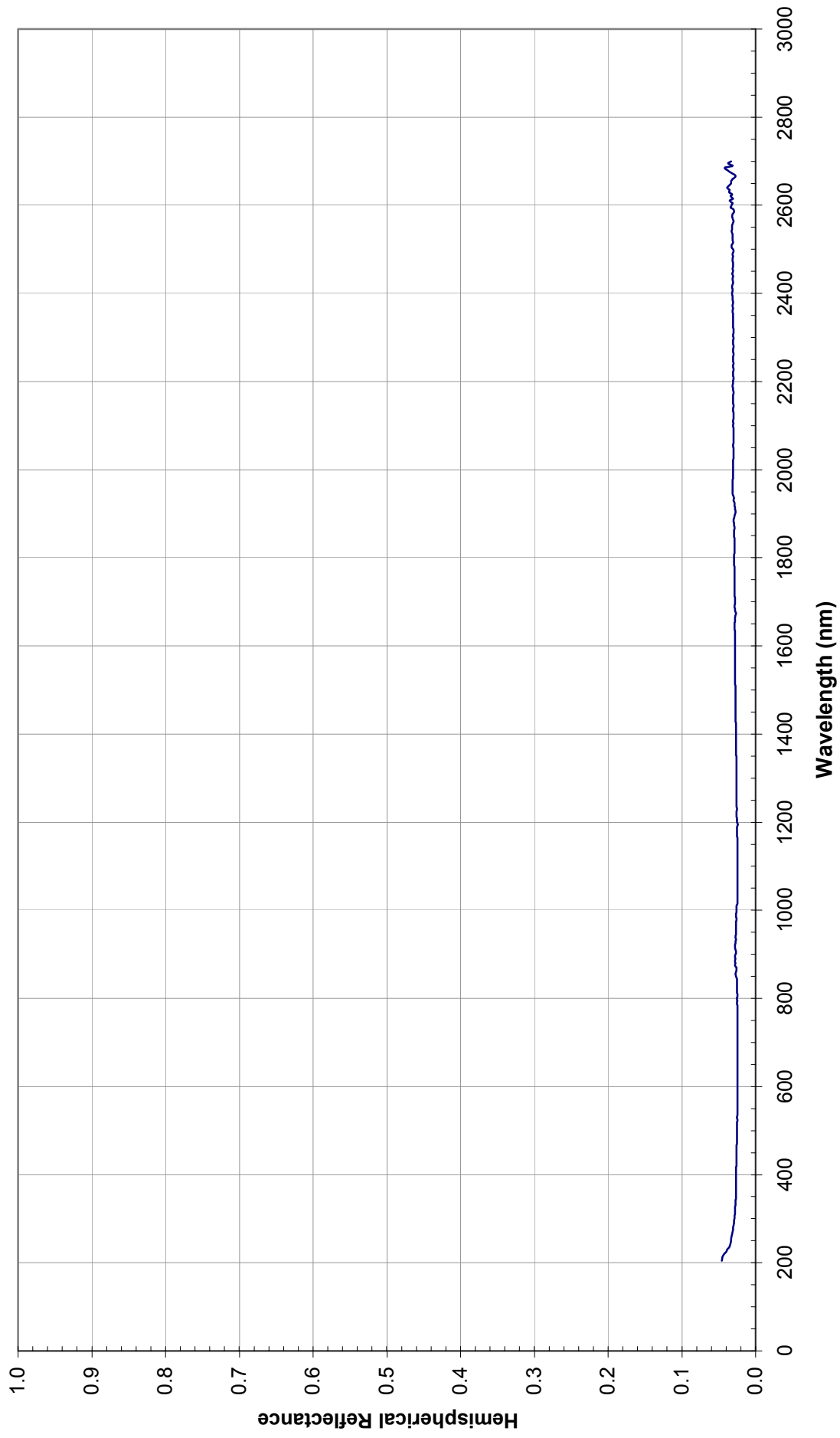


Figure 5.29

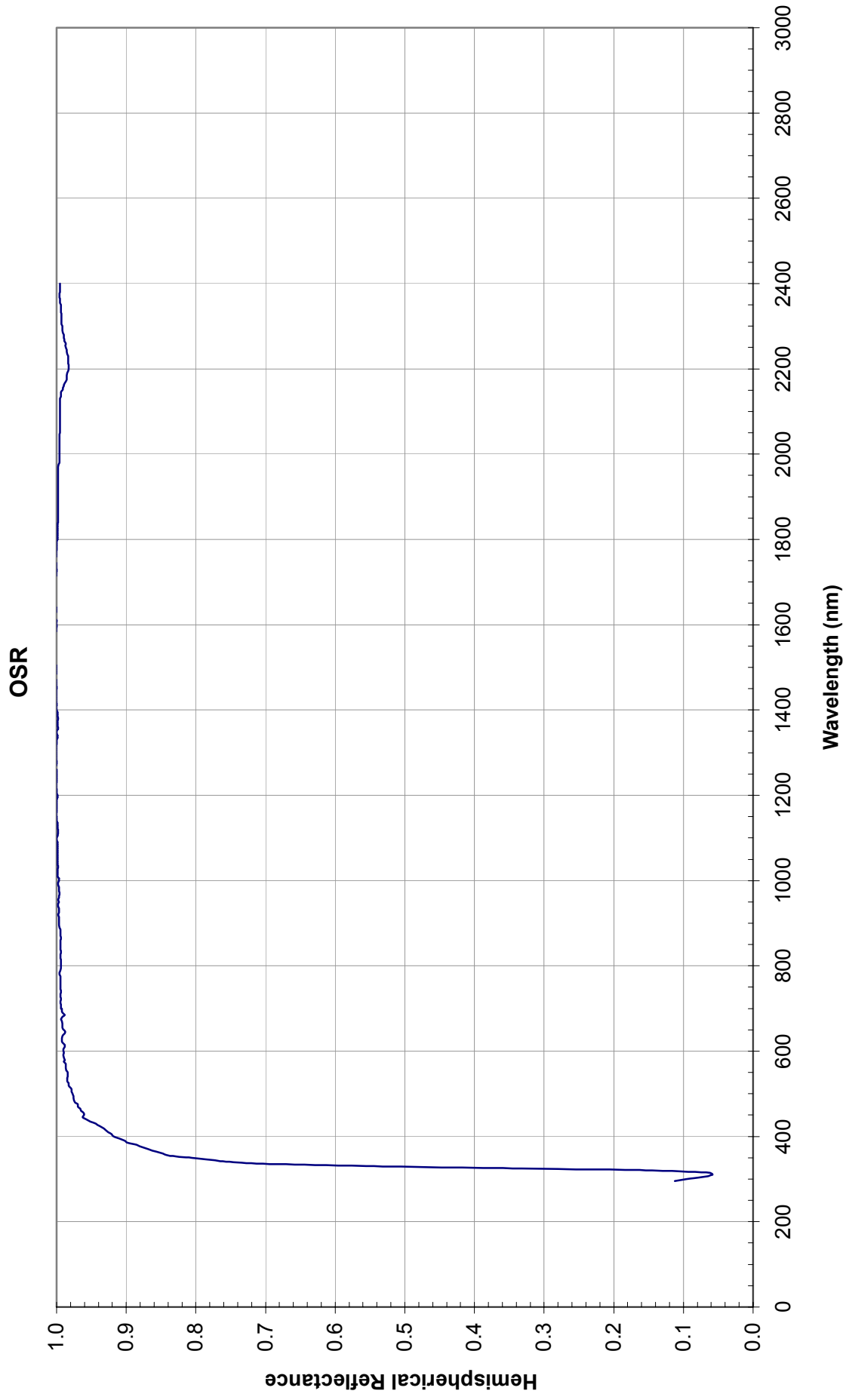


Figure 5.30

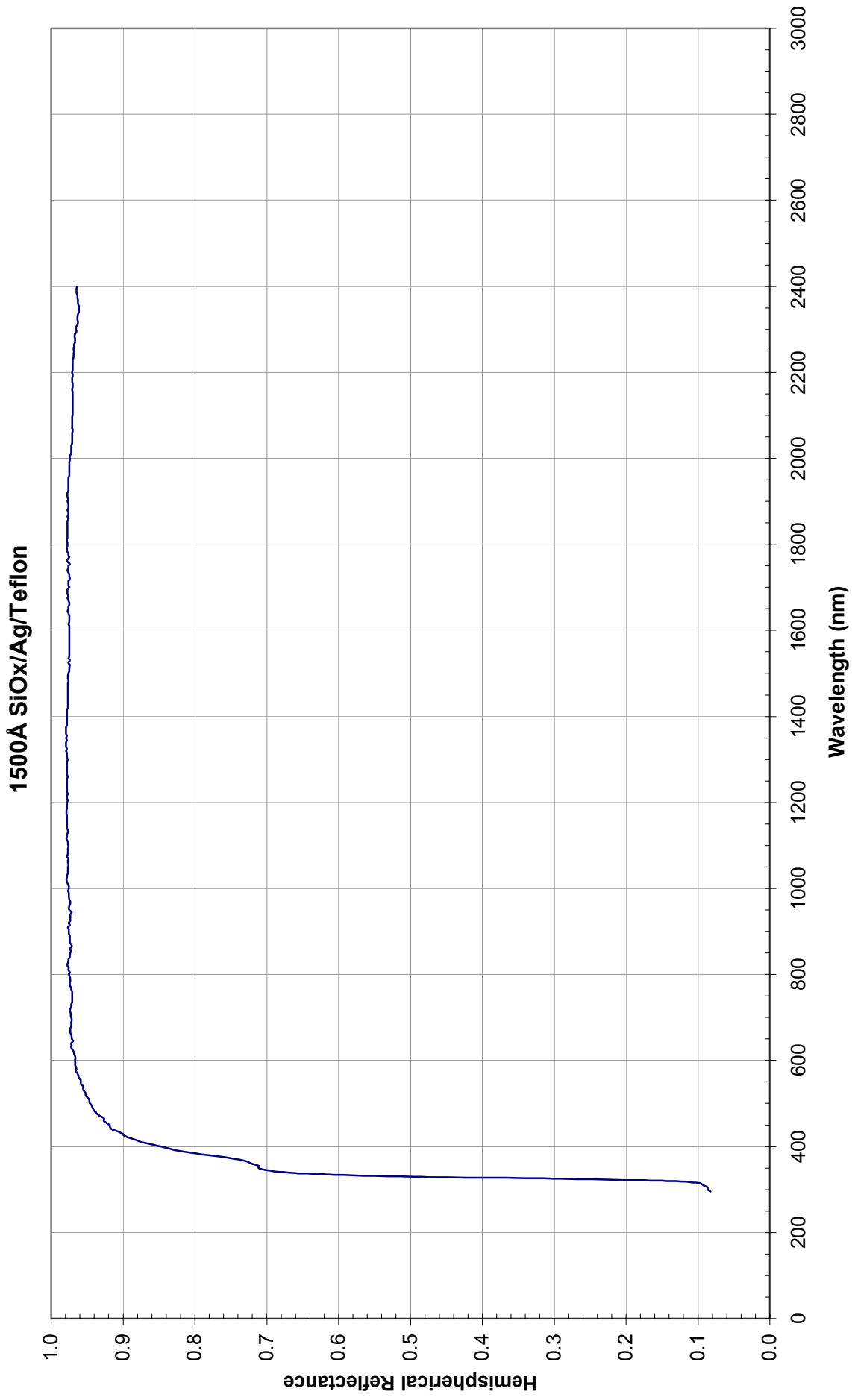


Figure 5.31

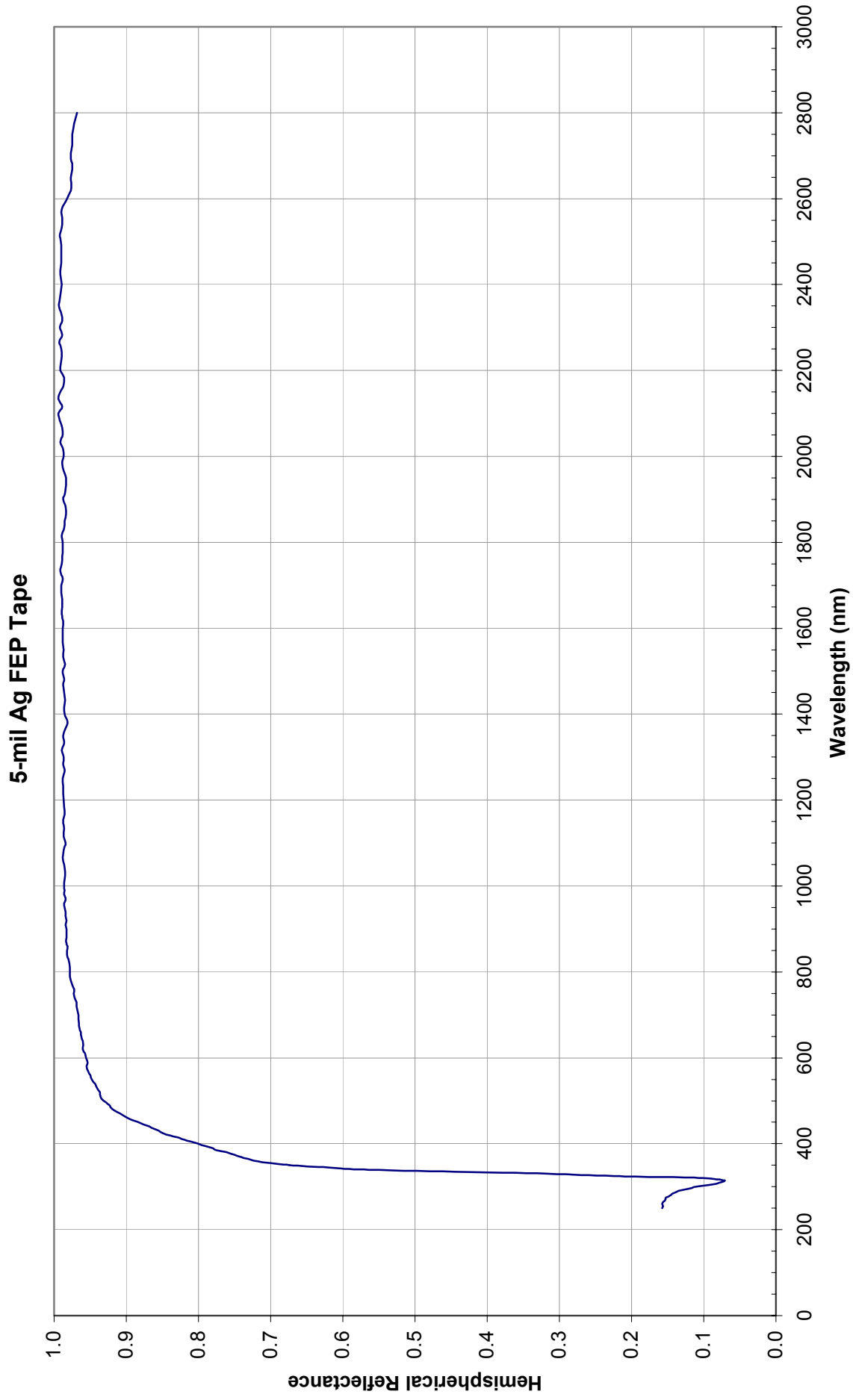


Figure 5.32

CIC Solar Cells -- ST-5

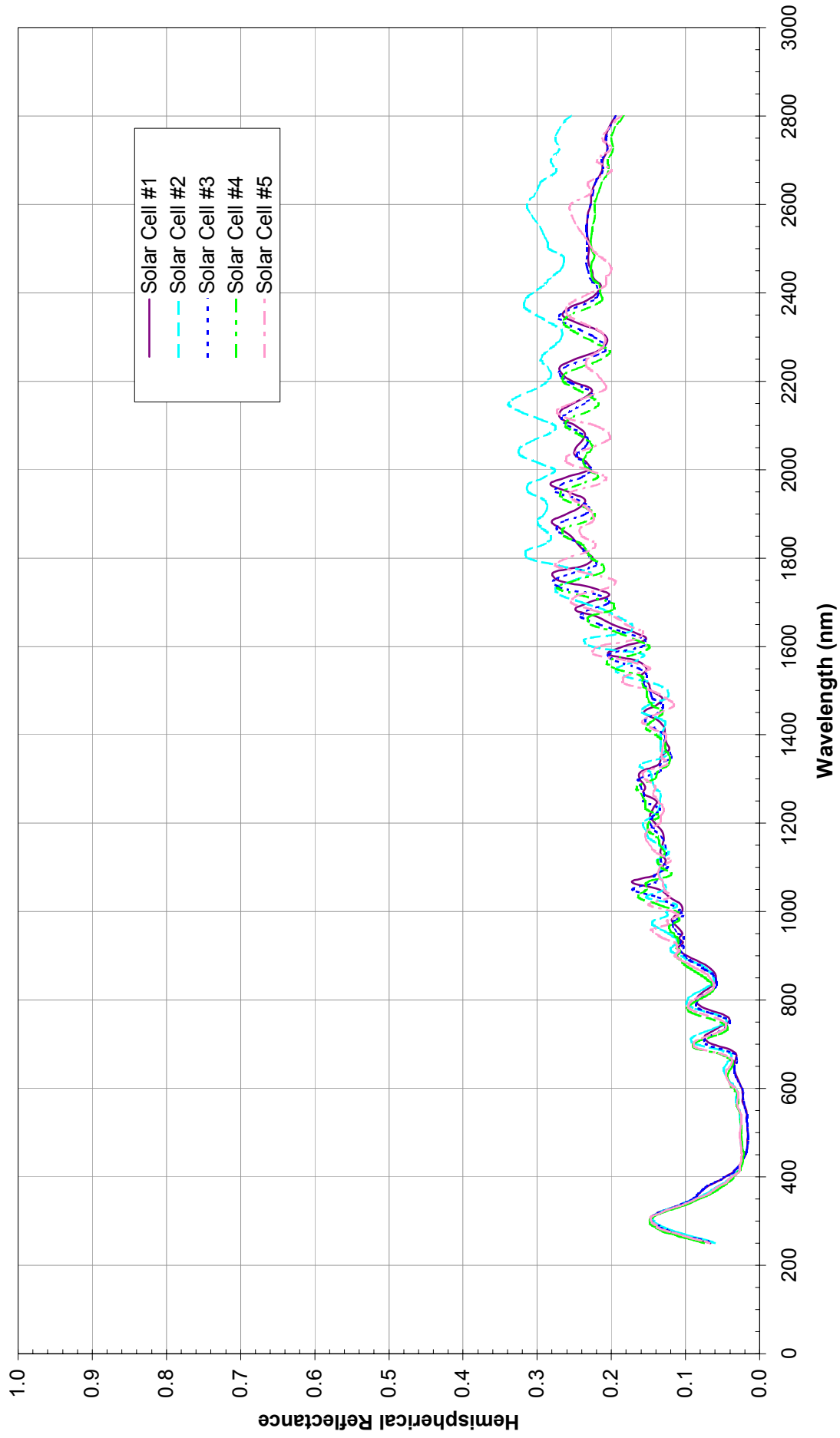


Figure 5.33

HST SAIH Solar Cell

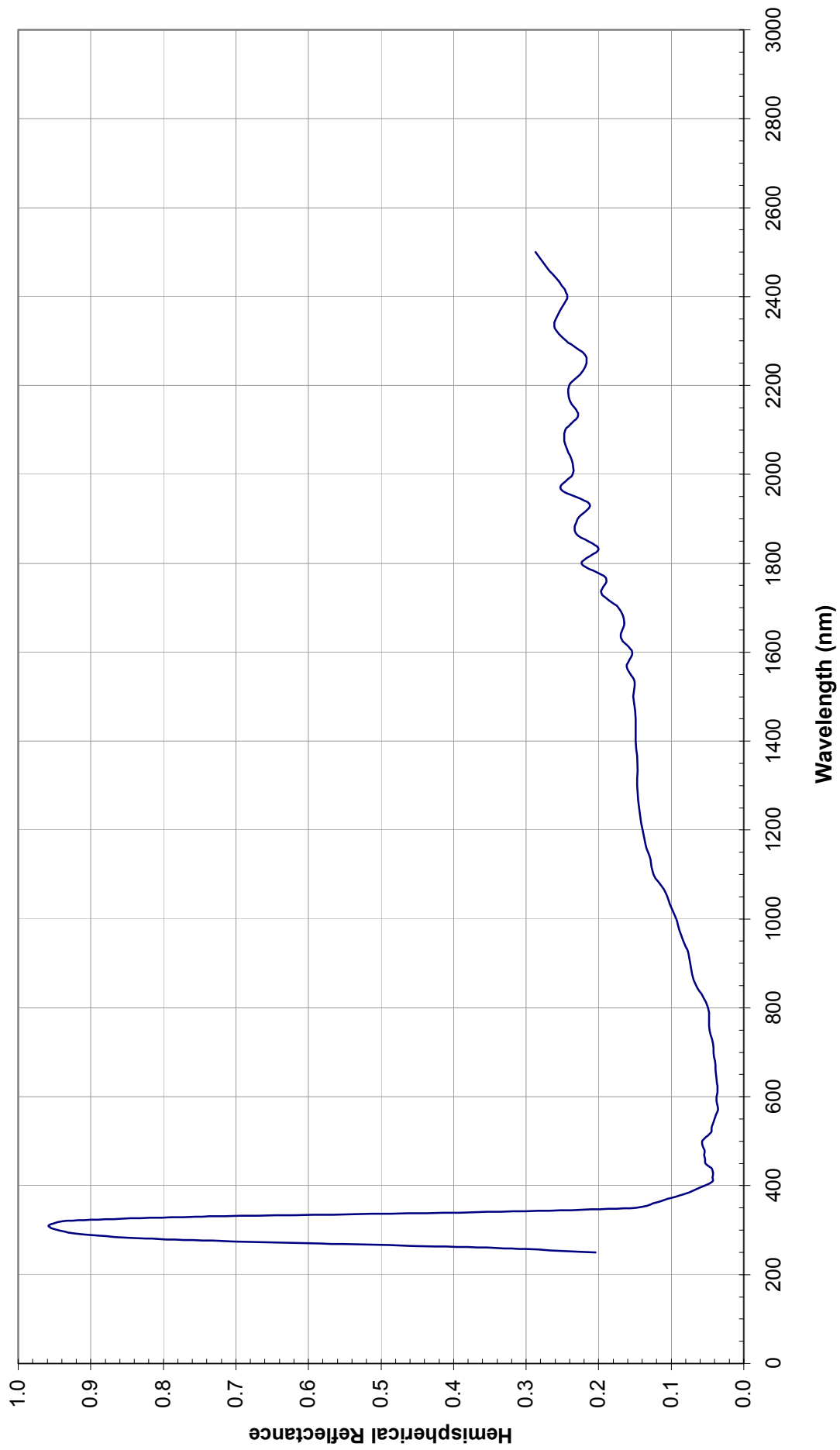


Figure 5.34

Electropolished Stainless Steel

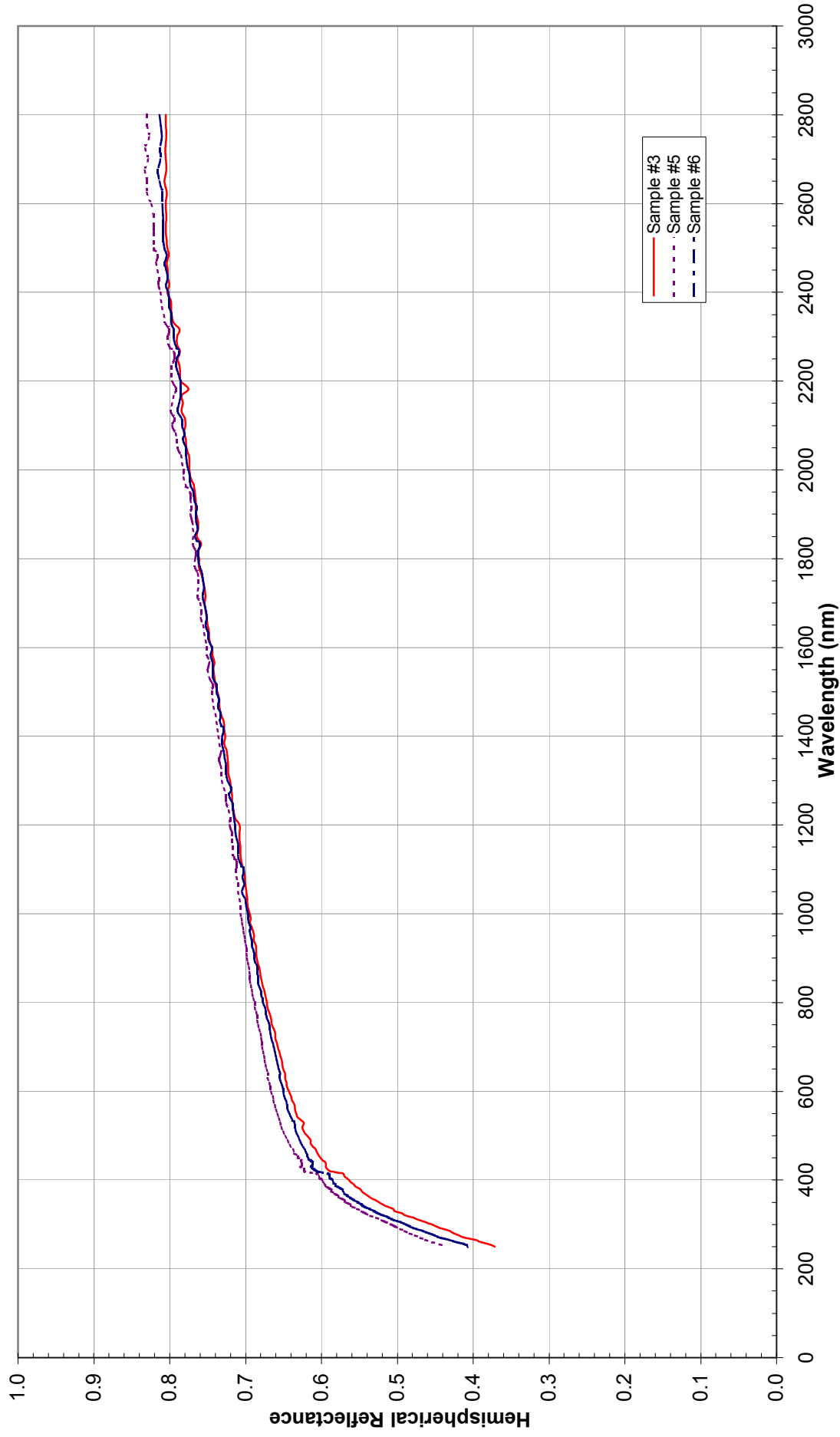


Figure 5.35

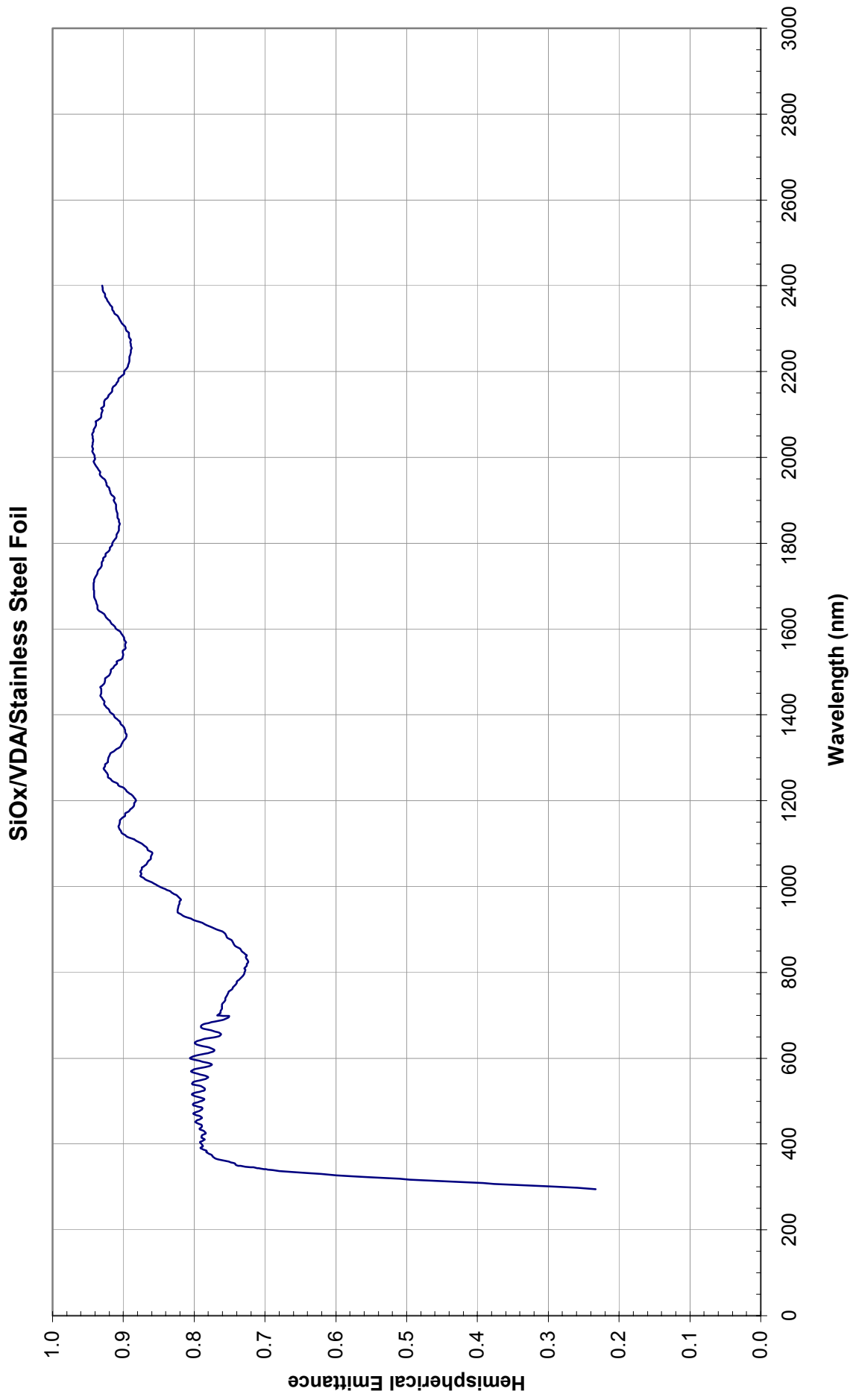


Figure 5.36

SiOx/Tedlar 1.5 mils

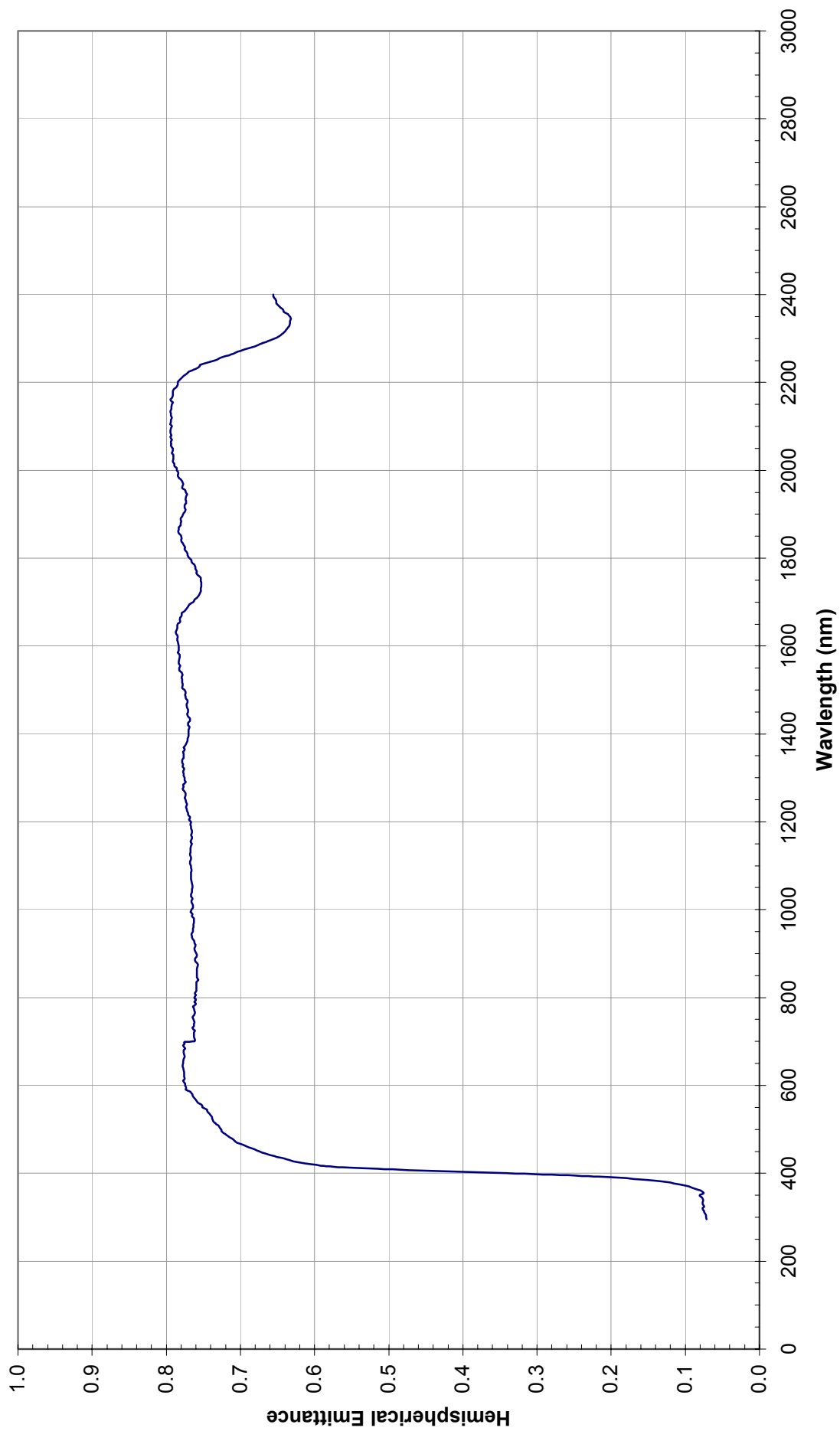


Figure 5.37

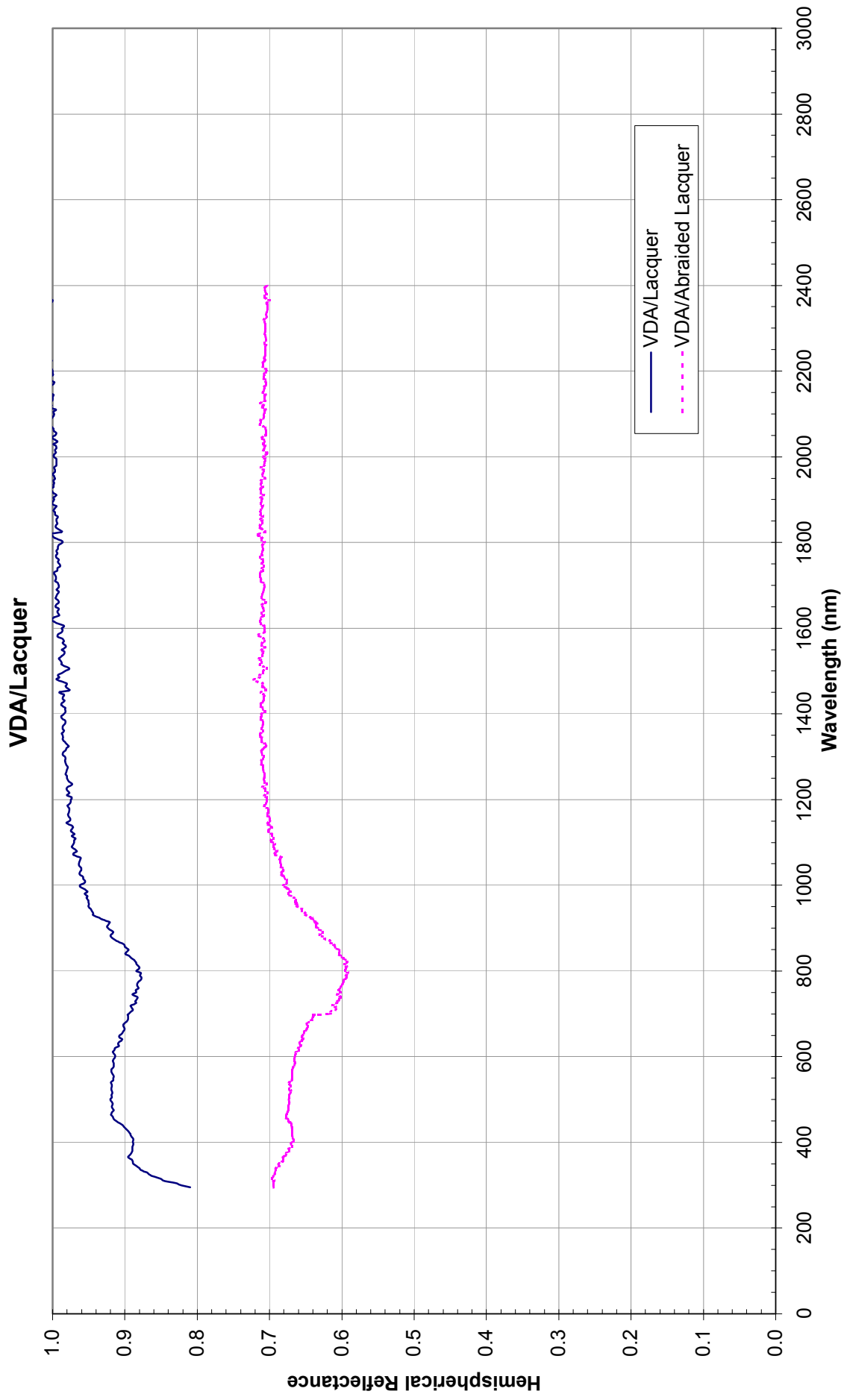


Figure 5.38

YB71

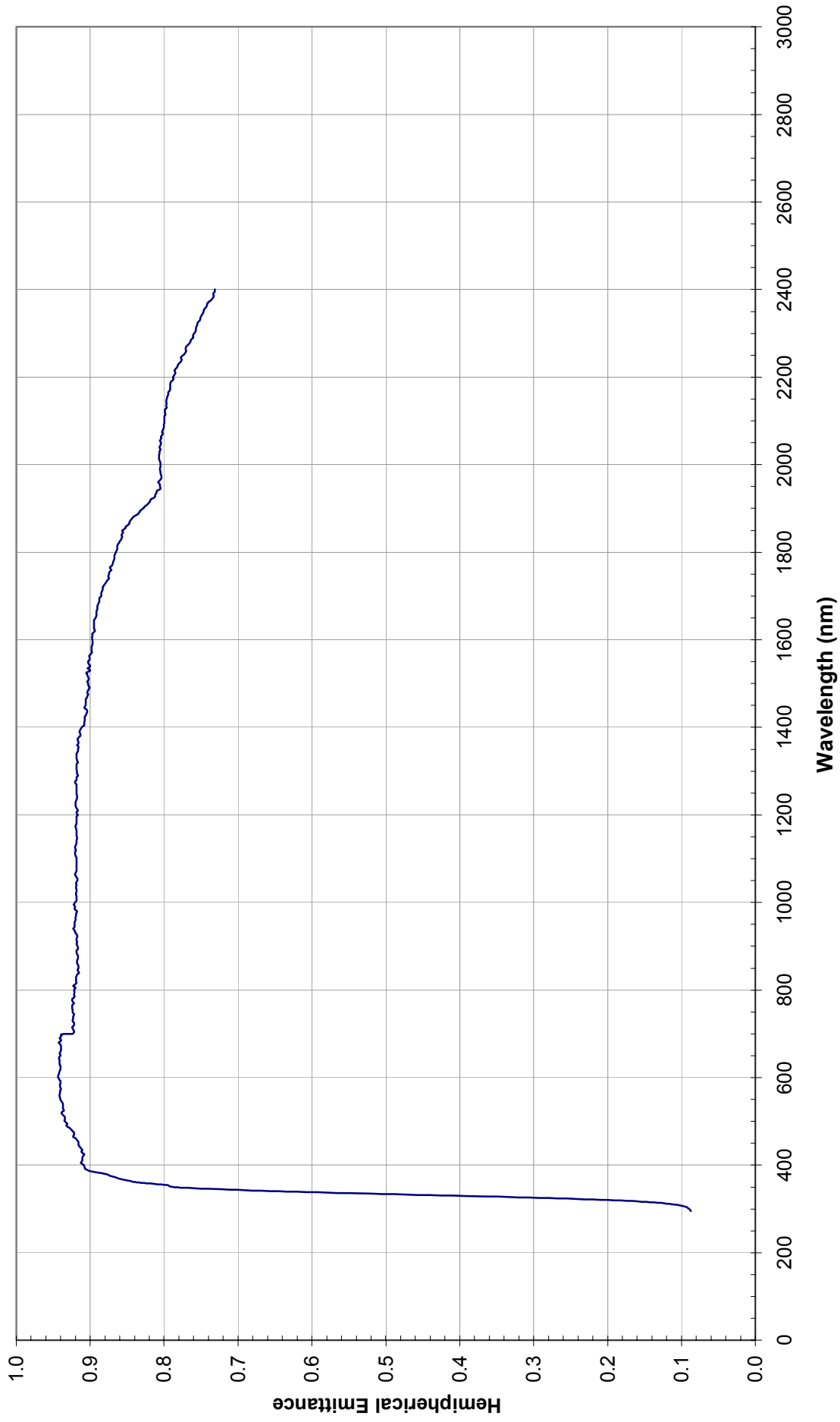


Figure 5.39

VI. Total Hemispherical Emittance as a Function of Temperature For Selected Thermal Control Coatings

The emittance measurements that follow were determined by a calorimetric technique as described in section 3.2.3. The thickness of each coating has been noted in parentheses on each chart and all coatings were on an Aluminum substrate unless otherwise noted. It is important to note that the emittance of each coating is a function of thickness, if a different coating thickness is used the resulting emittance as a function of temperature may be somewhat different. These tests represent data collected over a 10-year period by Lonny Kauder.

Aeroglaze A276 (3.0 mils)

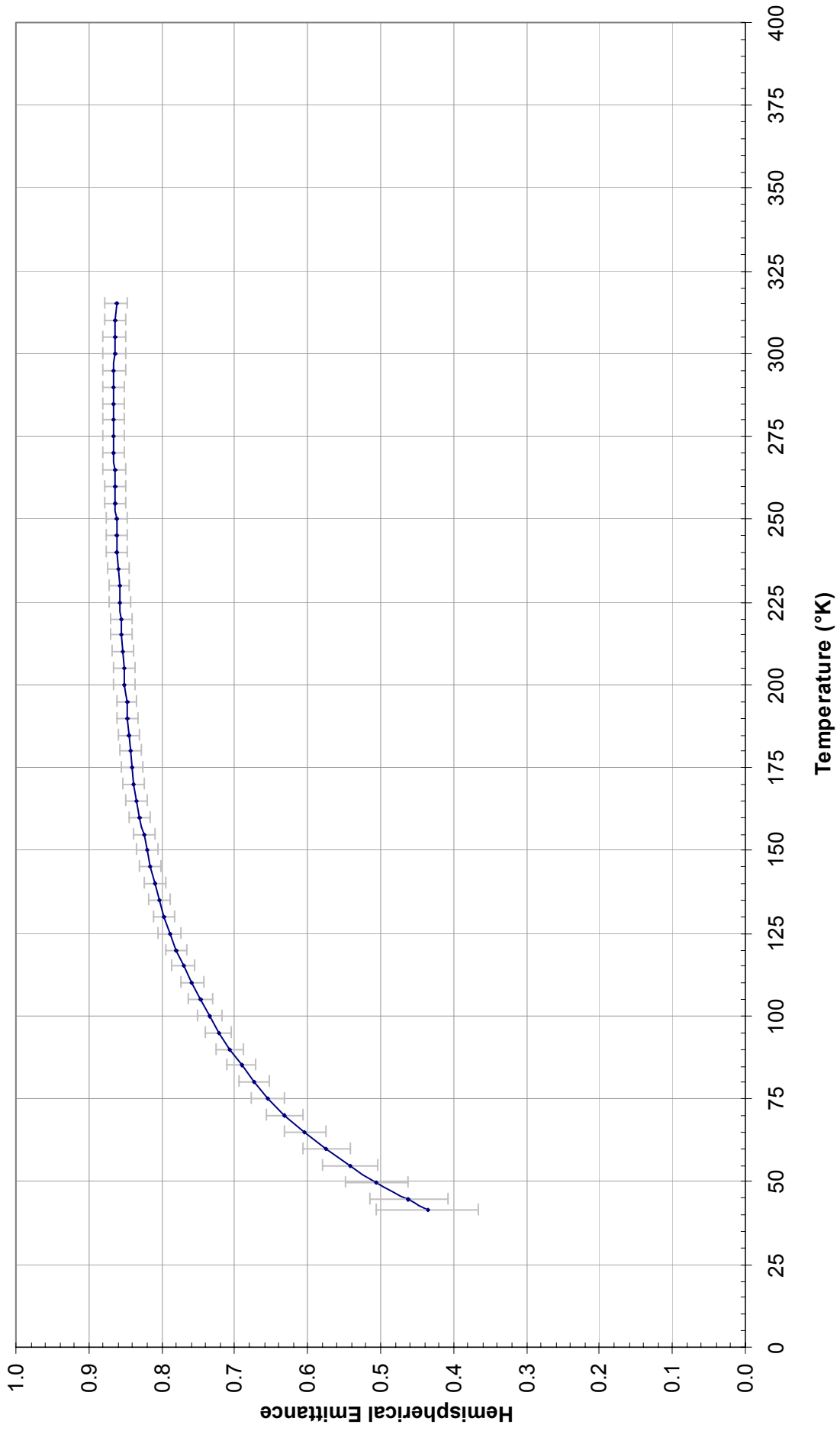


Figure 6.1

Chemglaze Z202 (1.6mils)

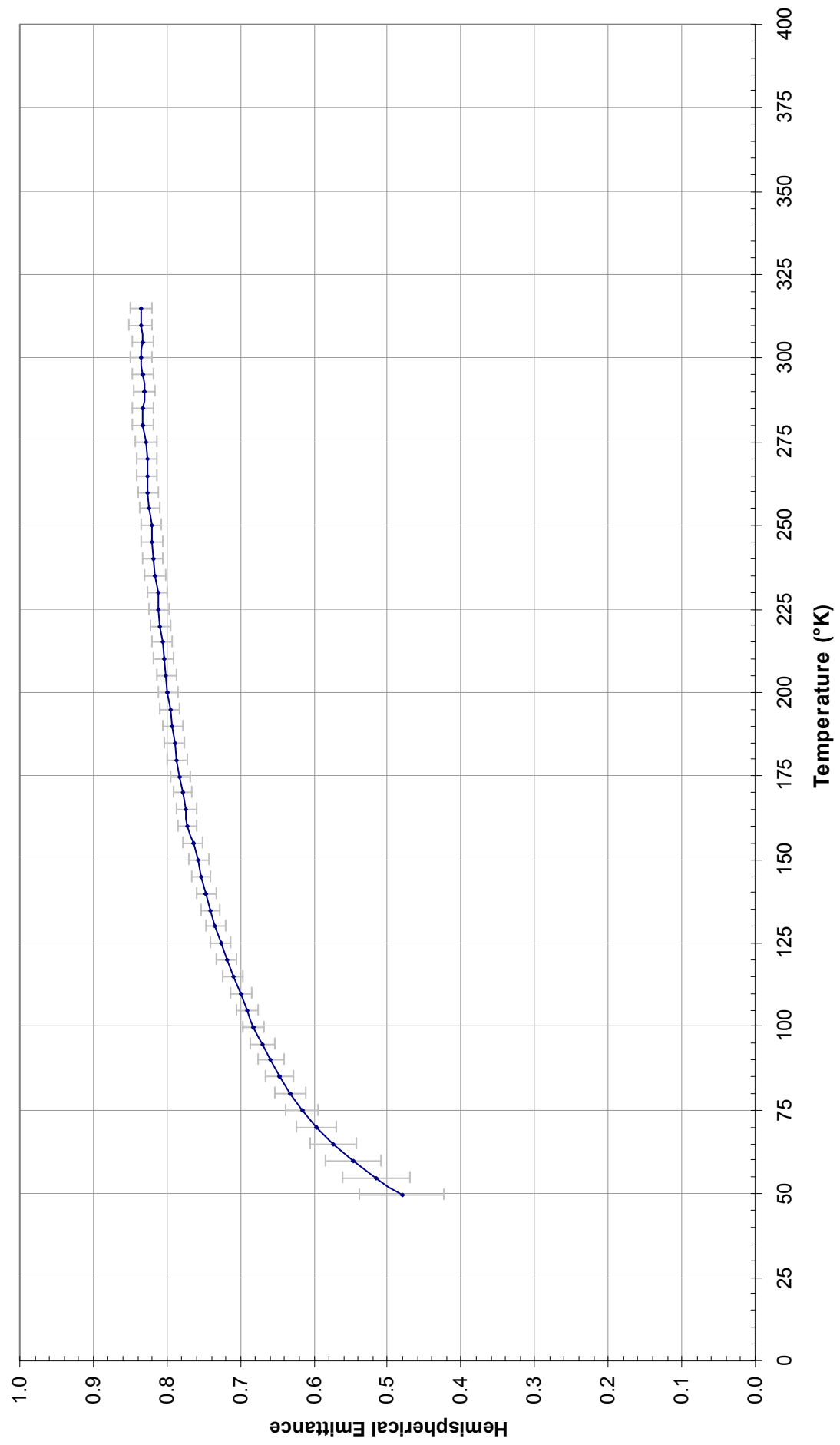


Figure 6.2

Chemglaze Z302 (2.2mils)

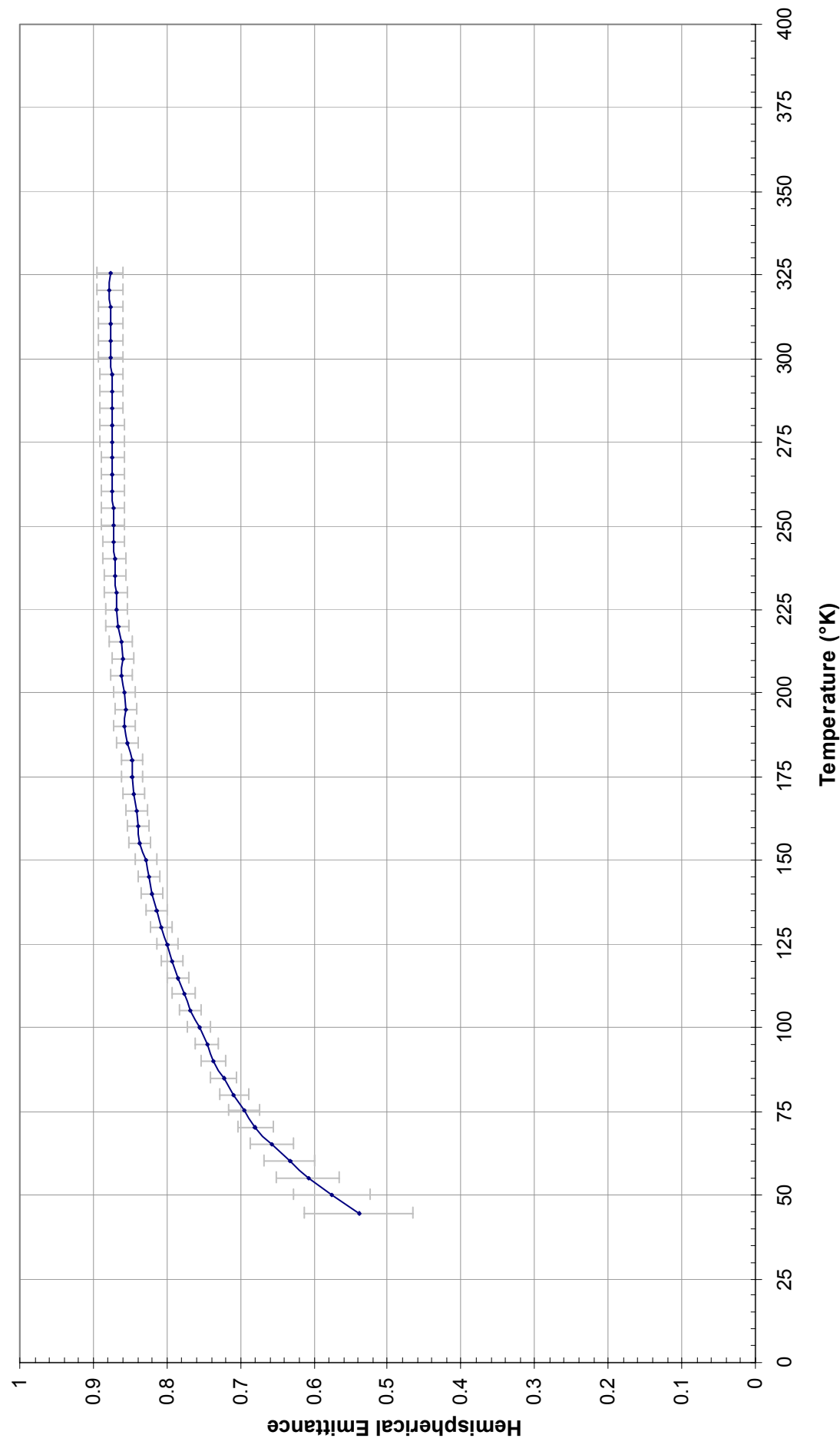


Figure 6.3

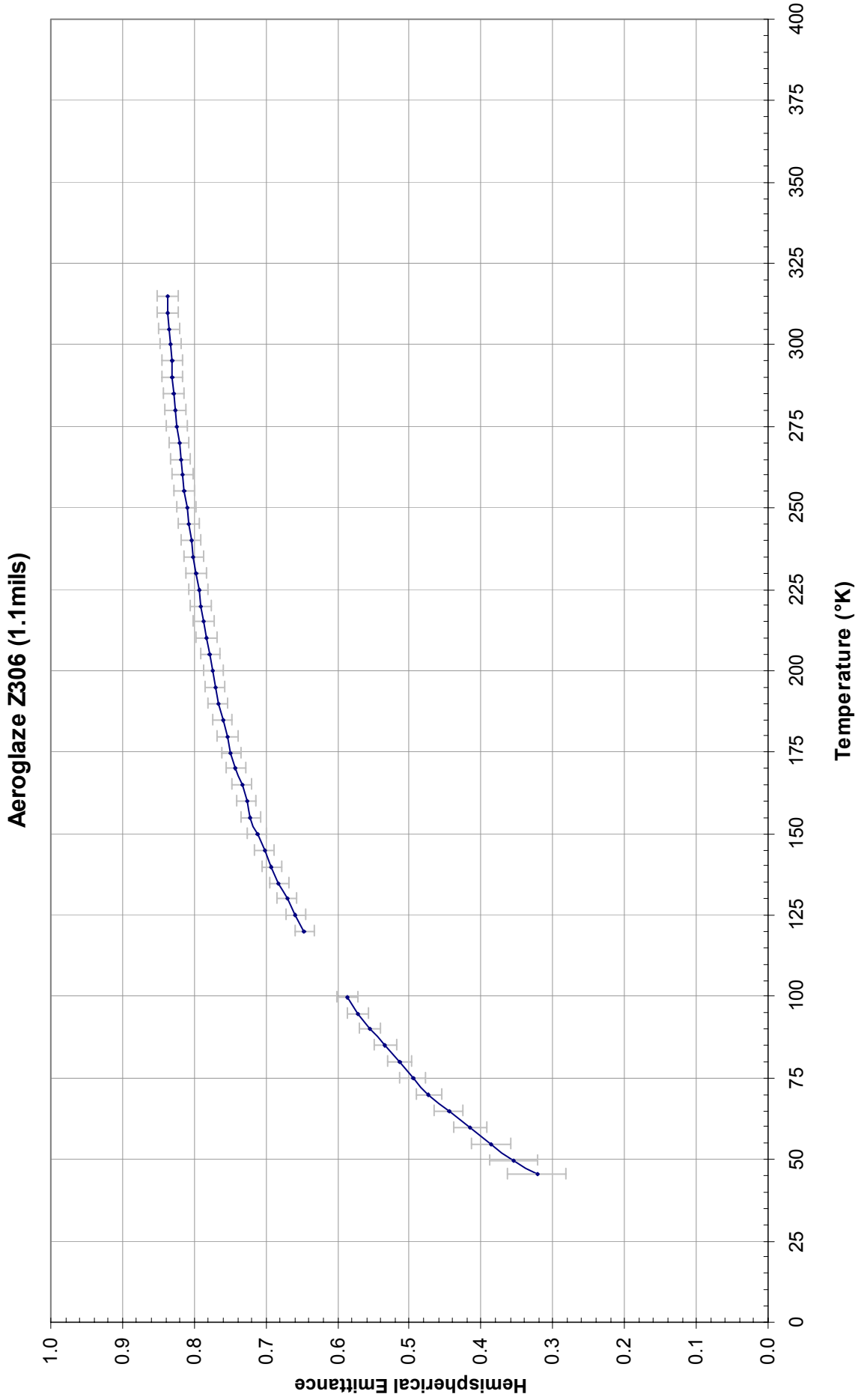


Figure 6.4

AeroGlaze Z306 (1.5 mils)

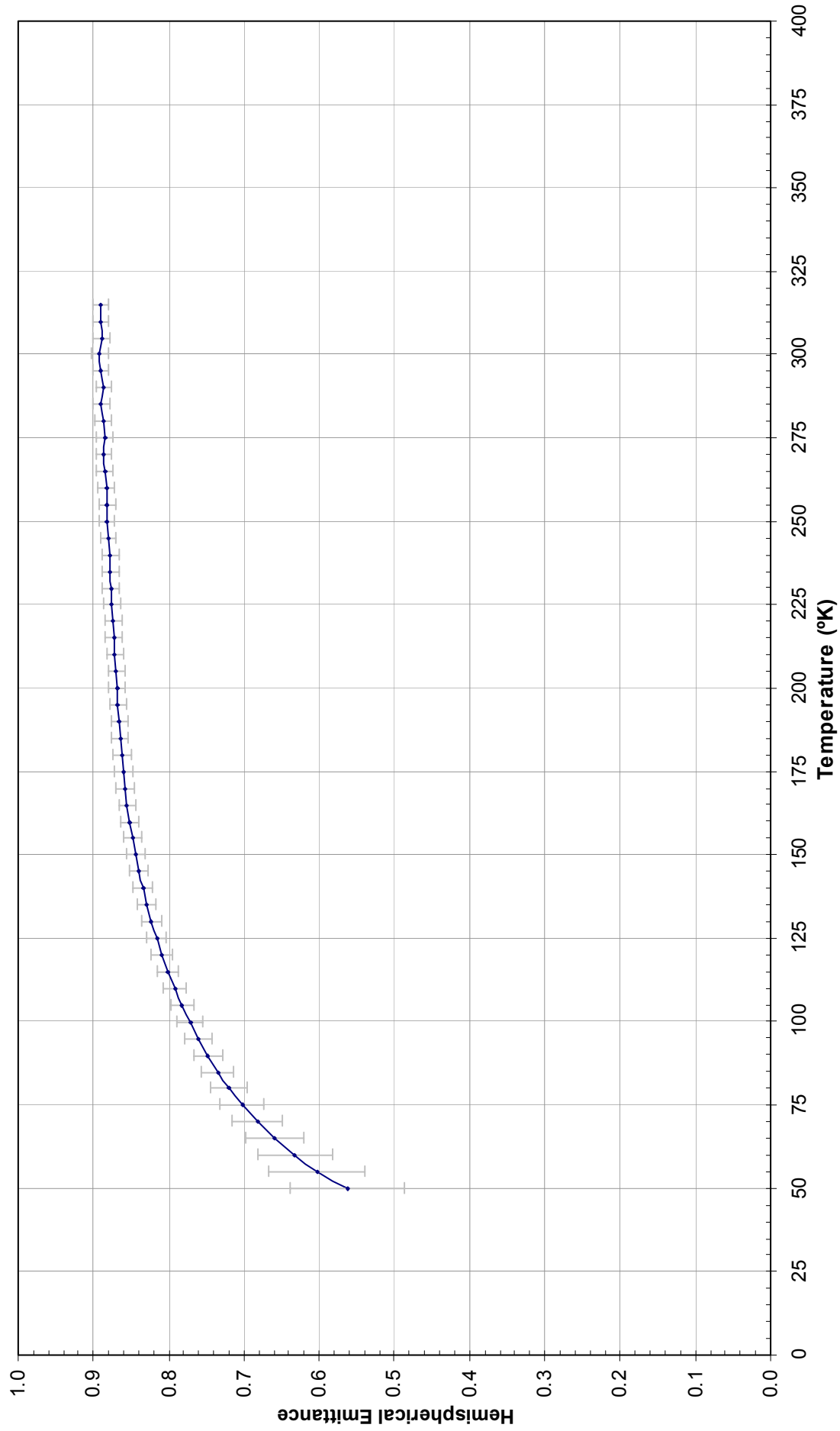


Figure 6.5

Chemglaze Z307 (1.4 mils)

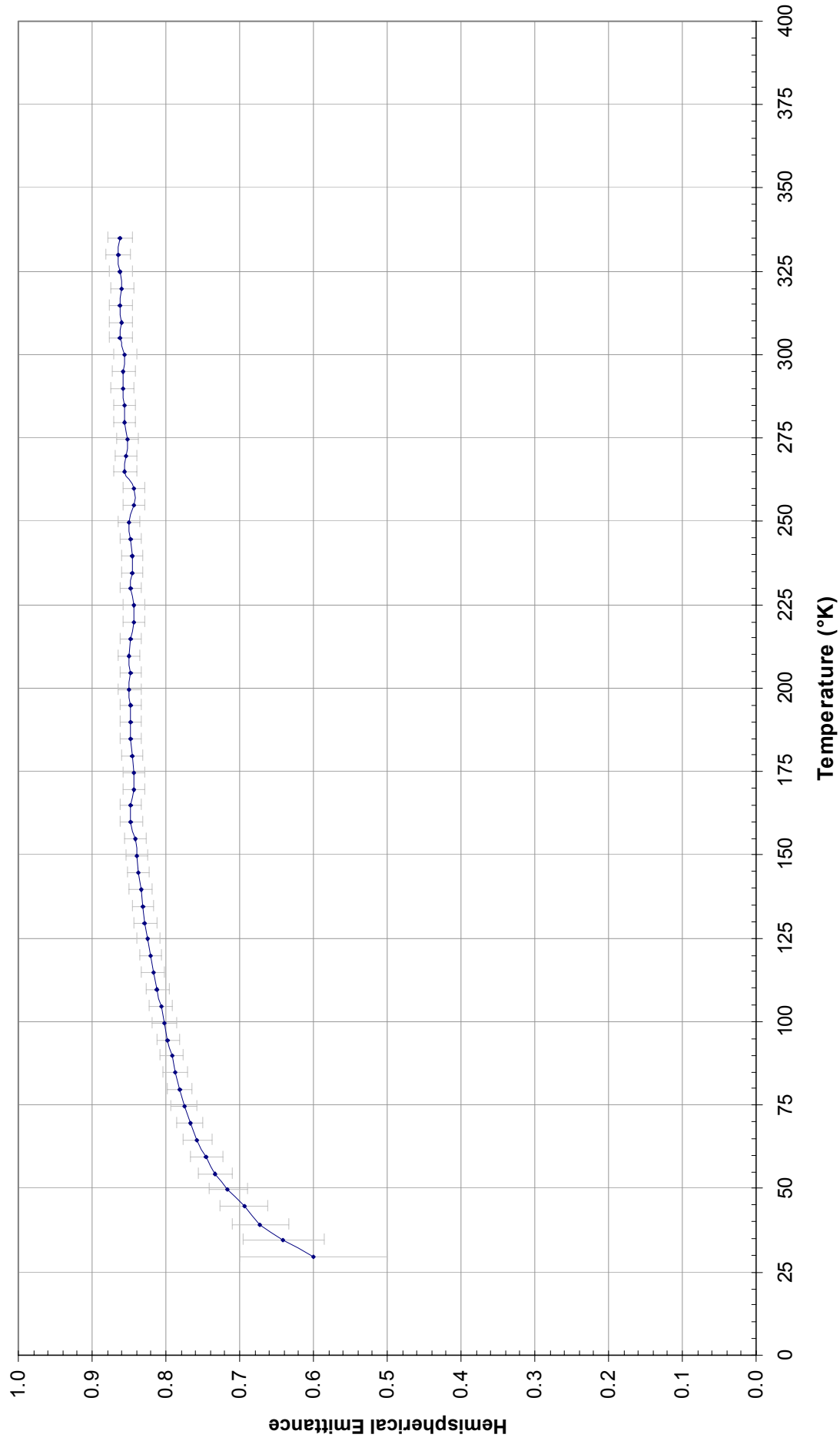


Figure 6.6

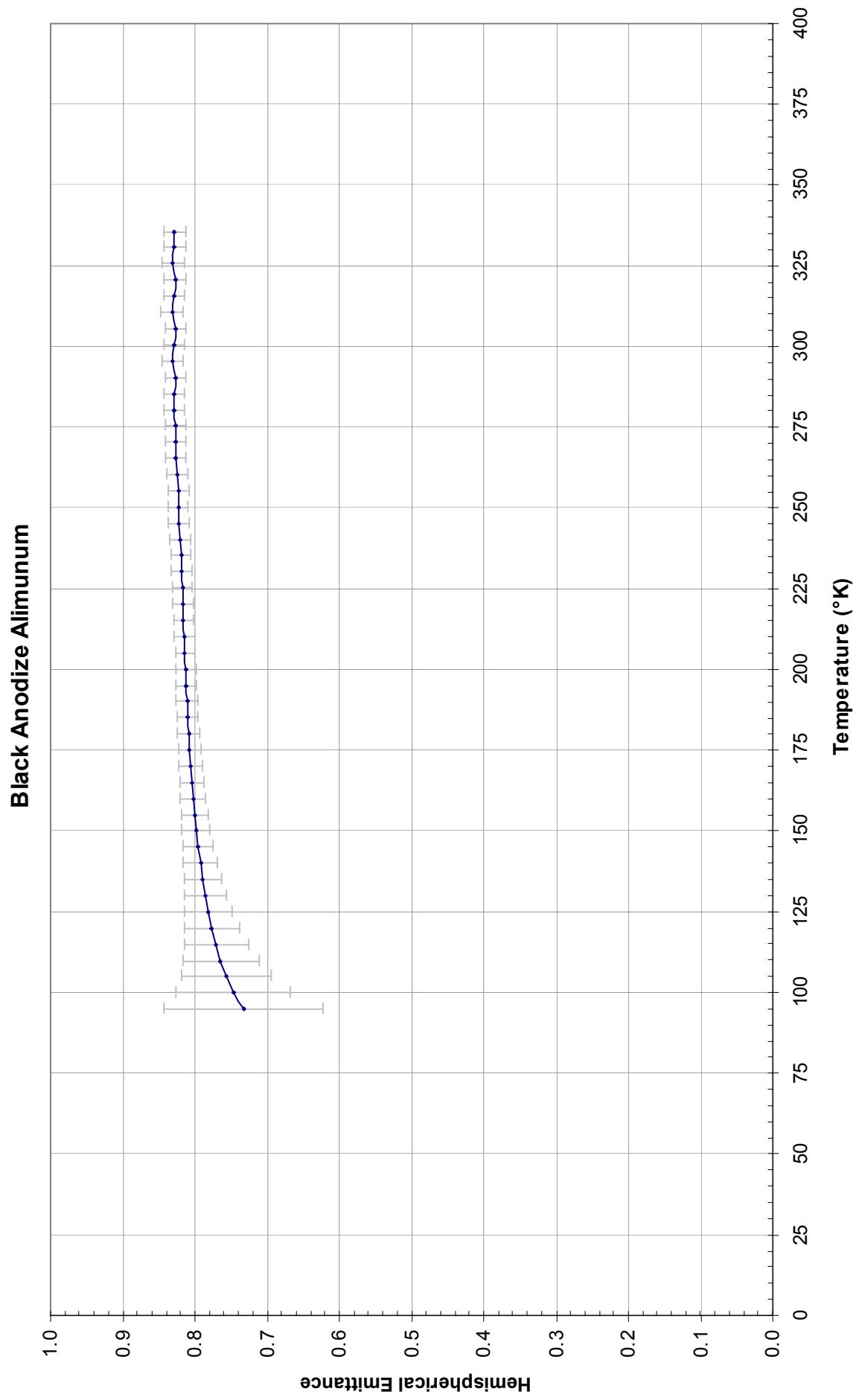


Figure 6.7

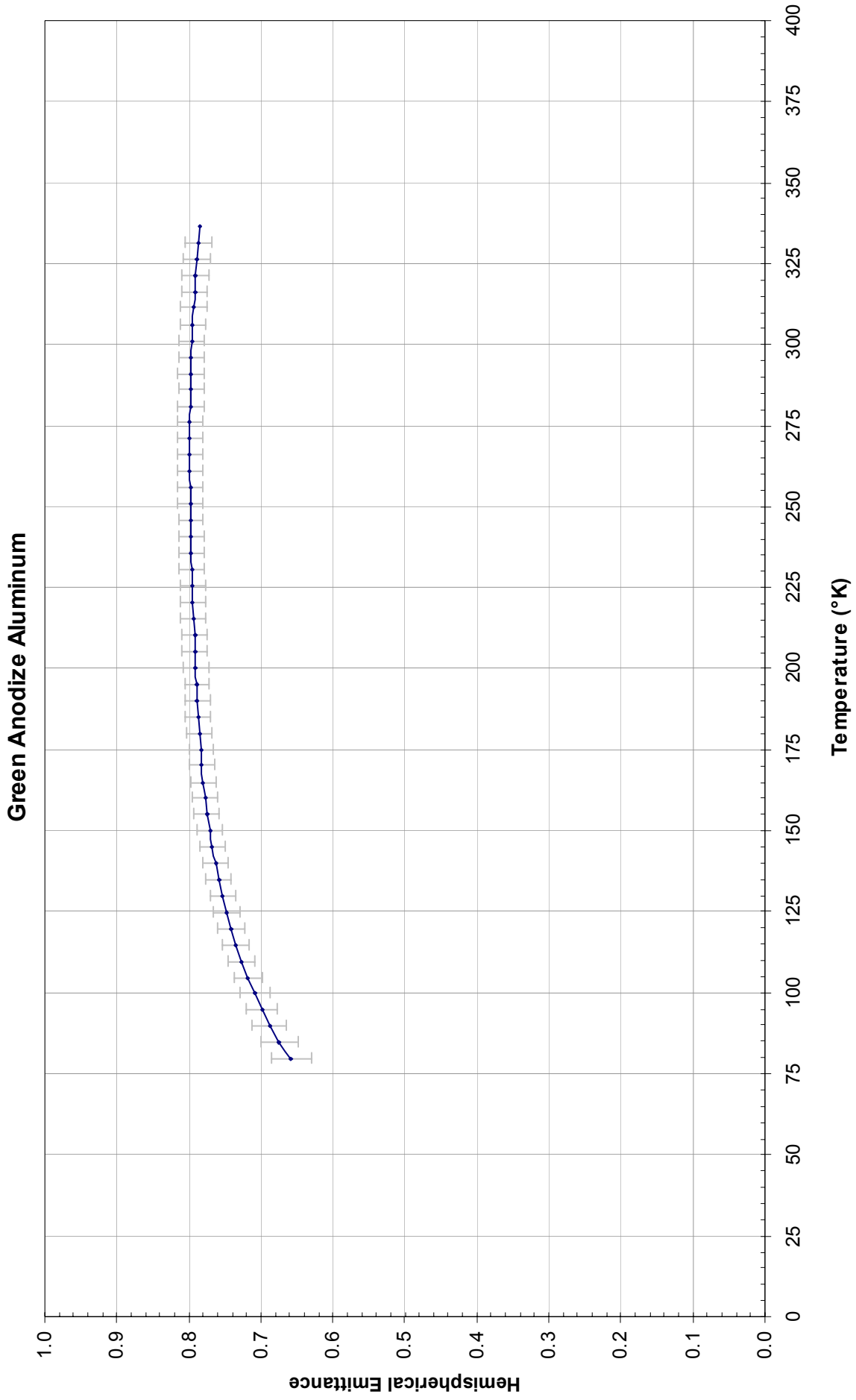


Figure 6.8

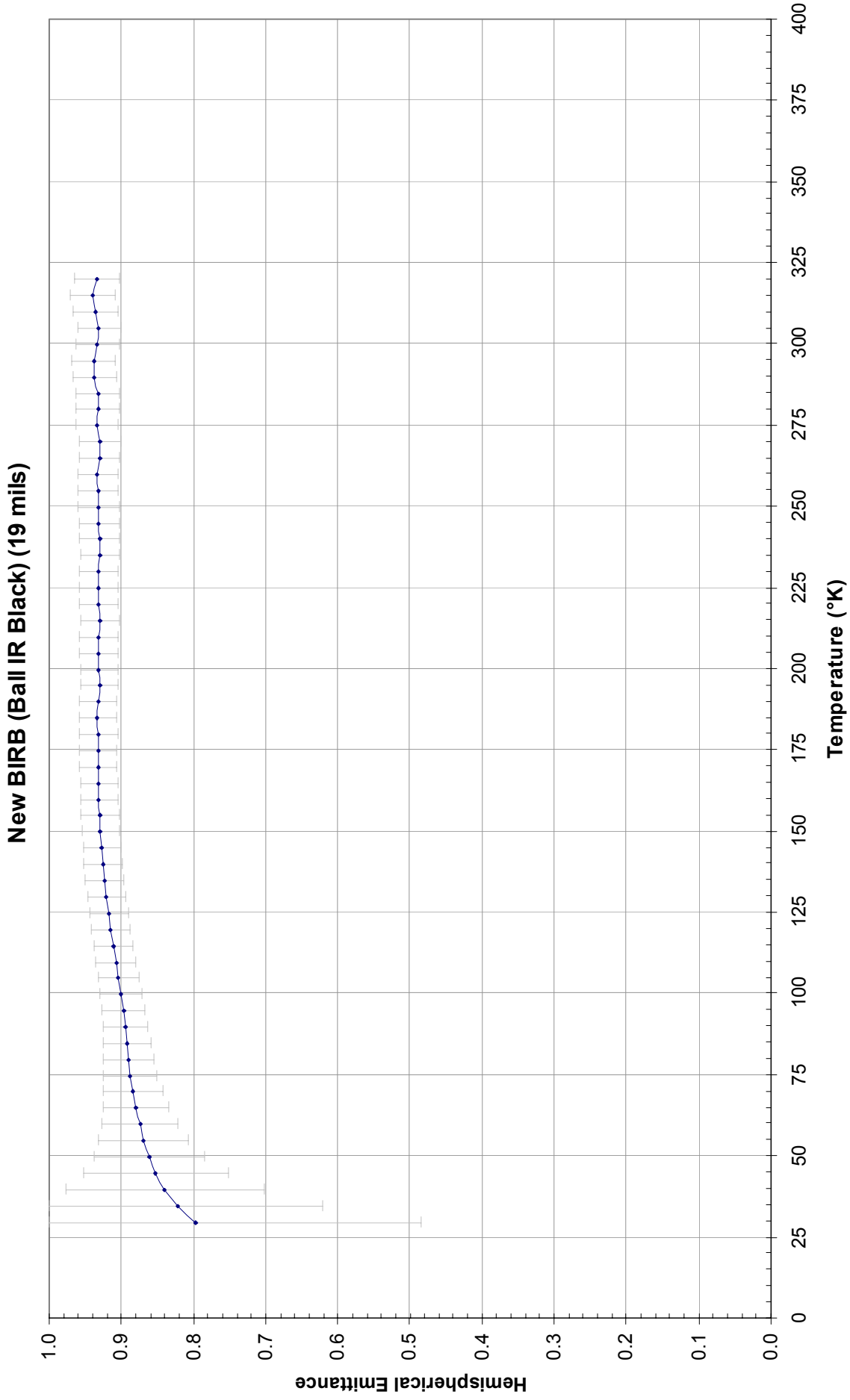


Figure 6.9

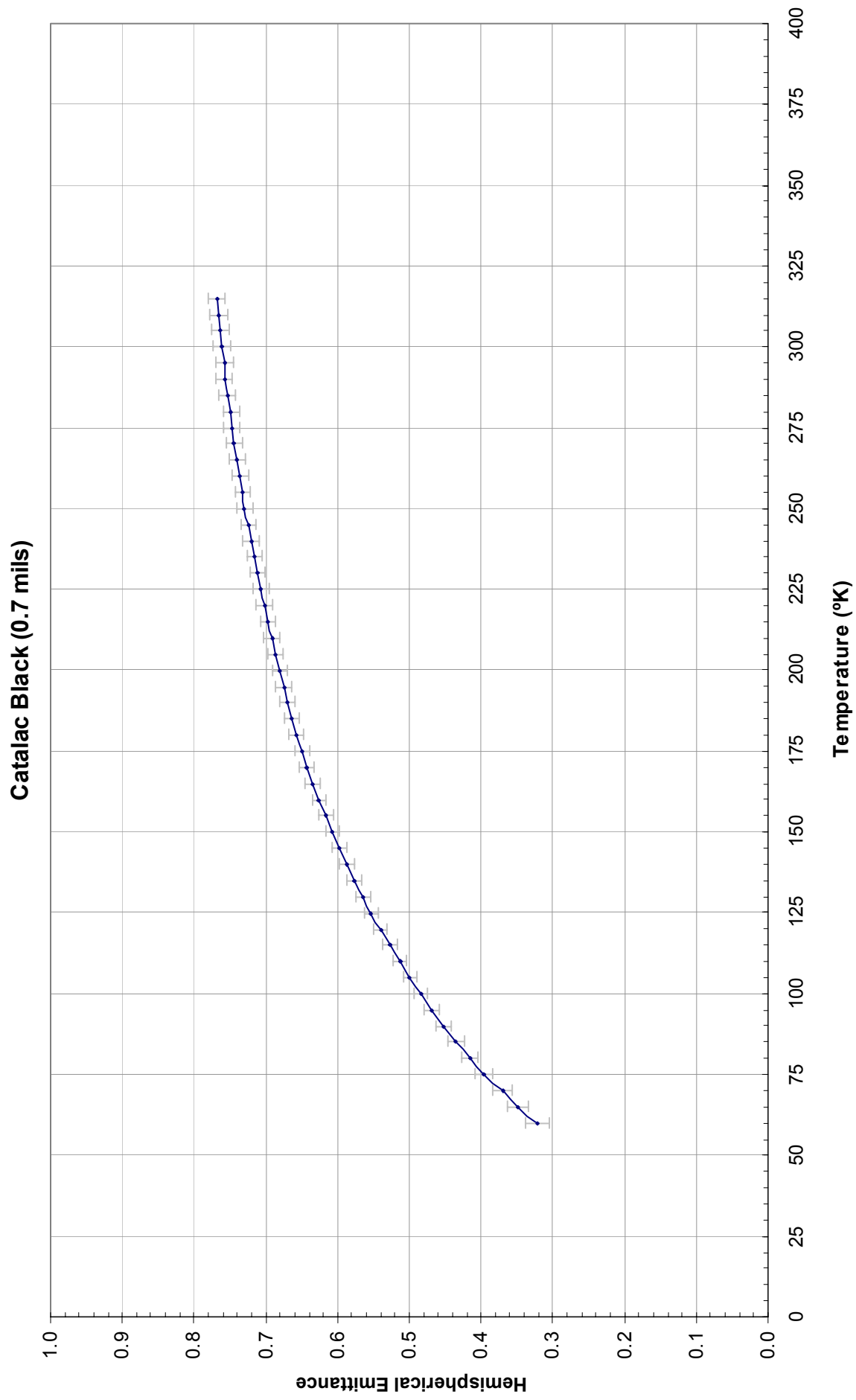


Figure 6.10

CTL15 Gloss Black Paint (4.1 mils)

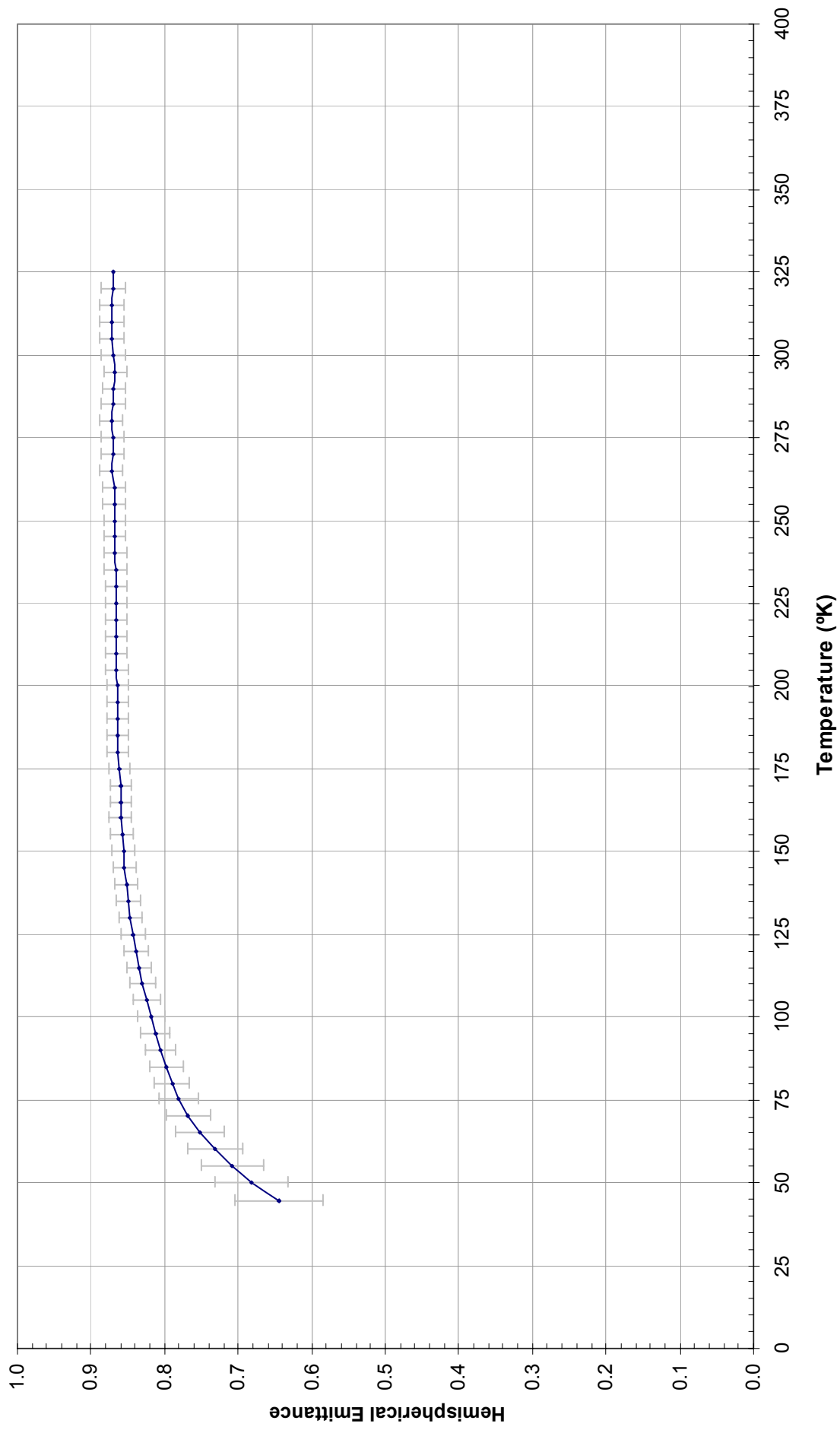


Figure 6.11

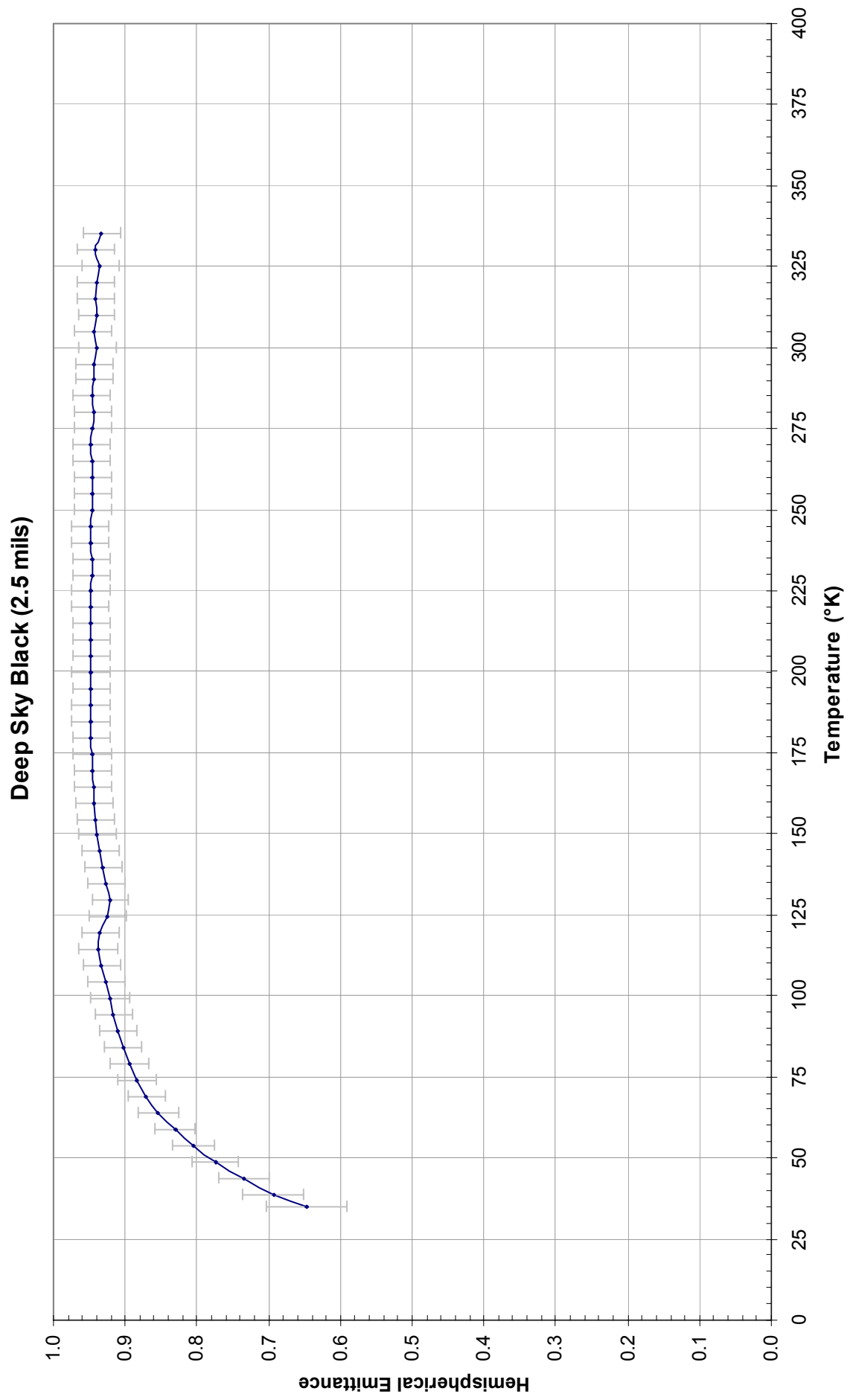


Figure 6.12

Dexter Flat Black Epoxy (2.0 mils)

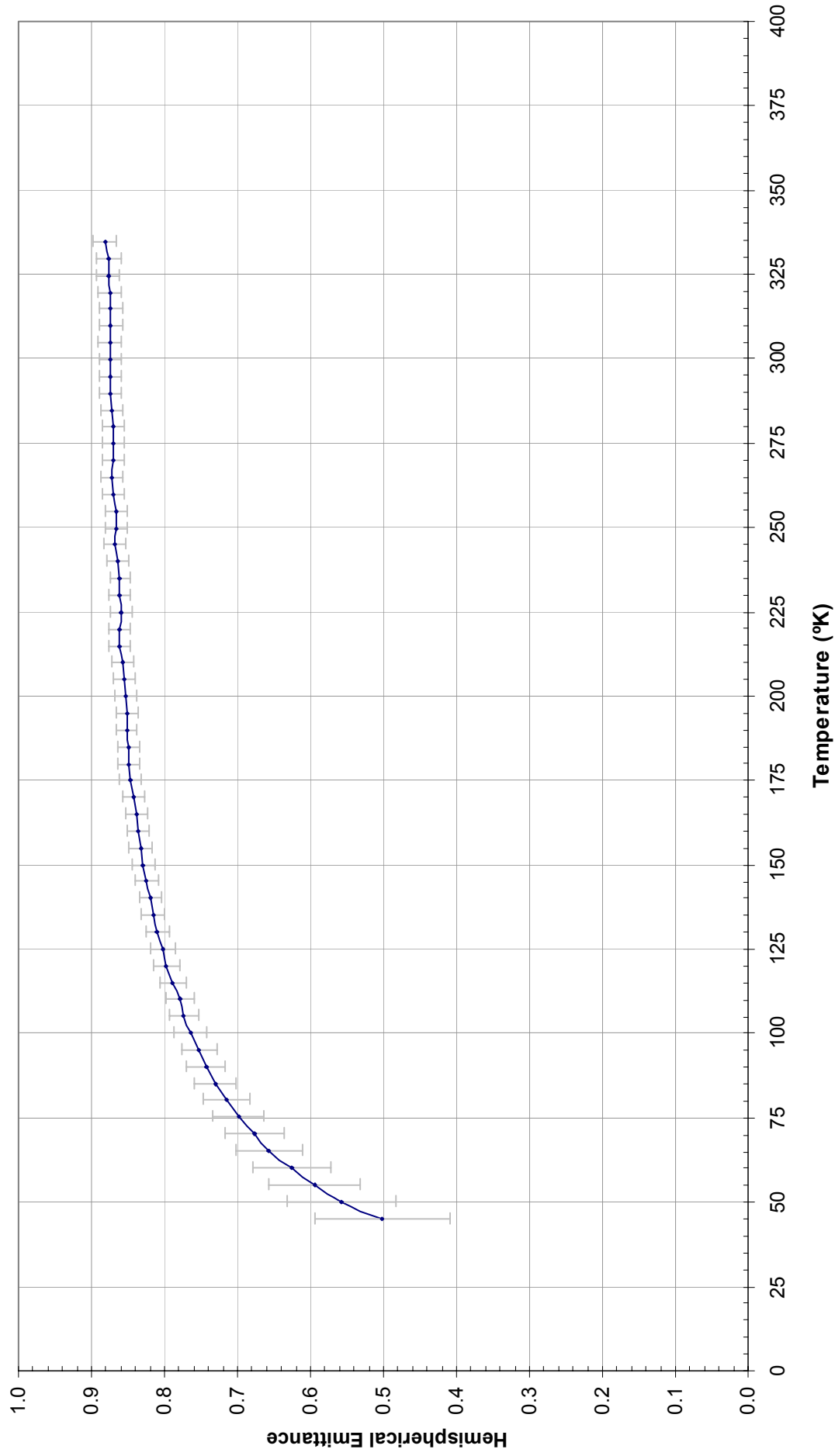


Figure 6.13

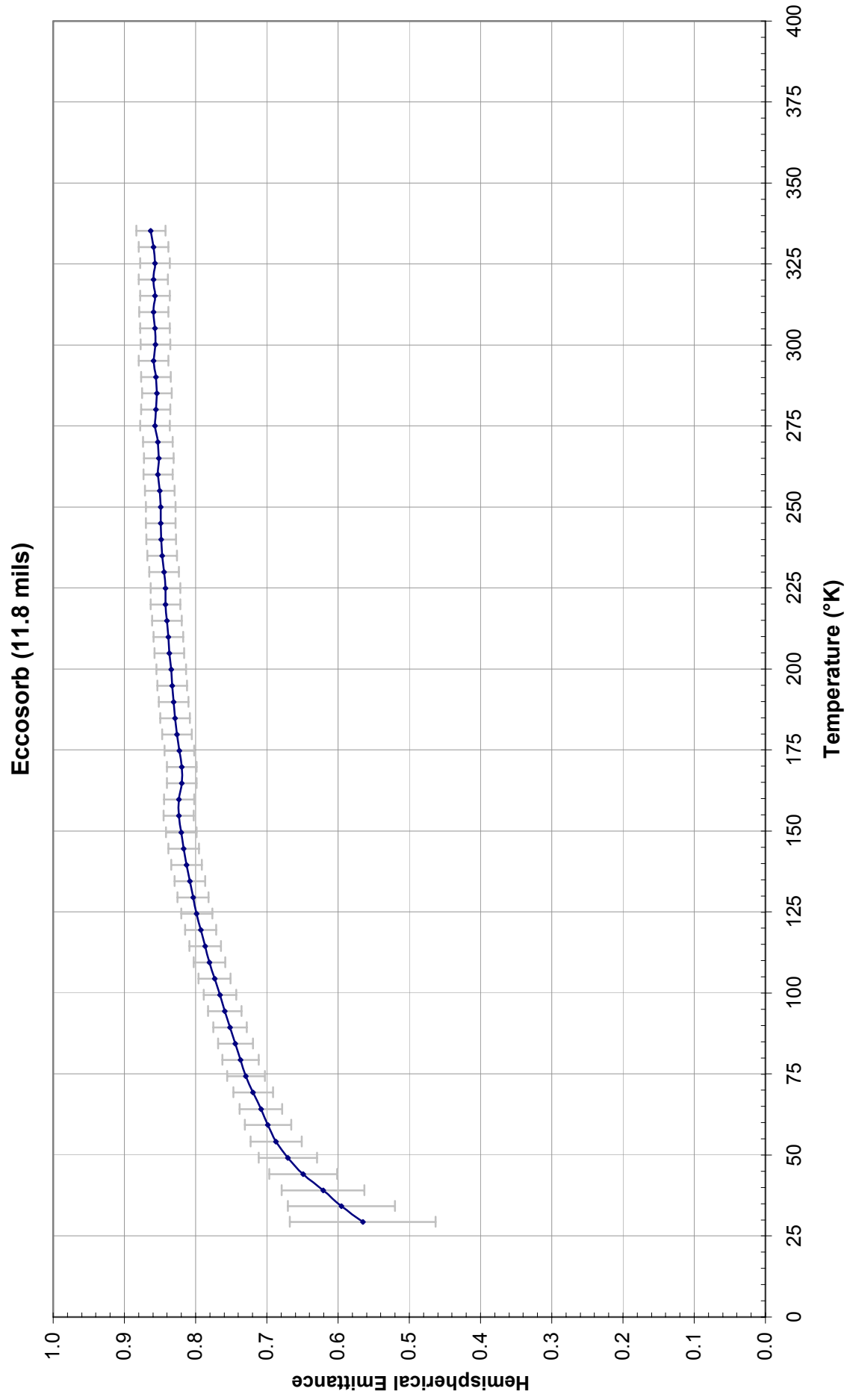


Figure 6.14

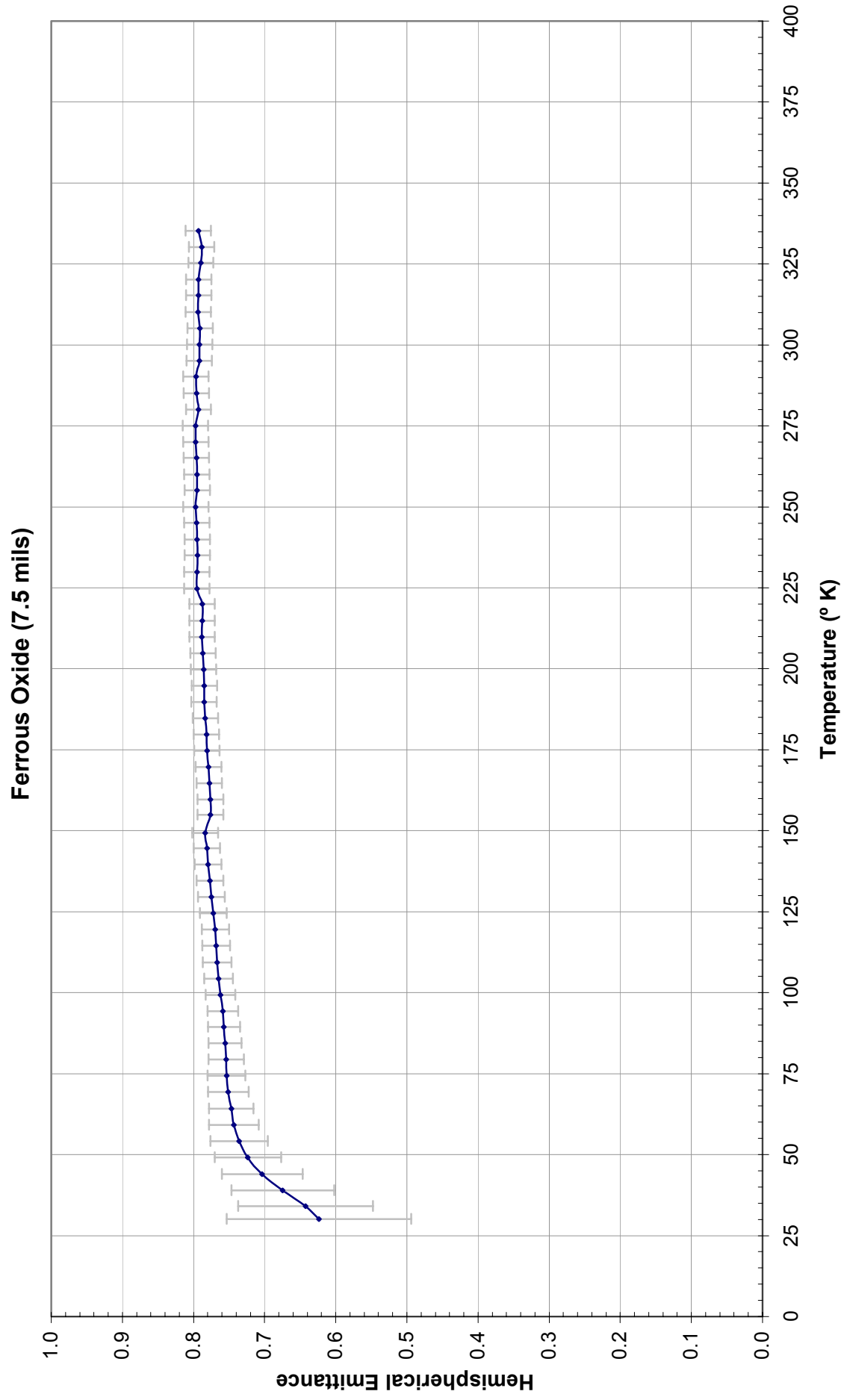


Figure 6.15

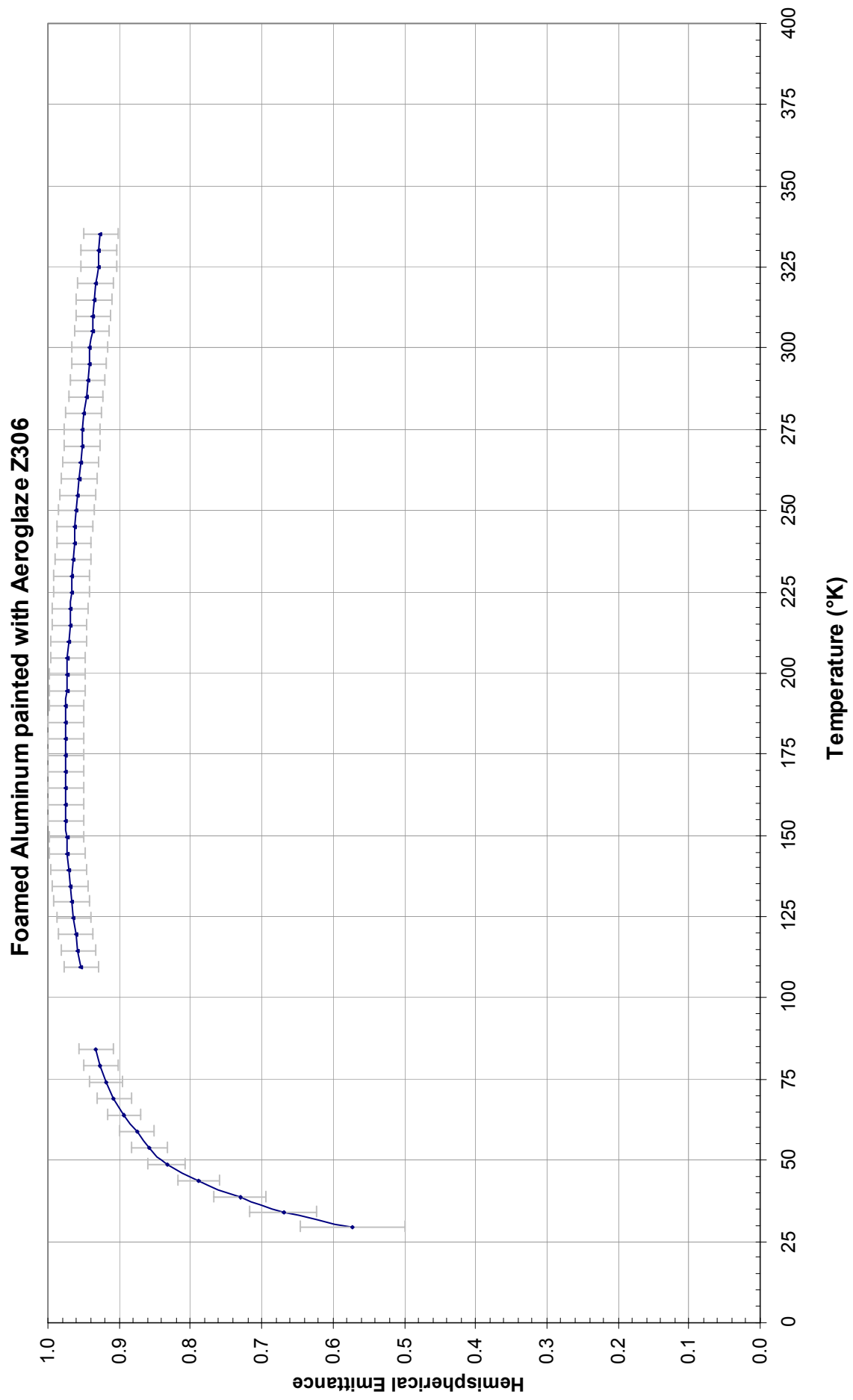


Figure 6.16

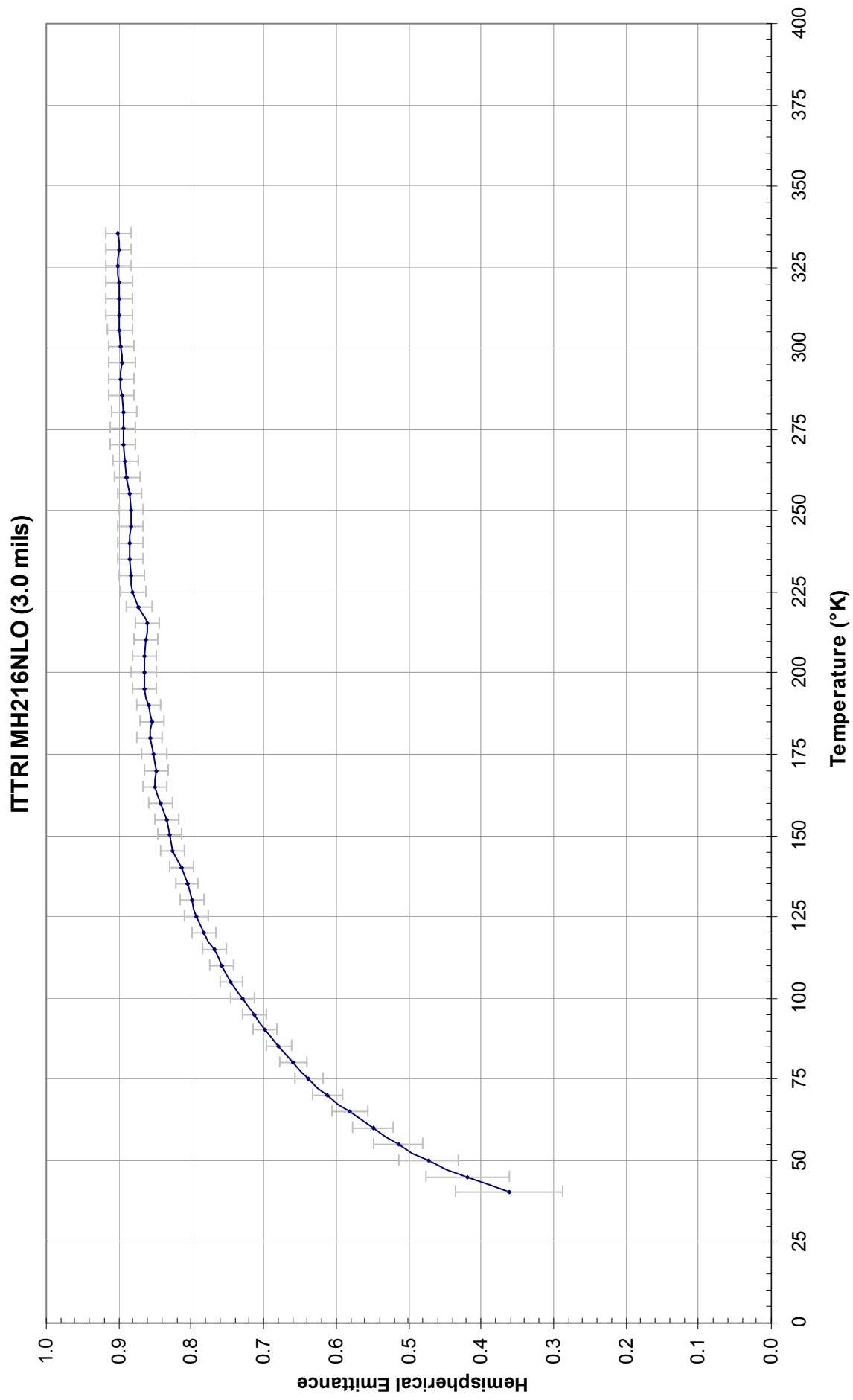


Figure 6.17

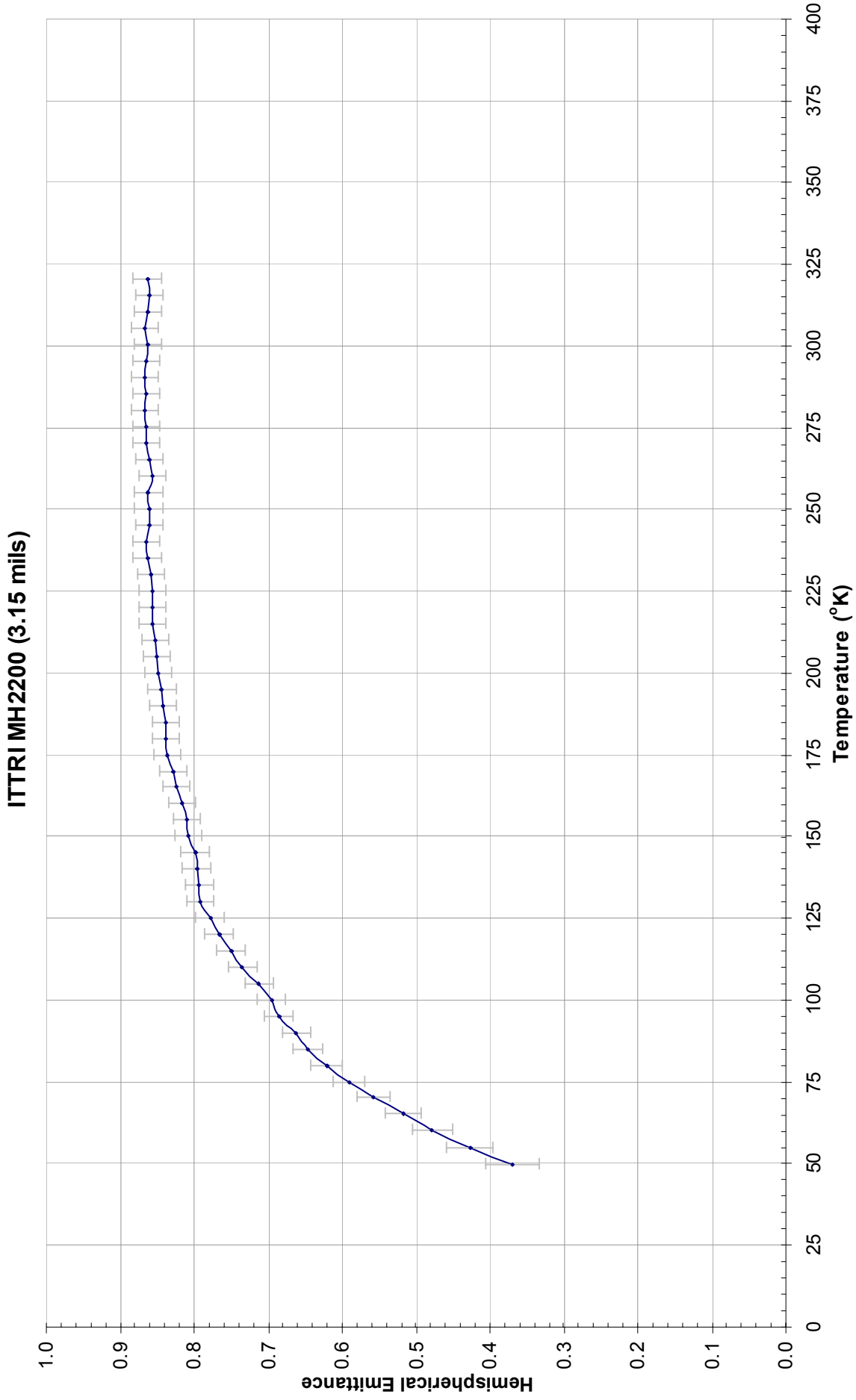


Figure 6.18

ITTRI S13GPLO (5.42 mils)

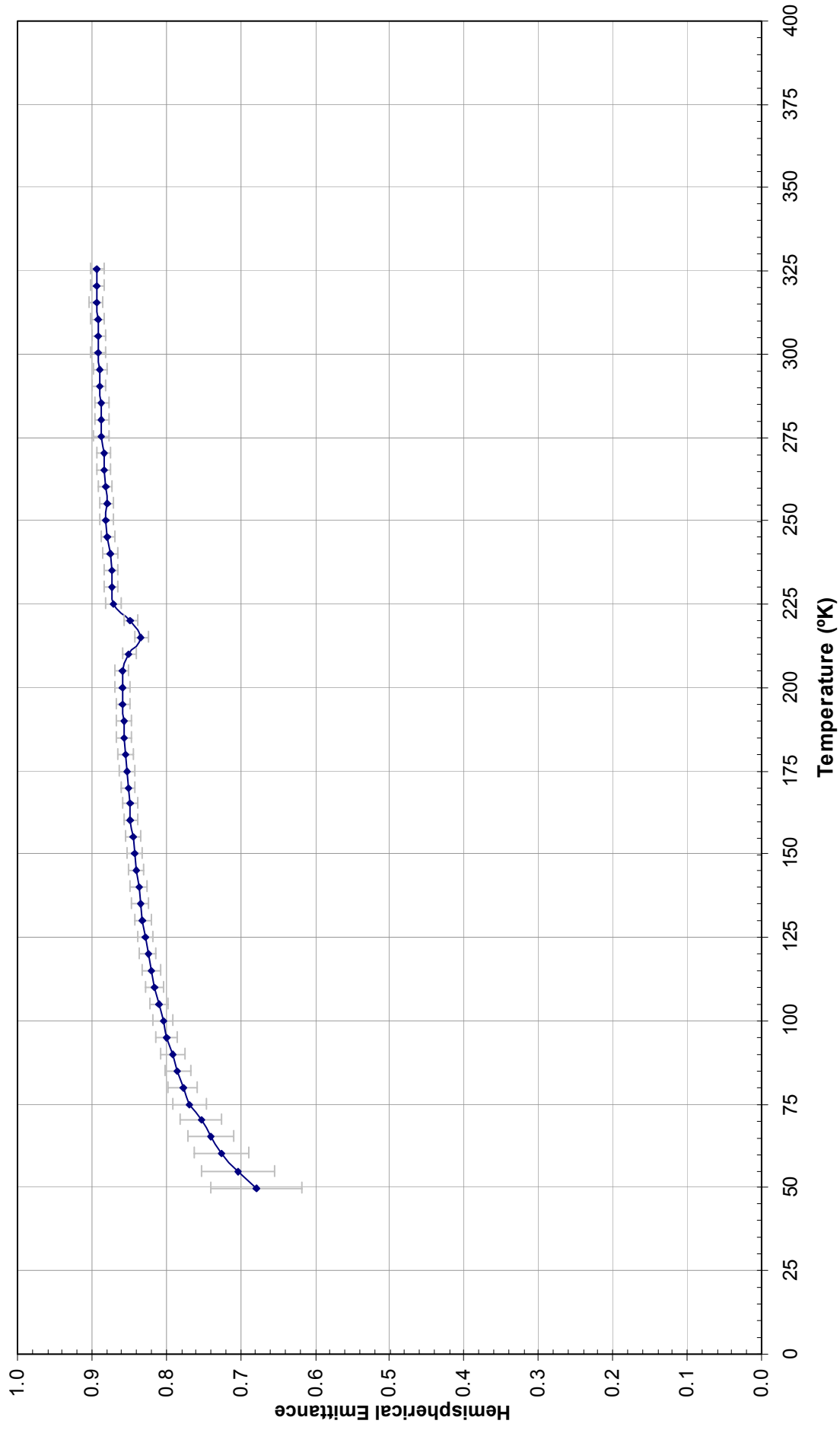


Figure 6.19

ITTRI Z93sc55 (5.43 mils)

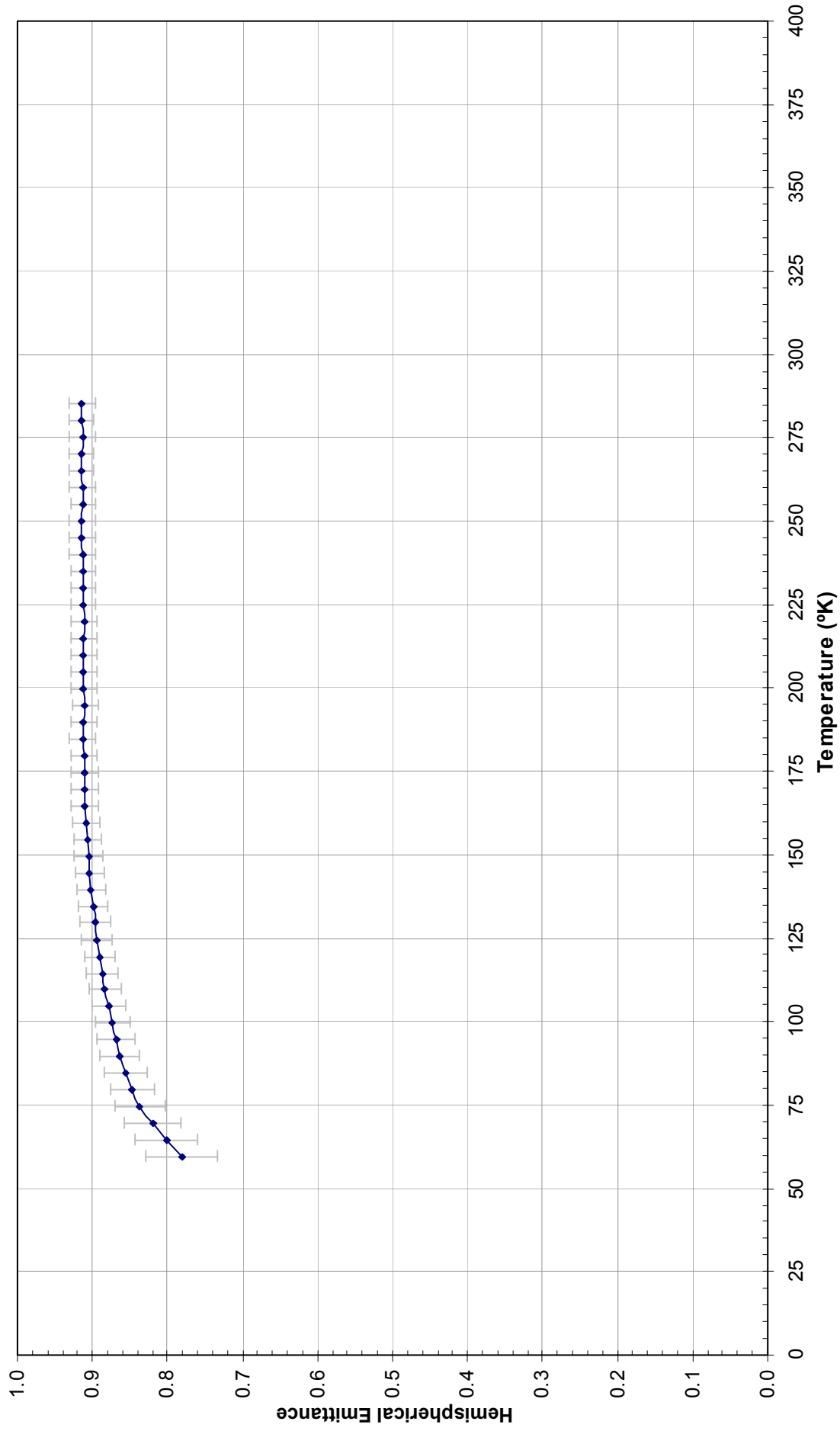


Figure 6.20

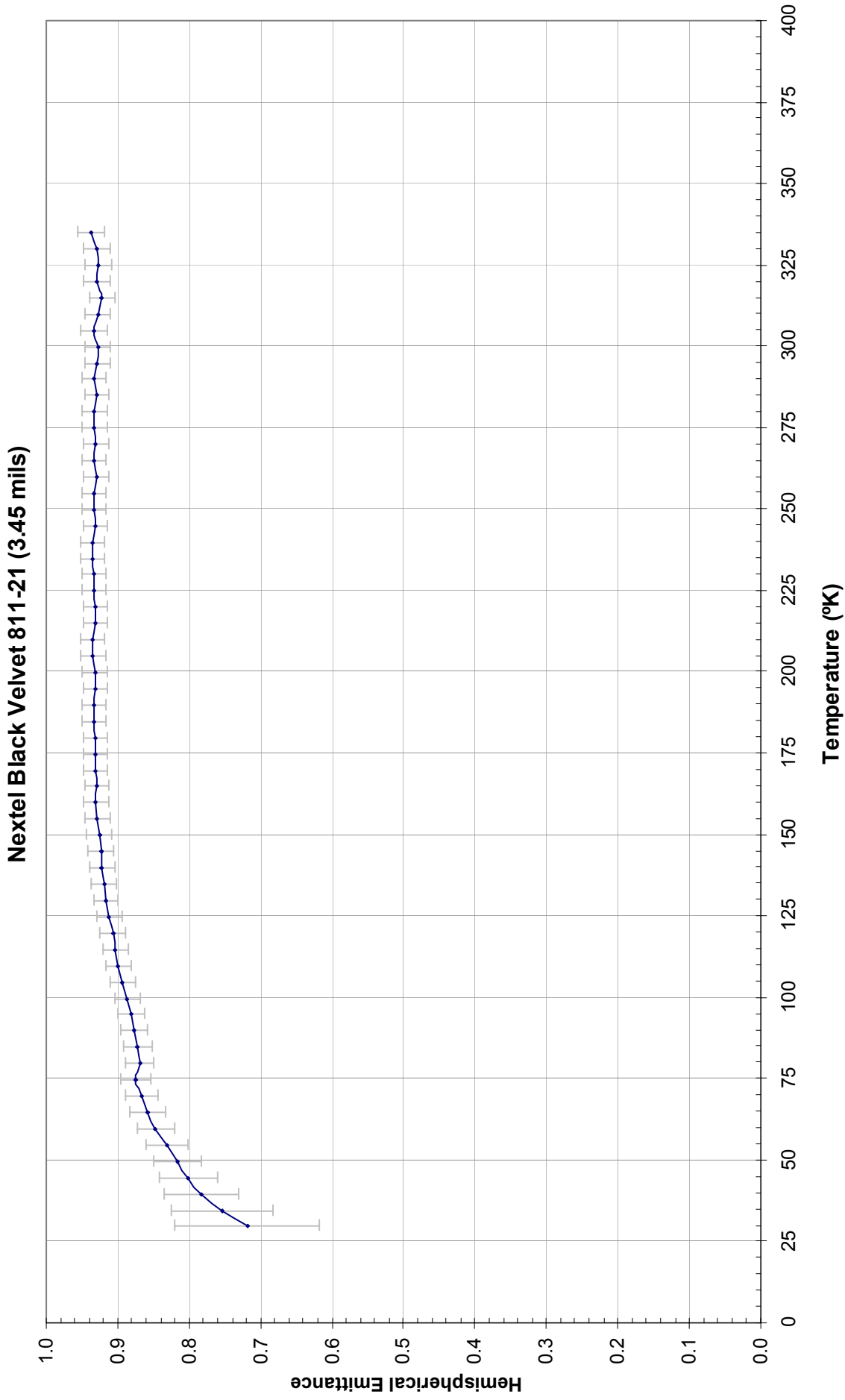


Figure 6.21

NPL Super Black (2.4 mils)

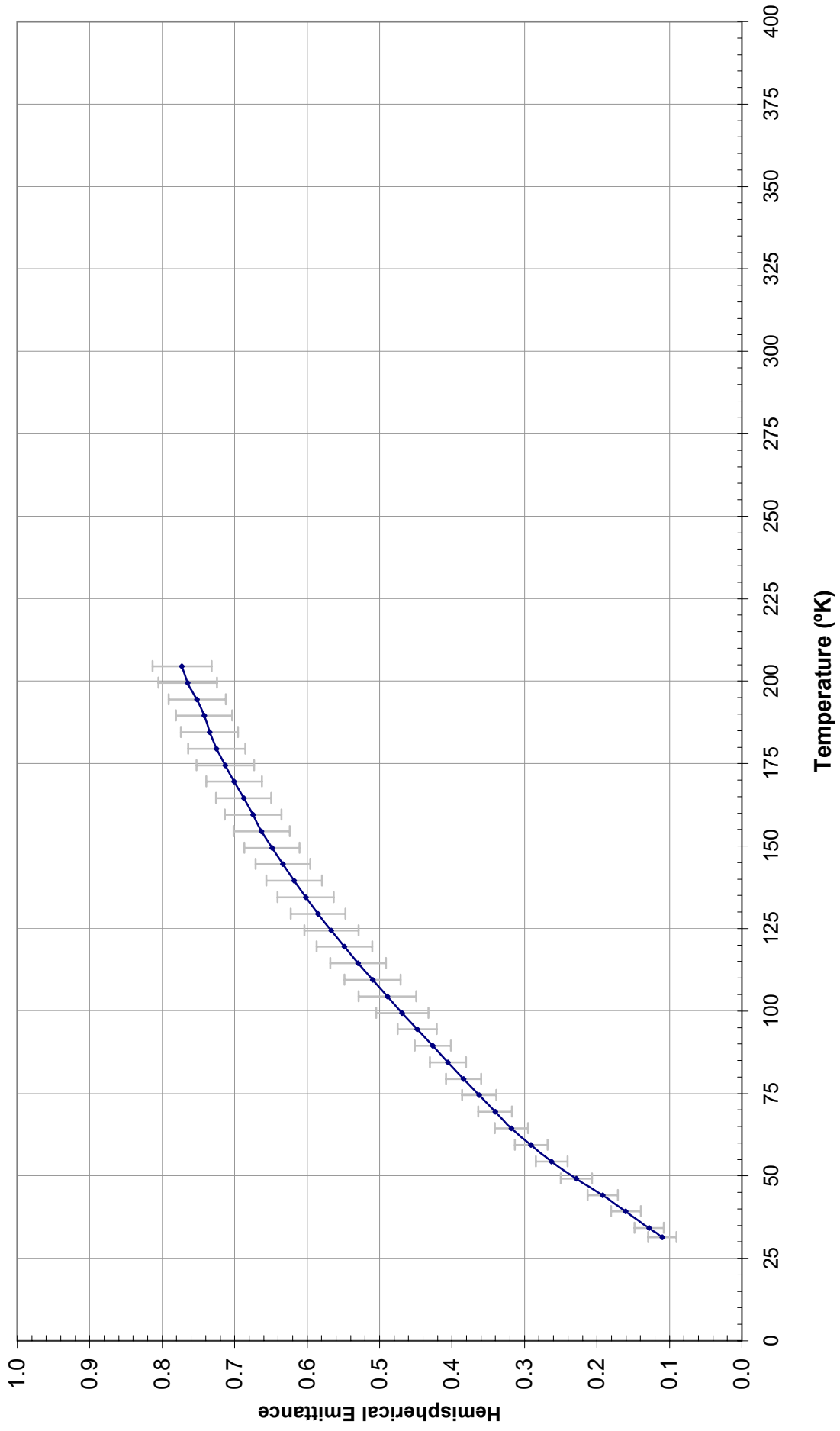


Figure 6.22

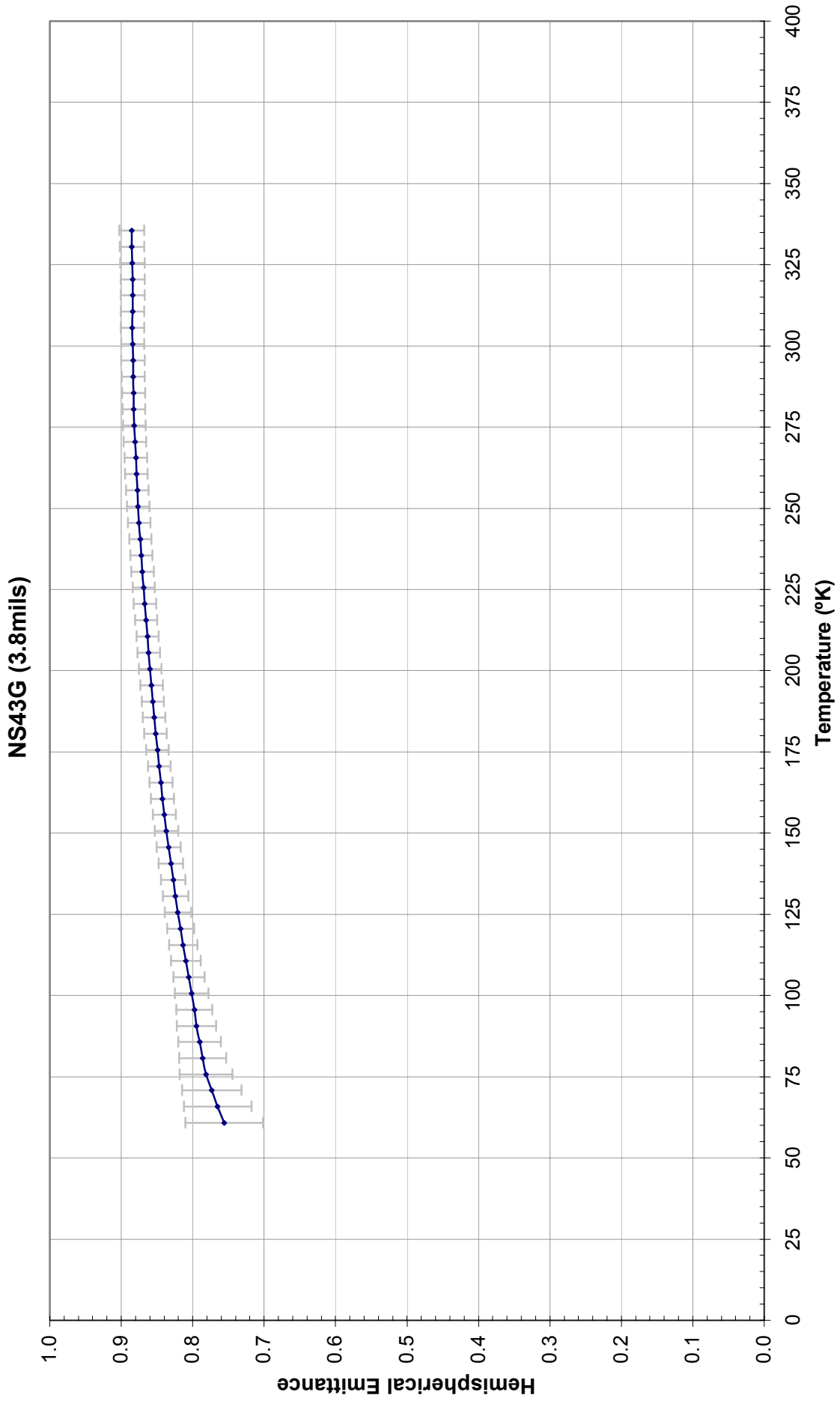


Figure 6.23

Parylene/Aluminum

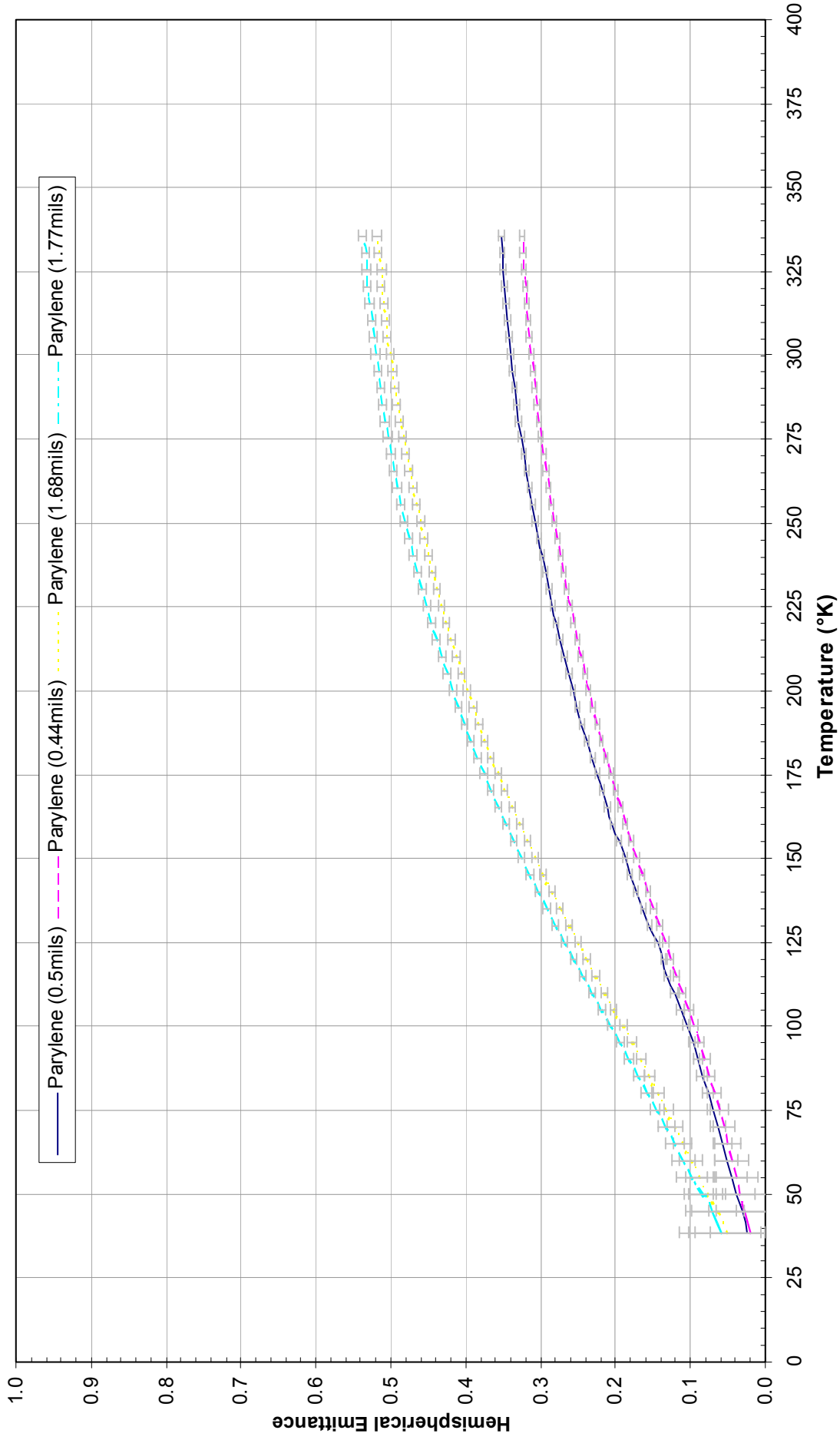


Figure 6.24

PT401 Semi-Gloss Black Paint (0.65mils)

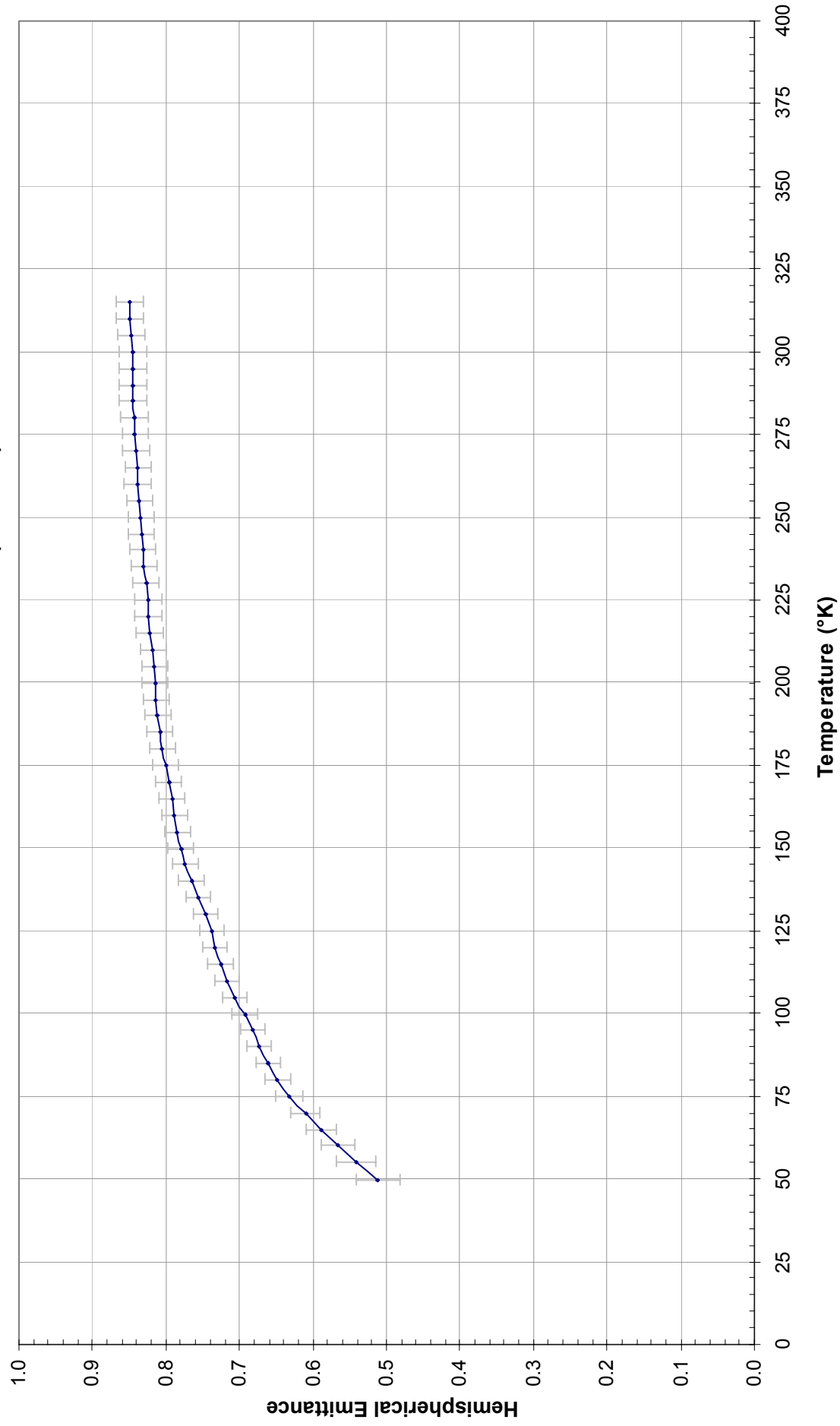


Figure 6.25

PT401 Semi-Gloss White Paint (2.1mils)

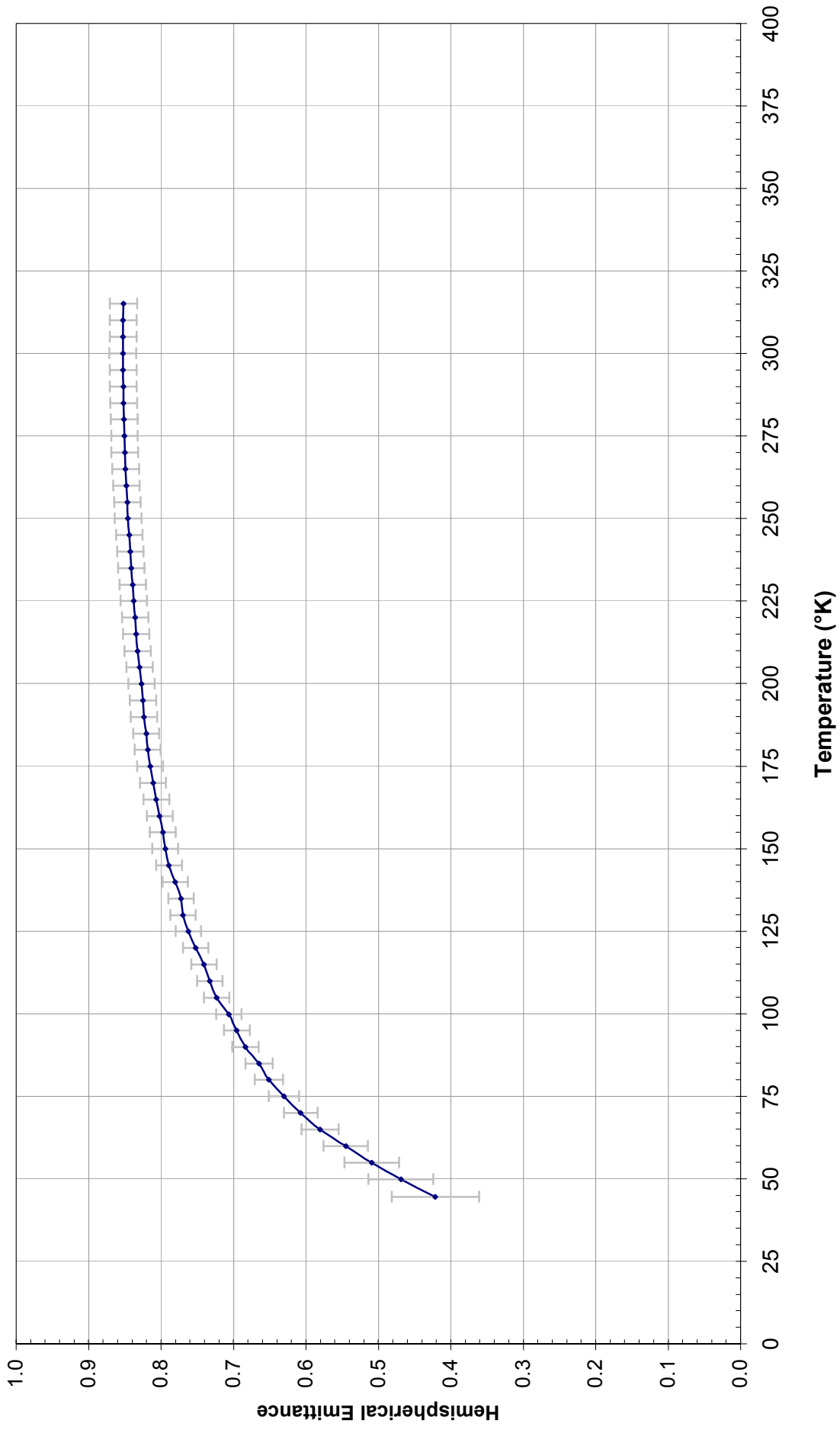


Figure 6.26

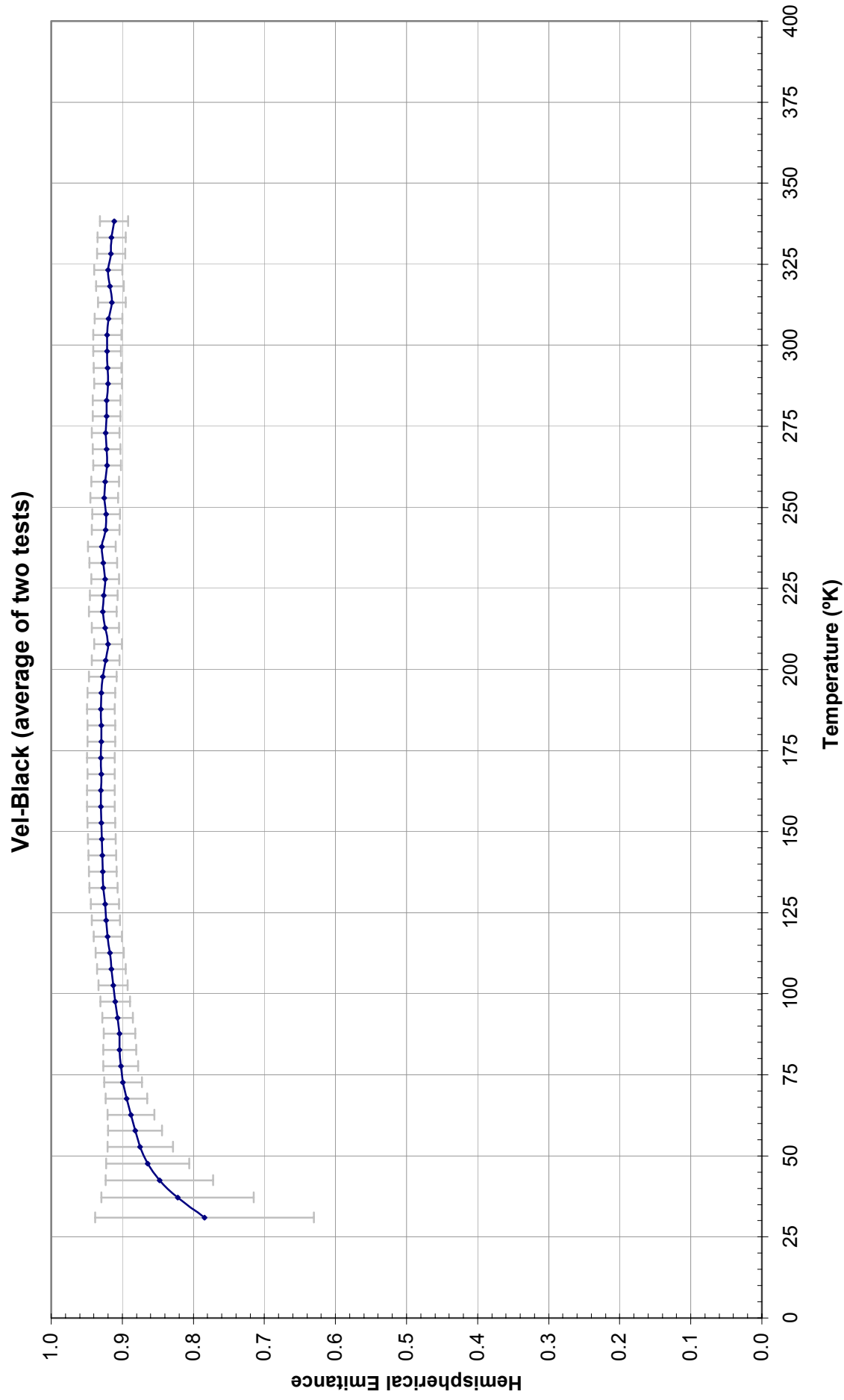


Figure 6.27

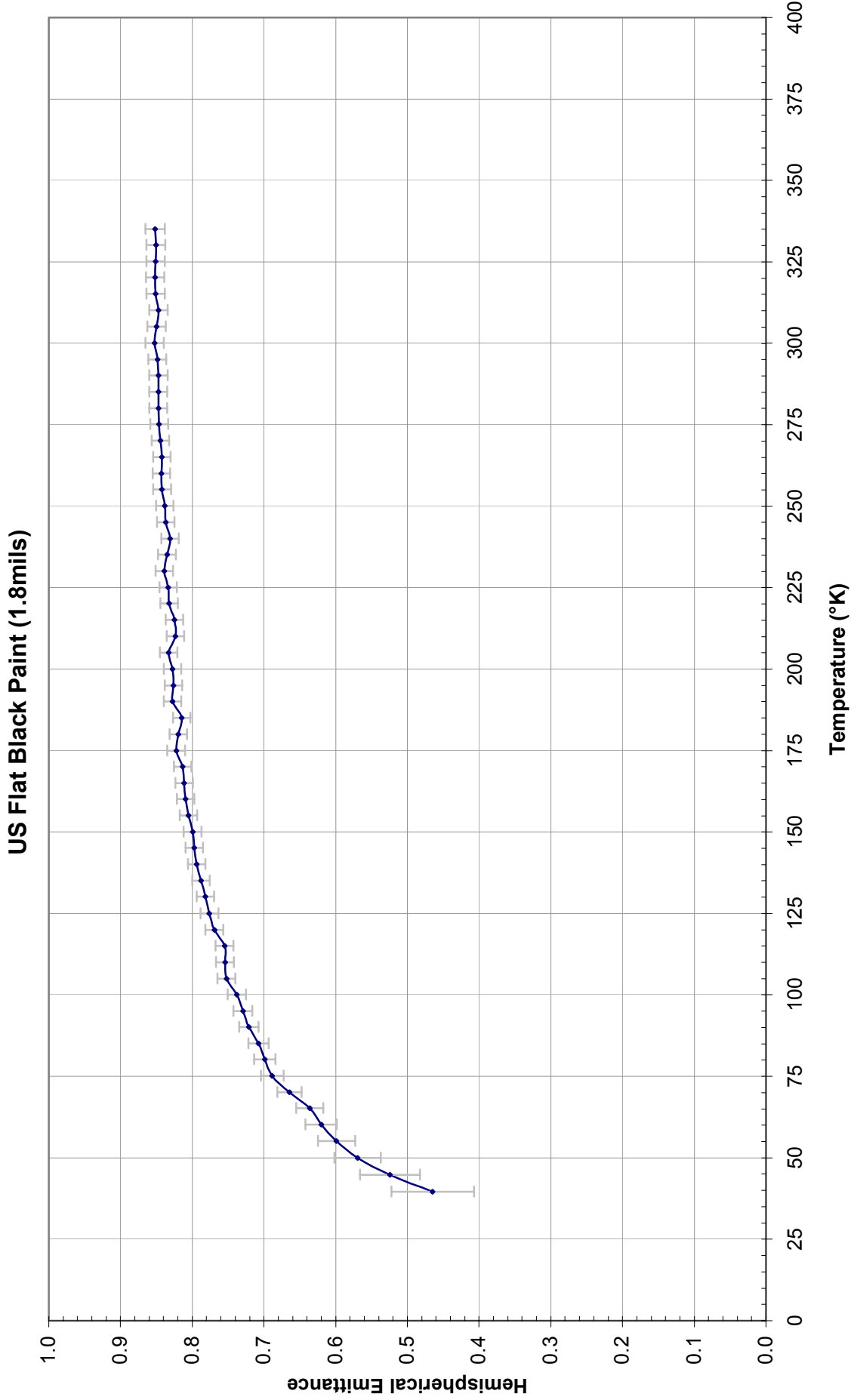


Figure 6.28

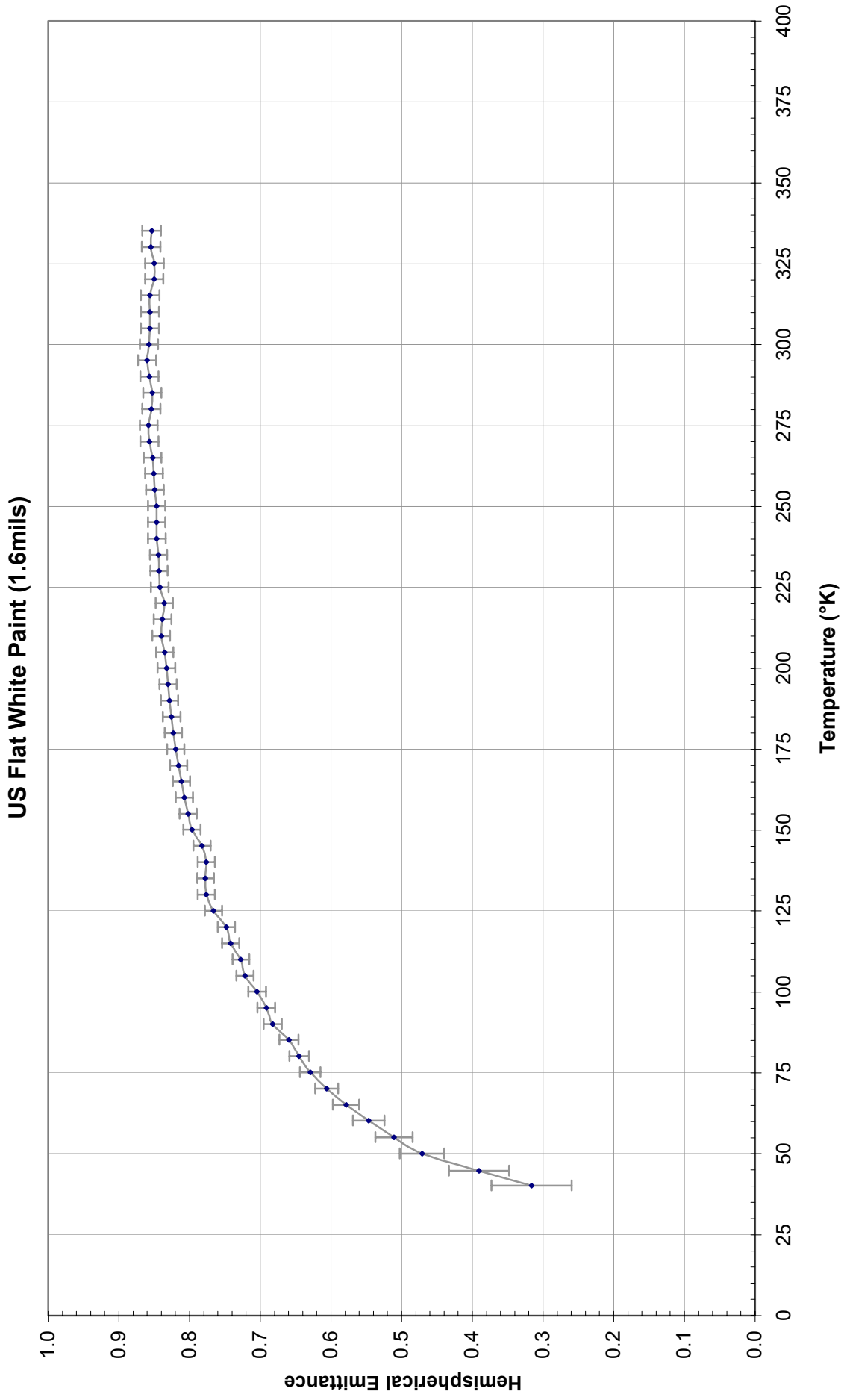


Figure 6.29

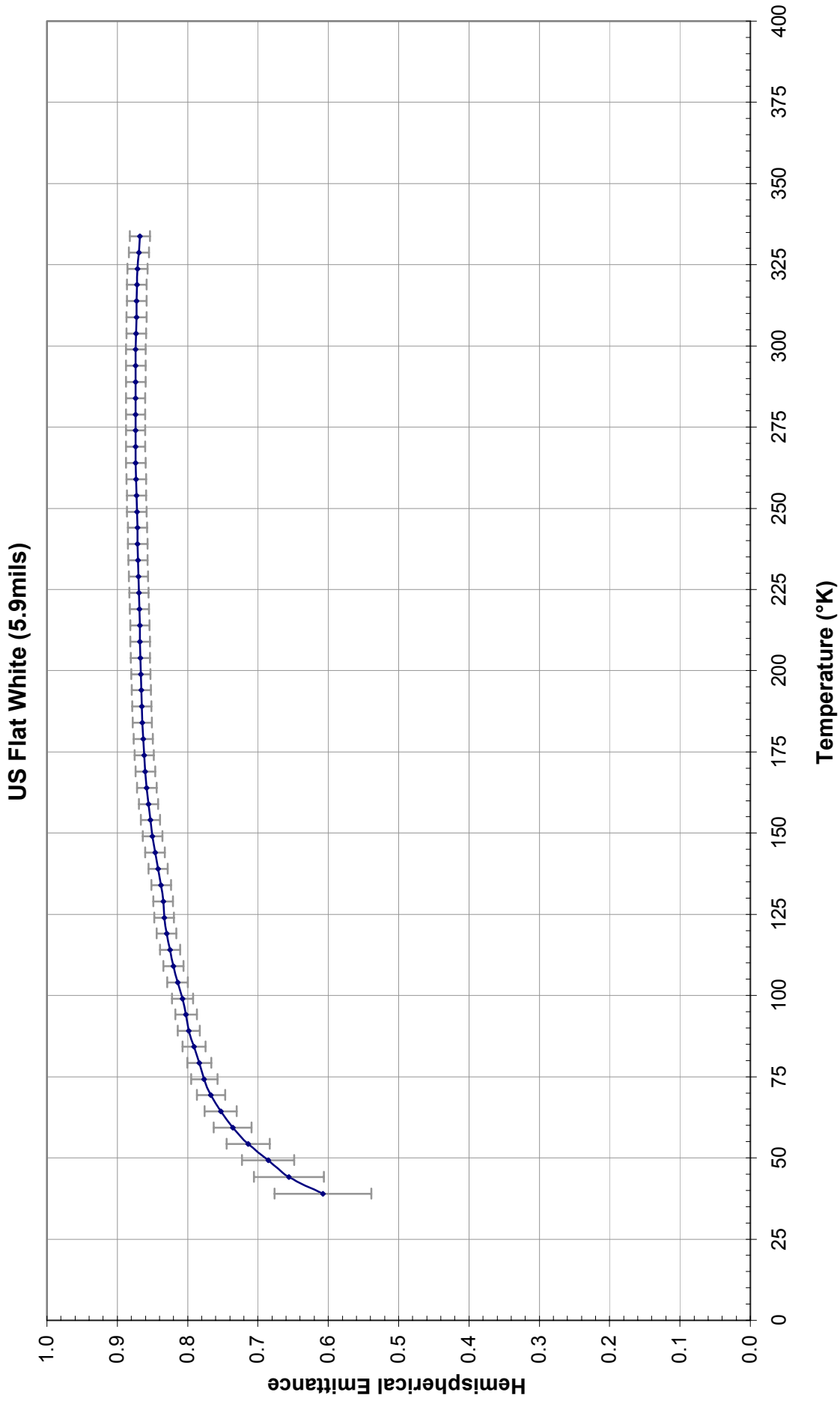


Figure 6.30

Stycast with Iron Microspheres (5.0 mils)

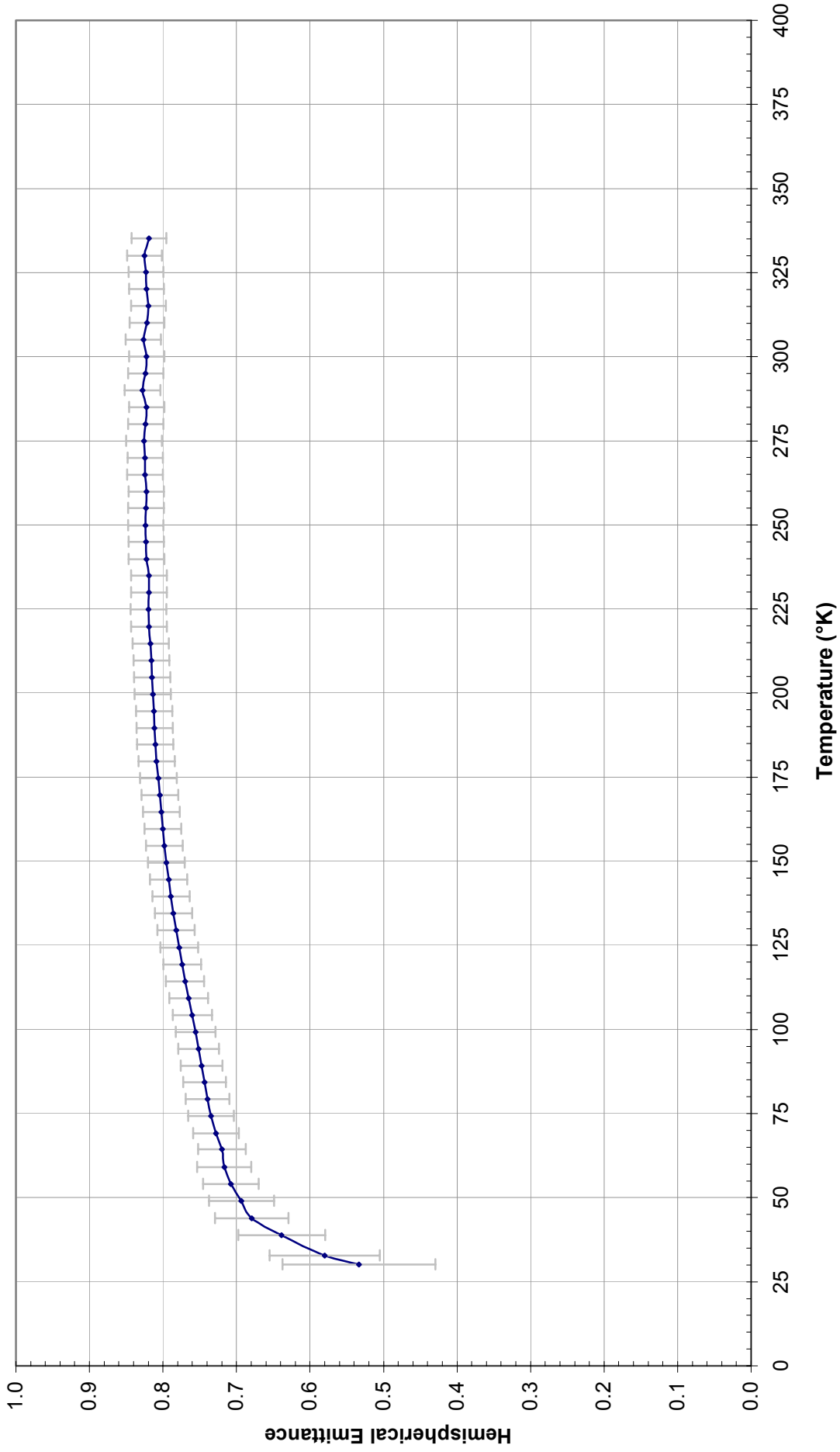


Figure 6.31

REPORT DOCUMENTATION PAGE

*Form Approved
OMB No. 0704-0188*

The public reporting burden for this collection of information is estimated to average 1 hour per response, including the time for reviewing instructions, searching existing data sources, gathering and maintaining the data needed, and completing and reviewing the collection of information. Send comments regarding this burden estimate or any other aspect of this collection of information, including suggestions for reducing this burden, to Department of Defense, Washington Headquarters Services, Directorate for Information Operations and Reports (0704-0188), 1215 Jefferson Davis Highway, Suite 1204, Arlington, VA 22202-4302. Respondents should be aware that notwithstanding any other provision of law, no person shall be subject to any penalty for failing to comply with a collection of information if it does not display a currently valid OMB control number.

PLEASE DO NOT RETURN YOUR FORM TO THE ABOVE ADDRESS.

1. REPORT DATE (DD-MM-YYYY)			2. REPORT TYPE		3. DATES COVERED (From - To)	
4. TITLE AND SUBTITLE					5a. CONTRACT NUMBER	
					5b. GRANT NUMBER	
					5c. PROGRAM ELEMENT NUMBER	
6. AUTHOR(S)					5d. PROJECT NUMBER	
					5e. TASK NUMBER	
					5f. WORK UNIT NUMBER	
7. PERFORMING ORGANIZATION NAME(S) AND ADDRESS(ES)					8. PERFORMING ORGANIZATION REPORT NUMBER	
9. SPONSORING/MONITORING AGENCY NAME(S) AND ADDRESS(ES)					10. SPONSORING/MONITOR'S ACRONYM(S)	
					11. SPONSORING/MONITORING REPORT NUMBER	
12. DISTRIBUTION/AVAILABILITY STATEMENT						
13. SUPPLEMENTARY NOTES						
14. ABSTRACT						
15. SUBJECT TERMS						
16. SECURITY CLASSIFICATION OF:			17. LIMITATION OF ABSTRACT	18. NUMBER OF PAGES	19a. NAME OF RESPONSIBLE PERSON	
a. REPORT	b. ABSTRACT	c. THIS PAGE			19b. TELEPHONE NUMBER (Include area code)	

